High-Fidelity, Computational Modeling of Non-Equilibrium Discharges for Combustion Applications

Laxminarayan L. Raja

Contributions:
Douglas Breden, Rochan Upadhyay, Shankar Mahadevan

Dept. of Aerospace Engr. and Engr. Mech,
The University of Texas at Austin
Austin, Texas 78712

AFOSR Plasma-Assisted Combustion

Multi-University Research Initiative Review (MURI) Review

Arlington, VA, USA

(22nd – 24th October 2013)

Report Documentation Page

Form Approved
OMB No. 0704-0188

Public reporting burden for the collection of information is estimated to average 1 hour per response, including the time for reviewing instructions, searching existing data sources, gathering and maintaining the data needed, and completing and reviewing the collection of information. Send comments regarding this burden estimate or any other aspect of this collection of information, including suggestions for reducing this burden, to Washington Headquarters Services, Directorate for Information Operations and Reports, 1215 Jefferson Davis Highway, Suite 1204, Arlington VA 22202-4302. Respondents should be aware that notwithstanding any other provision of law, no person shall be subject to a penalty for failing to comply with a collection of information if it does not display a currently valid OMB control number.

1. REPORT DATE	2. REPORT TYPE	3. DATES COVERED
OCT 2013		**00-00-2013 to 00-00-2013**

4. TITLE AND SUBTITLE	5a. CONTRACT NUMBER
High-Fidelity, Computational Modeling of Non-Equilibrium Discharges for Combustion Applications	5b. GRANT NUMBER
	5c. PROGRAM ELEMENT NUMBER
6. AUTHOR(S)	5d. PROJECT NUMBER
	5e. TASK NUMBER
	5f. WORK UNIT NUMBER
7. PERFORMING ORGANIZATION NAME(S) AND ADDRESS(ES) **University of Texas at Austin,Department of Aerospace Engr. and Engr. Mech,Austin,TX,78712**	8. PERFORMING ORGANIZATION REPORT NUMBER
9. SPONSORING/MONITORING AGENCY NAME(S) AND ADDRESS(ES)	10. SPONSOR/MONITOR'S ACRONYM(S)
	11. SPONSOR/MONITOR'S REPORT NUMBER(S)

12. DISTRIBUTION/AVAILABILITY STATEMENT
Approved for public release; distribution unlimited

13. SUPPLEMENTARY NOTES

14. ABSTRACT

15. SUBJECT TERMS

16. SECURITY CLASSIFICATION OF:			17. LIMITATION OF ABSTRACT	18. NUMBER OF PAGES	19a. NAME OF RESPONSIBLE PERSON
a. REPORT	b. ABSTRACT	c. THIS PAGE			
unclassified	**unclassified**	**unclassified**	**Same as Report (SAR)**	**86**	

Motivation

- There is significant evidence to show cold (non-equilibrium) plasma discharges have distinct advantages as combustion ignition / stabilization sources
- At high pressures relevant to applications, cold plasmas generated by nanosecond pulsing that result in streamer like constricted discharges
- Significant experimental difficulty in probing the structure and properties of streamers (small length scales, short time scales)
- High-fidelity computational modeling can play an important role in describing physics and chemistry in these discharges

Cold (non-equilibrium) plasma discharge in plasma parameter space

- Thermal plasmas (“Hot”)
  - Most electrical energy goes into gas heating (~10,000 K)
  - All species can be characterized by the same temperature (in thermal equilibrium)
- Non-thermal plasmas (“Cold”)
  - Electrical power is absorbed by electrons which in turn produce radicals and ions.
  - Electrons have high temperature (~10,000 K and more)
  - Ions and Neutrals remain at lower temperature (~300-1000 K)
  - Not in thermal equilibrium (non-equilibrium plasma)

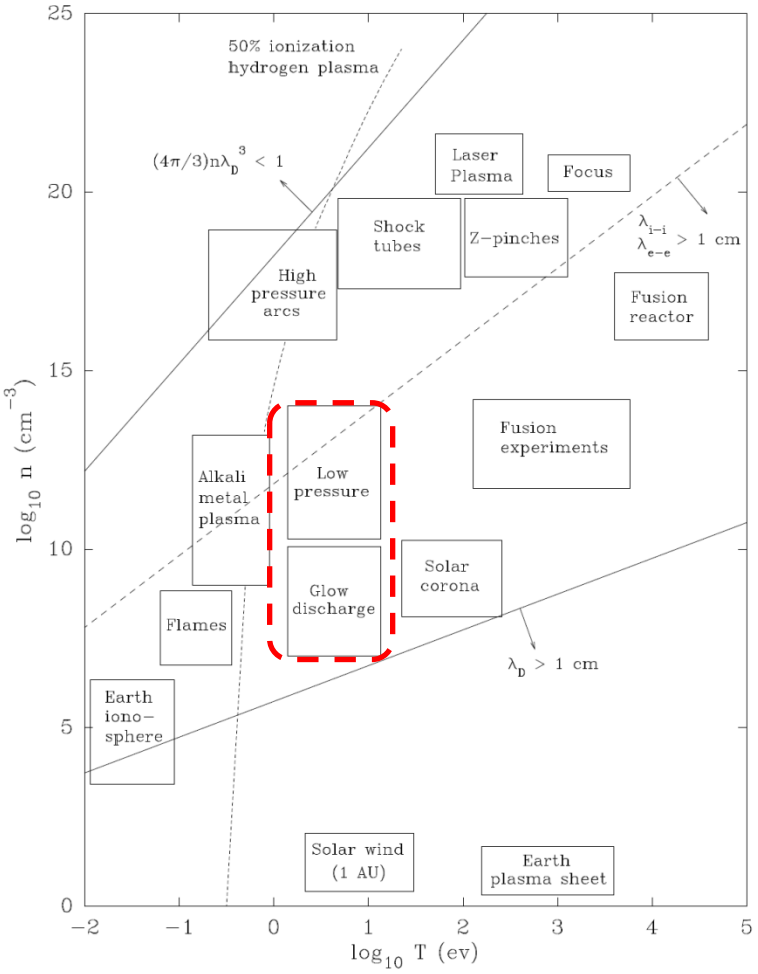

From : NRL plasma formulary
http://wwwppd.nrl.navy.mil/nrlformulary/

Characteristic molecular energies and electron energy loss pathways

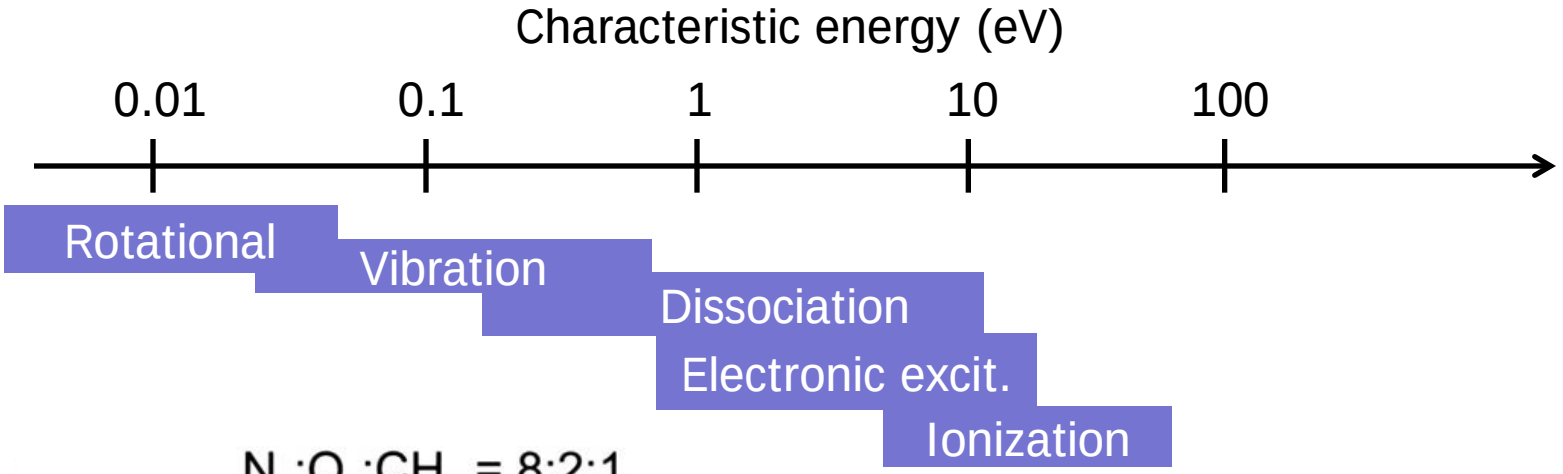

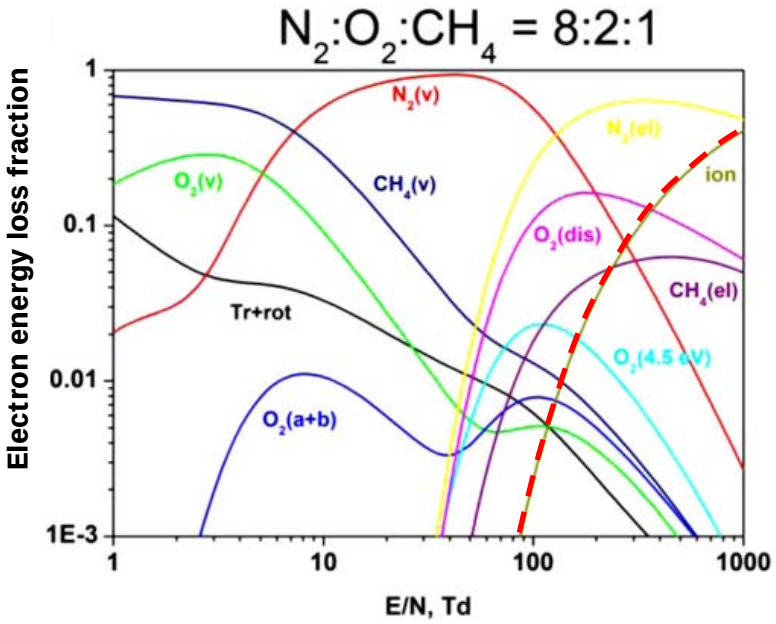

- Reduced electric field E/N is an important parameter for plasmas (1 Td = 10^{-17} V cm^2)
- Note: Breakdown threshold ~ 100 Td (e.g. 120 Td for air)

Ref : Starikovskiy and Alexsandrov, Prog. Energy Comb. Sci., 2013

Approach to sustain non-equilibrium at high pressures (automotive and aerospace appl.)

- In principle can maintain non-equilibrium by high discharge voltages (i.e. high E/n)
  - (Rate of energy gain by electrons) > (Rate of energy loss to gas heating)
- However at high pressures non-equilibrium discharges are susceptible to Glow-to-Arc Transitions (GAT)
  - Discharge instabilities cause gas temperature to rise rapidly
- GAT has time-scale of ~100's ns
- Can sustain non-equilibrium, by repeated pulsing on nanosecond time scales
  - First demonstration in early 2000 [Kruger et al. 2002]

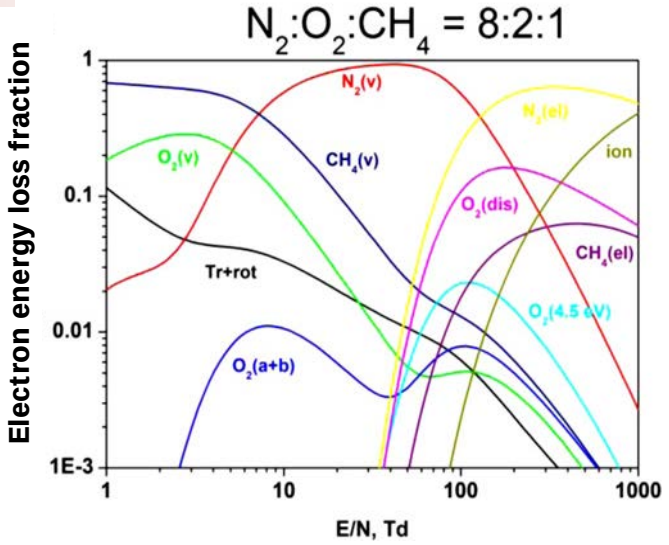

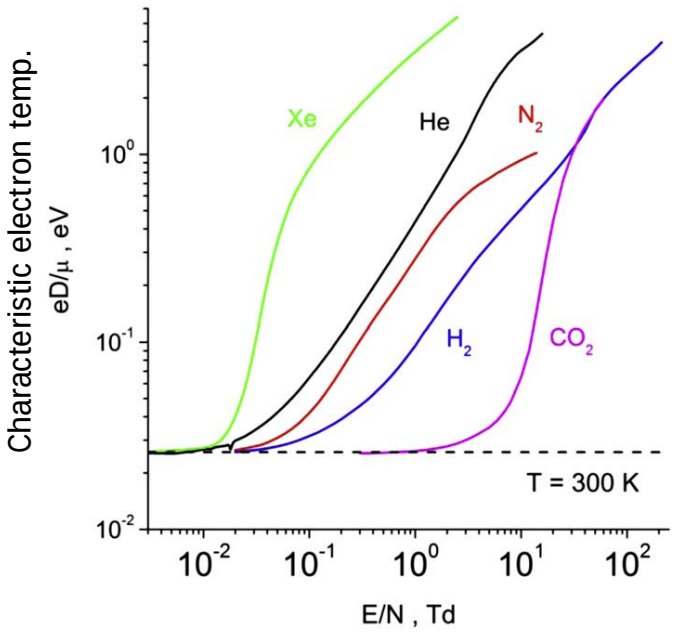

Ref : Starikovskiy and Alexsandrov, Prog. Energy Comb. Sci., 2013
Kruger, Laux, Yu, Packan, Perriot, Pure and Appl. Chem., 74, 2002, pp. 334

Nanosecond pulsing produces enhanced tail in the electron Energy Dist. Func. (EEDF)

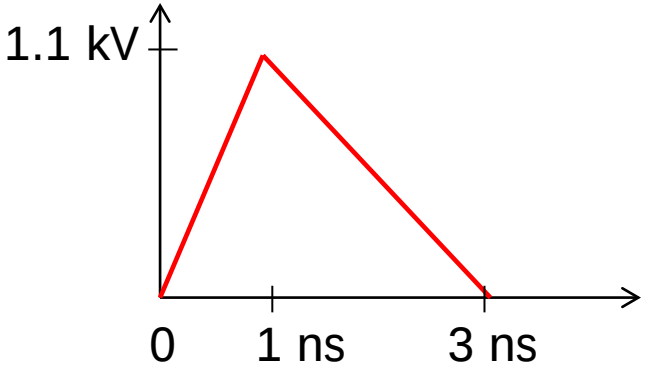

Air, p=1 Torr, 300 K, 3 cm gap
(E/n = 1140 Td)

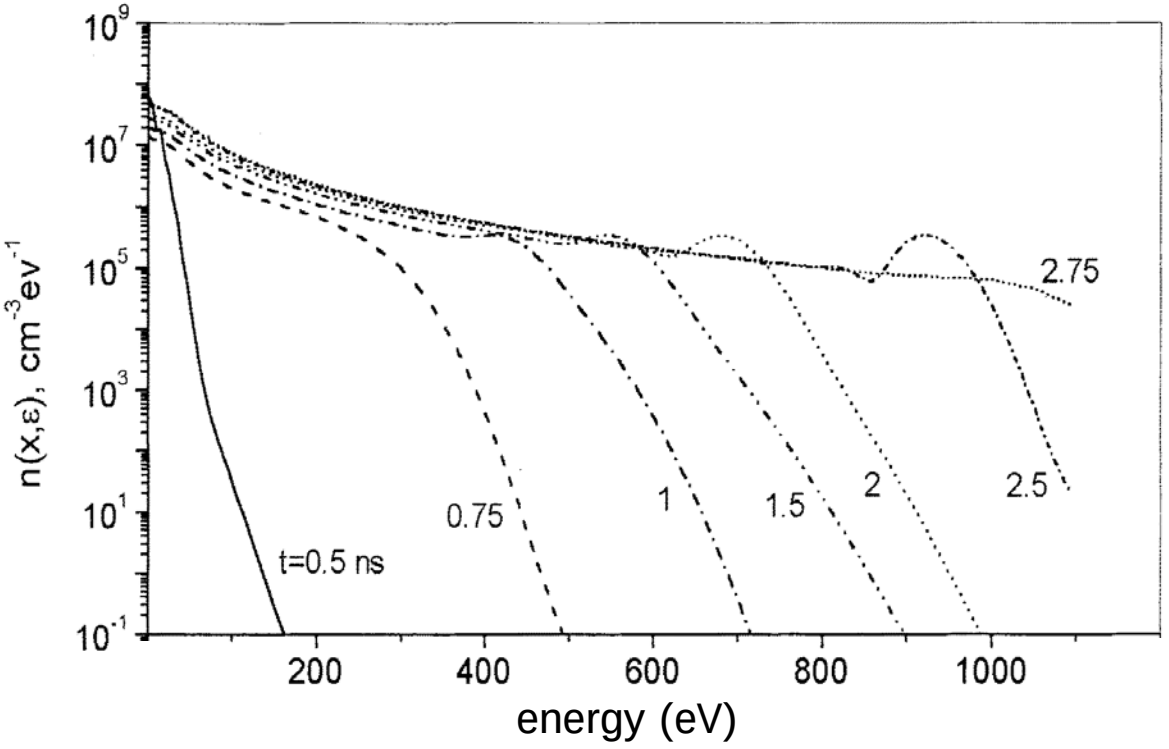

- Power budget for nanosecond pulsed discharge is much lower than a DC discharge

From: Macheret et al., IEEE Trans. Plasma Sci. 30, 2002, pp. 1301.

Computational challenges for plasma ignition and flame spread prediction

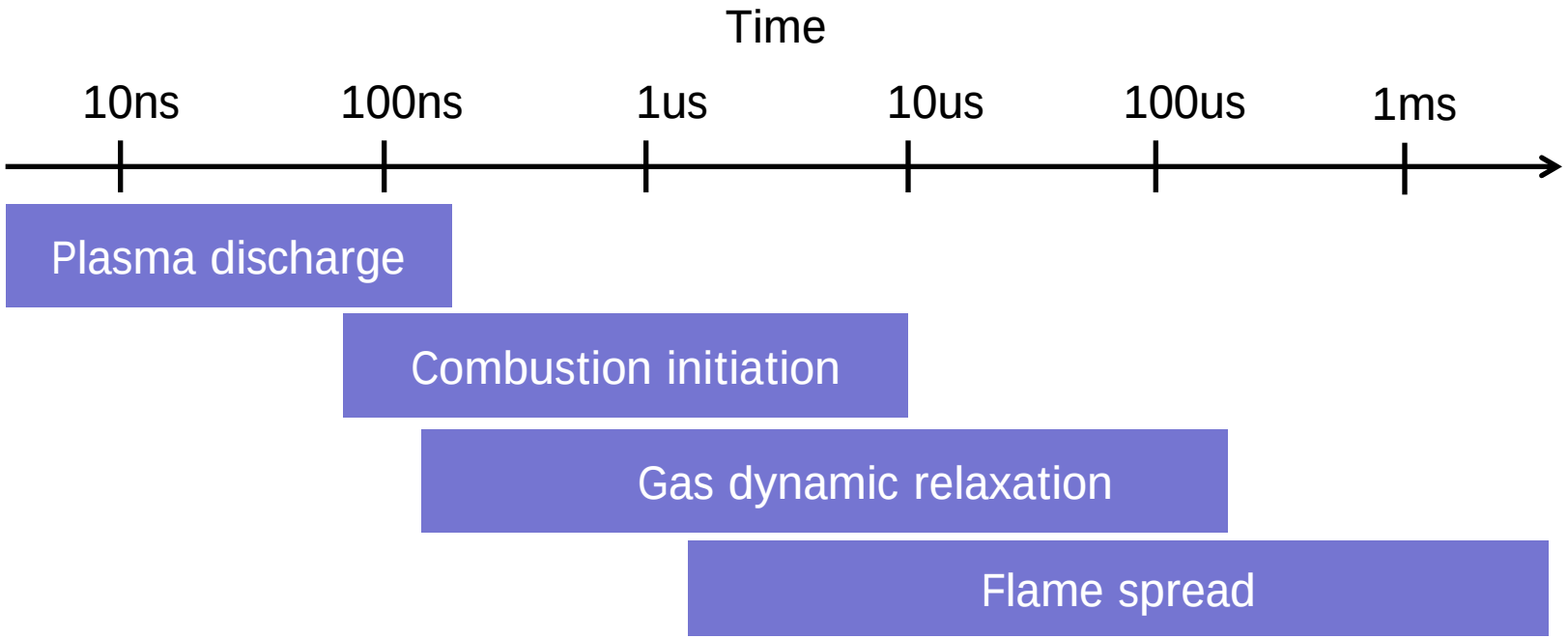

- Multiple physical and chemical processes with vast disparity in time scales
- Complex chemistries with high degree of uncertainty

Coaxial electrode cold plasma igniter for automotive combustion applications

Coaxial electrode igniter

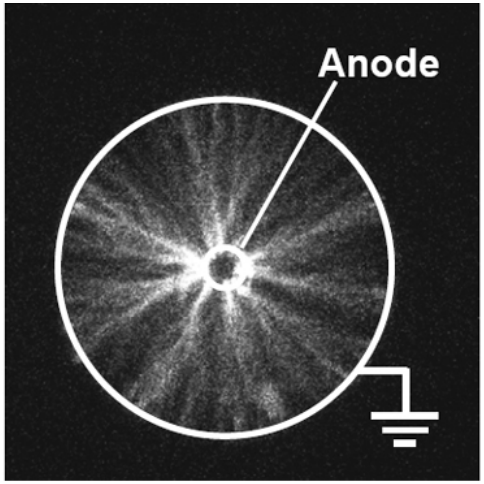

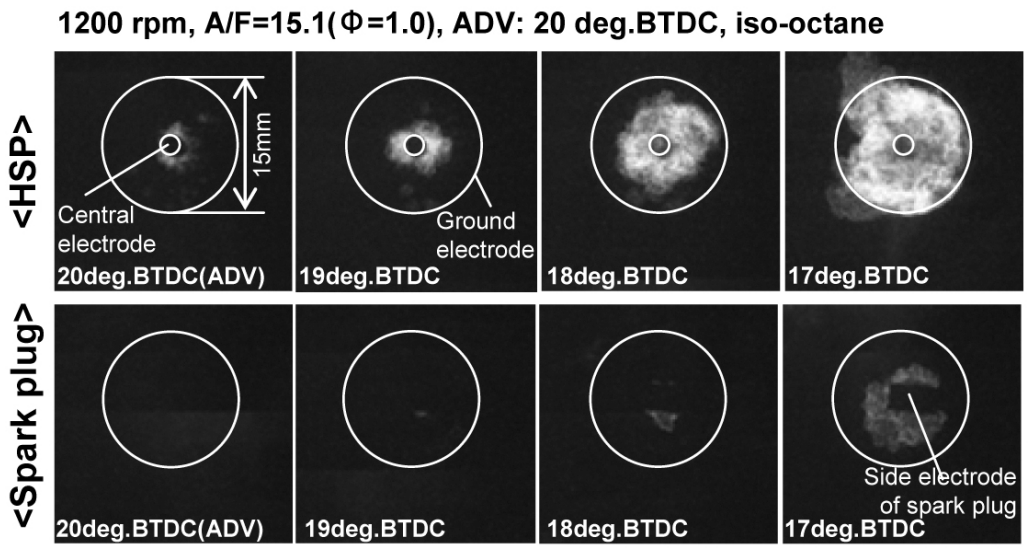

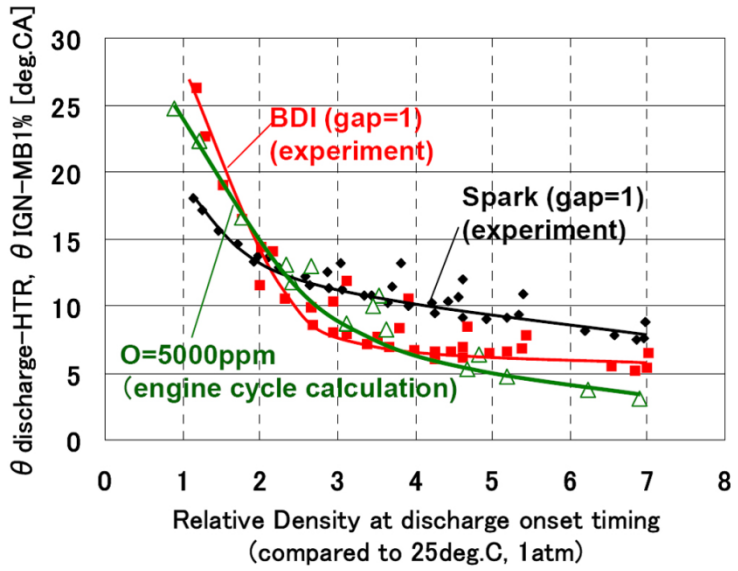

From: Shiraishi et al. SAE Paper 2011-01-0660

Single electrode (Corona) excitation for automotive ignition applications

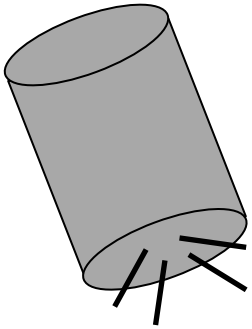

RF : Freq. ~10 MHz
Voltage ~100kV

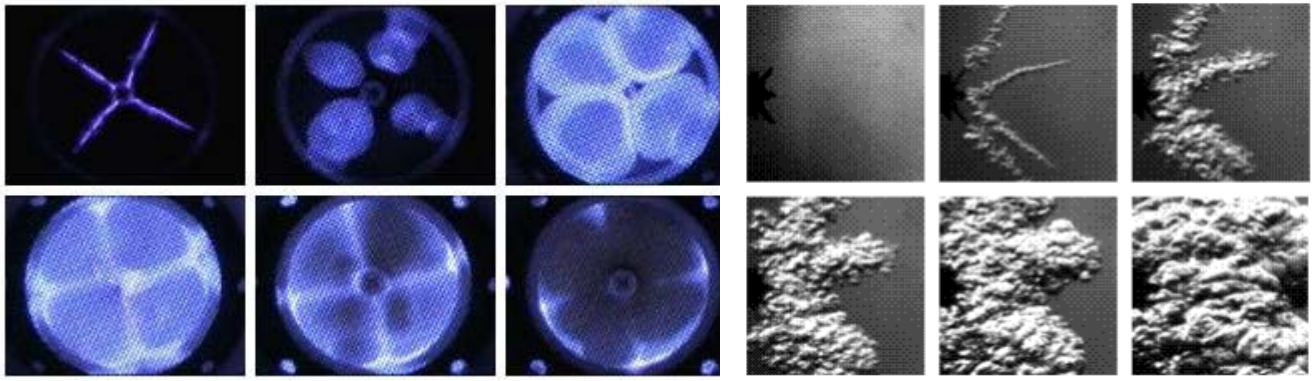

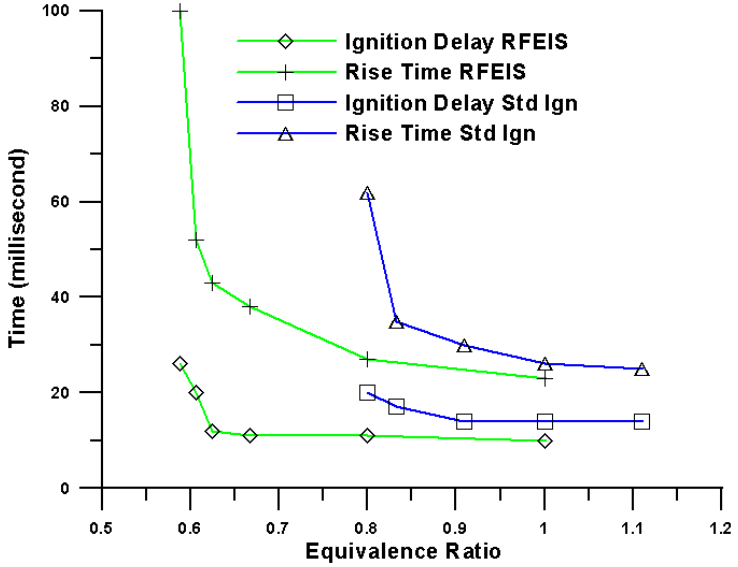

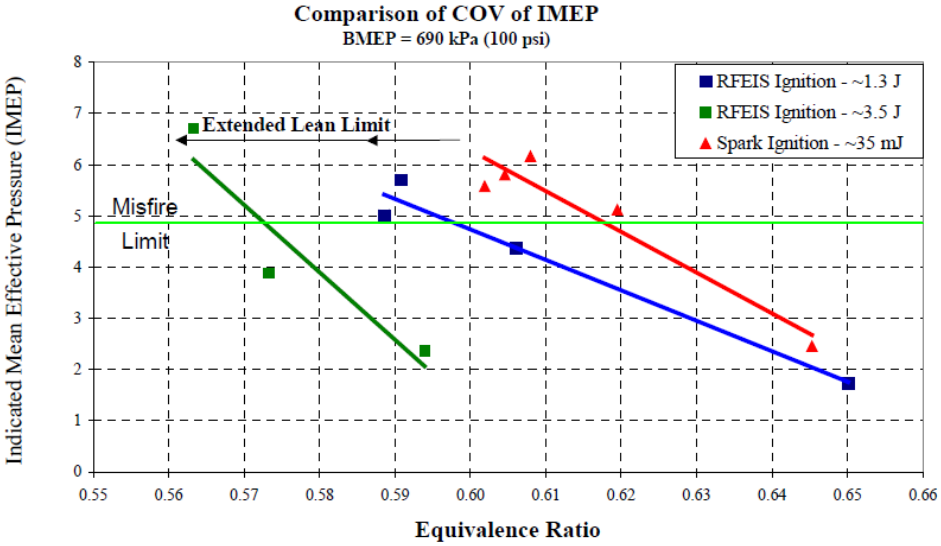

Figure 18. Lean Misfire Limit Comparison at 690 kPa BMEP

Ref: P. Freen, “Radio Frequency Electrostatic Ignition System Feasibility Demonstration, EISG Final Report,2005

Nanosecond pulsed ignition of supersonic combustion

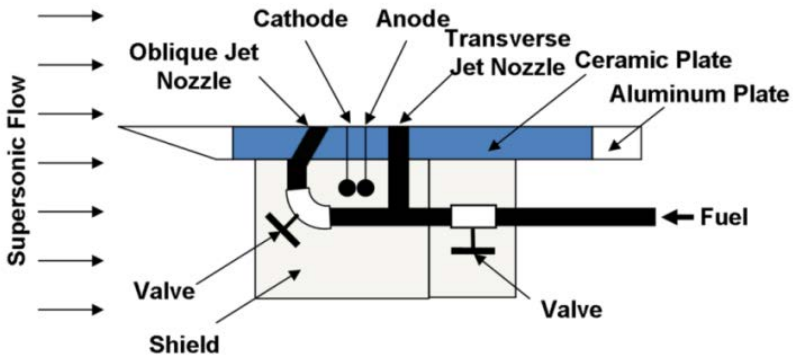

- 7 kV unipolar pulses
- 20 ns pulse width
- 50 kHz pulse freq.

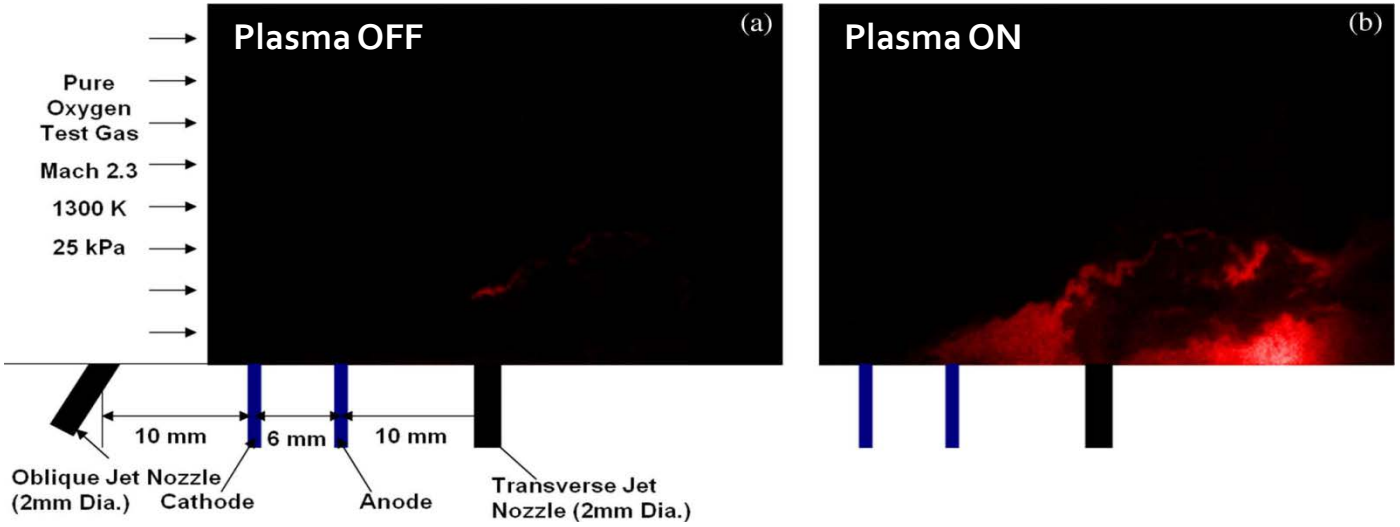

OH PLIF

Ref: H. Do, M. G. Mungal and M. A. Cappelli., "Jet Flame Ignition in a Supersonic Crossflow using a Pulsed Nonequilibrium Plasma Discharge," IEEE Tran. On Plasma Sci. Vol.36 , 2008, pp. 2918-2923

Approach

- High fidelity multi-dimensional computational simulations of the plasma processes relevant to plasma assisted combustion
  - Self-consistent plasma
  - Multi-species
  - Multi-temperature
  - Gas-phase kinetics
  - Surface kinetics
- Plasma model + Gas dynamic model
  - Two-way gas dynamic / plasma coupling

Plasma model

- Species continuity

$$\frac{\partial n_k}{\partial t} + \vec{\nabla} \cdot \vec{f}_k = \dot{G}_k \qquad k = 1,...,K_g (k \neq k_b)$$

- Ideal Gas Law

$$p = \sum_k n_k k_B T_k$$

- Drift-Diffusion approximation with bulk convection

$$\vec{f}_k \equiv n_k \vec{u}_k = -\mu_k n_k \vec{\nabla}\phi - D_k \vec{\nabla} n_k + n_k \vec{V}$$

- Poisson's equation

$$\nabla^2 \phi = -\frac{e}{\varepsilon_0} \sum_k Z_k n_k$$

- Electron Energy Equation

$$\frac{\partial e_e}{\partial t} + \vec{\nabla} \cdot \left(\left(\tfrac{5}{3} \mu_e \vec{E} + \vec{V} \right) e_e - \kappa_e \vec{\nabla} e_e \right) = \left(+ e \vec{f}_e \cdot \vec{\nabla} \phi \right) - \frac{3}{2} k_B n_e \frac{2 m_e}{m_{k_b}} (T_e - T_g) \bar{\nu}_{k,k_b} - e \sum_i \Delta E_i^e r_i$$

Plasma model

- Gas Energy Equation
  - Ions and Neutrals have temperature T_g
  - T_g assumed constant, or obtained by solving Gas Energy

$$\frac{\partial \sum_{k\in H} n_k h_k}{\partial t} + \vec{\nabla}\cdot\left(\sum_{k\in H}\vec{f}_k h_k - \sum_{k\in H}\kappa_k \vec{\nabla} T_g\right) = \eta_{\mathrm{Th}}\underbrace{\left(-e\sum_{k\in H}\vec{f}_k\cdot\vec{\nabla}\phi\right) + \frac{3}{2}k_B n_e \frac{2m_e}{m_{k_b}}(T_e - T_g)\bar{\nu}_{k,k_b} - e\sum_i \Delta E_i^g r_i}_{S_{T_g}}$$

  - If plasma model is solved with flow model, T_g is obtained from Navier-Stokes solver and only source terms are calculated by Gas Energy module

Flow model (Compressible Navier-Stokes)

$$\iiint_V \frac{\partial \mathbf{U}}{\partial t} dV + \iint_{\partial V} \vec{\mathbf{F}}_{\text{inviscid}} . \hat{n} dS = \iint_{\partial V} \vec{\mathbf{F}}_{\text{viscous}} . \hat{n} dS + \iiint_V \mathbf{S} dV$$

$$\mathbf{U} = \begin{bmatrix} \rho \\ \rho u \\ \rho v \\ \rho e_t \end{bmatrix} \qquad \mathbf{F}_{\text{inviscid}} = \begin{bmatrix} \rho u \\ \rho u^2 + p \\ \rho uv \\ (\rho e_t + p)u \end{bmatrix} \hat{i} + \begin{bmatrix} \rho v \\ \rho vu \\ \rho v^2 + p \\ (\rho e_t + p)v \end{bmatrix} \hat{j}$$

$$\mathbf{F}_{\text{viscous}} = \begin{bmatrix} 0 \\ \tau_{xx} \\ \tau_{xy} \\ u\tau_{xx} + v\tau_{xy} - \dot{q}_x \end{bmatrix} \hat{i} + \begin{bmatrix} 0 \\ \tau_{yx} \\ \tau_{yy} \\ u\tau_{yx} + v\tau_{yy} - \dot{q}_y \end{bmatrix} \hat{j} \qquad \mathbf{S} = \begin{bmatrix} 0 \\ f_x \\ f_y \\ S + \vec{f}_{ES} \cdot \vec{V} \end{bmatrix}$$

Photoionization (3-term Helmholtz equation model)

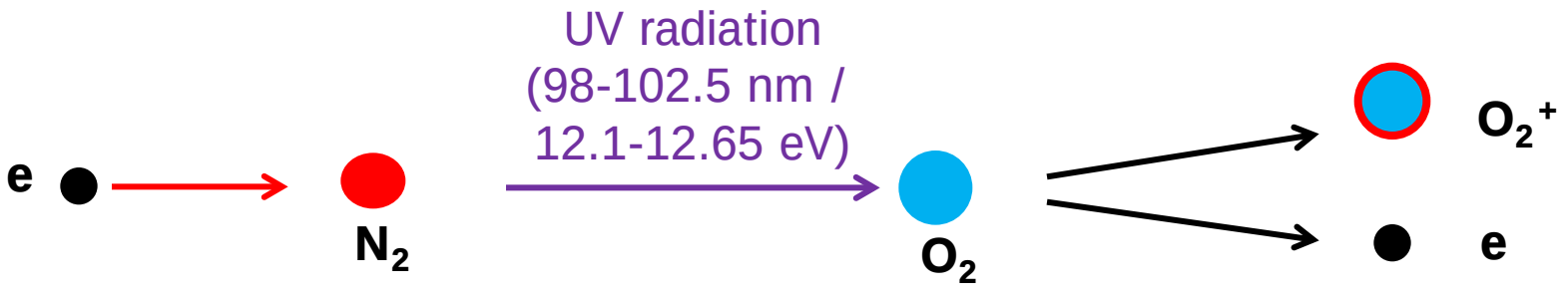

$e + N_2 \rightarrow e + N_2 + h\nu$

$O_2 + h\nu \rightarrow e + O_2^+$

IP: O_2=12.07 eV

Integral Model (Zheleznyak et al 1982):

$$S_{ph}(\vec{r}) = \iiint \frac{I(\vec{r}\prime)g(R)}{4\pi R^2} dV$$

Emission function:

$$I(\vec{r}) = \frac{P_q}{P + P_q} \xi S_i(\vec{r})$$

Absorption function:

$$\frac{g(R)}{P_{O2}} = \frac{exp^{-\chi_{min} P_{O2} R} - exp^{-\chi_{max} P_{O2} R}}{P_{O2}\, R\, ln(\chi_{max}/\chi_{min})}$$

3-term expansion approach :

$$\nabla^2 S_{ph}^j - (\lambda_j P_{O2})^2 S_{ph}^j = -A_j P_{O2}^2 I(\vec{r})$$

(j = 1,2,3)

$$S_{ph}(\vec{r}) = S_{ph}^1 + S_{ph}^2 + S_{ph}^3$$

	A_j (cm^{-1} Torr $^{-1}$)	λ_j (cm^{-1} Torr^{-1})
S_{ph}^1	0.0067	0.0447
S_{ph}^2	0.0346	0.1121
S_{ph}^3	0.3059	0.5994

* Luque A, Ebert U, Montijn C and Hundsdorfer W 2007 Appl. Phys. Lett. 90 08150
+ Bourdon A, Pasko NP, Liu NY, Celestin S, Segue P and Maroude E 2007 Plasma Sources Sci. Technol. 16 656

Mathematical approach to coupling plasma and flow physics

Electrostatic Force Term (No Magnetic field):

$$\vec{f}_{ES} = e\sum_k Z_k n_k \vec{E}$$

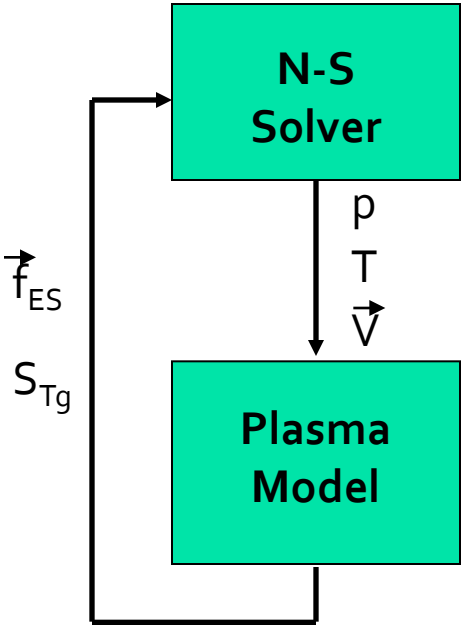

Gas Energy Source Term

$$S_{T_g} = \eta_{\mathrm{Th}}\left(-e\sum_{k\in H}\vec{f}_k \cdot \vec{\nabla}\phi\right) + \frac{3}{2}k_B n_e \frac{2m_e}{m_{k_b}}(T_e - T_g)\bar{\nu}_{k,k_b} - e\sum_i \Delta E_i^g r_i$$

Numerical approach

- 1D, 2D, 3D
- Fully unstructured, hybrid mesh
- Finite-volume spatial discretization, backward Euler time discretization (formally 1st order in space and time)
- Flow model:
  - AUSM family of spatial discretization
    (2nd order accuracy through gradient reconstruction)
  - 4th order RK time integration
- Domain decomposition parallel enabled

Plasma chemistry mechanism

- Methane-air plasma chemistry mechanism
  - Species and pathways relevant to plasma time scale (~10's ns)

  - 26 Species :

E, O, N_2 , O_2 , H , N_2^+ , O_2^+ , N_4^+ , O_4^+ , $O_2^+N_2$, O_2^- , O^- , O_2(a1) , O_2(b1) , O_2* , N_2(A) , N_2(B) , N_2C , N_2(a1), CH_4 , CH_3 , CH_2 , CH_4^+ , CH_3^+ , CH_2^- , H^-

  - 85 Reactions :

1) electron impact, 2) ion-ion, 3) ion-neutral, 4) neutral-neutral

Methane-air plasma mechanism

	Rxn	Reaction	A	B	C	Activation energy (eV)	Ref.
E+N_2	G_1	E + N_2 → E + N_2 (rotational)		BOLSIG+		0.02	(22)
	G_2	E + N_2 → E + N_2 (vibrational)		BOLSIG+		1.0	(22)
	G_3	E + N_2 → E + N_2(A)		BOLSIG+		6.17	(22)
	G_4	E + N_2 → E + N_2(B)		BOLSIG+		7.35	(22)
	G_5	E + N_2 → E + N_2(B)		BOLSIG+		7.36	(22)
	G_6	E + N_2 → E + N_2(B)		BOLSIG+		8.16	(22)
	G_7	E + N_2 → E + N_2(a1)		BOLSIG+		8.4	(22)
	G_8	E + N_2 → E + N_2(a1)		BOLSIG+		8.55	(22)
	G_9	E + N_2 → E + N_2(a1)		BOLSIG+		8.89	(22)
	G_{10}	E + N_2 → E + N_2(C)		BOLSIG+		11.03	(22)
	G_{11}	E + N_2 → E + N_2 (electronic)		BOLSIG+		11.88	(22)
	G_{12}	E + N_2 → E + N_2 (electronic)		BOLSIG+		12.25	(22)
	G_{13}	E + N_2 → E + N_2 (electronic)		BOLSIG+		13.0	(22)
	G_{14}	E + N_2 → 2E + N_2^+		BOLSIG+		15.6	(22)
	G_{15}	E + O_2 → E + O_2 (rotational)		BOLSIG+		0.02	(22)
E+O_2	G_{16}	E + O_2 → E + O_2		BOLSIG+		0.0193	(22)
	G_{17}	E + O_2 → E + O_2(a1)		BOSLIG+		0.98	(22)
	G_{18}	E + O_2 → E + O_2(b1)		BOLSIG+		1.63	(22)
	G_{19}	E + O_2 → E + O_2*		BOLSIG+		4.5	(22)
	G_{20}	E + O_2 → E + O_2 (electronic)		BOLSIG+		6.0	(22)
	G_{21}	E + O_2 → E + O_2 (electronic)		BOLSIG+		8.4	(22)
	G_{22}	E + O_2 → E + O_2 (electronic)		BOLSIG+		9.97	(22)
	G_{23}	E + O_2 → E + 2O		BOLSIG+		5.58	(22)
	G_{24}	E + O_2 → E + 2O (O + O(^{1}D))		BOLSIG+		8.4	(22)
	G_{25}	E + O_2 → 2E + O_2^+		BOLSIG+		12.07	(22)
excitation →	G_{26}	E + O → E + O		BOLSIG+		6.34	(22)
E+CH_4	G_{27}	E + CH_4 → E + CH_4 (vibrational)		BOLSIG+		0.36	(23)
	G_{28}	E + CH_4 → E + CH_4		BOLSIG+		0.162	(23)
	G_{29}	E + CH_4 → 2E + CH_4^+		BOLSIG+		12.6	(23)
	G_{30}	E + CH_4 → 2E + CH_3^+ + H		BOLSIG+		14.3	(23)
	G_{31}	E + CH_4 → E + CH_3 + H		BOLSIG+		9.0	(23)
	G_{32}	E + CH_4 → E + CH_3 + H		BOLSIG+		10.0	(23)
	G_{33}	E + CH_4 → E + CH_3 + H		BOLSIG+		11.0	(23)
	G_{34}	E + CH_4 → E + CH_3 + H		BOLSIG+		12.0	(23)
dissociative recomb.	G_{35}	E+ O_2^+ → O + O		BOLSIG+		-0.691	(22)
	G_{36}	E + O_4^+ → O_2 + O_2		BOLSIG+		-12.07	(22)
attachment	G_{37}	E + O_2 → O^- + O		BOLSIG+		4.66	(22)
	G_{38}	E + CH_4 → H^- + CH_3		BOLSIG+		9.0	(22)
excitation →	G_{39}	E + CH_4 → CH_2^- + CH_2		BOLSIG+		10.8	(22)
dissociation →	G_{40}	E + O_2(a1) → E + O_2(b1)		BOLSIG+		0.65	(22)
attachment	G_{41}	E + O_2(a1) → E + 2O		BOLSIG+		6.34	(22)
	G_{42}	E + O_2(a1) → O- + O		BOLSIG+		3.9	(22)
	G_{43}	E + O_2(b1) → O- + O		BOLSIG+		3.7	(22)

Methane-air plasma mechanism

cluster ion formation

charge exchange

attachment

ion-ion recomb.

Neutral reactions

dissociative charge ex.

charge exchange

dissociative recomb.

Rxn	Reaction	A	B	C	Activation energy (eV)	Ref.
G_{44}	$N_2^+ + N_2 + M \rightarrow N_4^+ + M$	5.0e-41	0	0	1.0	(24)
G_{45}	$N_4^+ + O_2 \rightarrow O_2^+ + 2N_2$	2.5e-16	0	0	-3.51	(24)
G_{46}	$N_2^+ + O_2 \rightarrow O_2^+ + N_2$	1.04e-15	-0.5	0	-3.51	(24)
G_{47}	$O_2^+ + 2N_2 \rightarrow O_2{+}N_2 + N_2$	8.1e-38	-2.0	0	-	(24)
G_{48}	$O_2{+}N_2 + N_2 \rightarrow O_2^+ + 2N_2$	14.8	-5.3	2357	-	(24)
G_{49}	$O_2{+}N_2 + O_2 \rightarrow O_4^+ + N_2$	1.0e-15	0	0	-	(24)
G_{50}	$O_2^+ + O_2 + M \rightarrow O_4^+ + M$	2.03e-34	-3.2	0	-	(24)
G_{51}	$E + 2O_2 \rightarrow O_2^- + O_2$	6.0e-39	-1.0	0	-0.43	(24)
G_{52}	$O_2^- + O_4^+ \rightarrow 3O_2$	1.0e-13	0	0	-11.64	(24)
G_{53}	$O_2^- + O_4^+ + M \rightarrow 3O_2 + M$	3.12e-31	-2.5	0	-11.64	(24)
G_{54}	$O_2^- + O_2^+ + M \rightarrow 2O_2 + M$	3.12e-31	-2.5	0	-11.64	(24)
G_{55}	$O^- + O_2^+ \rightarrow O + O_2$	3.464e-12	-0.5	0	-10.61	(24)
G_{56}	$N_2A + O_2 \rightarrow N_2 + 2O$	1.7e-18	0	0	-1.05	(25)
G_{57}	$N_2A + O_2 \rightarrow N_2 + O_2(b1)$	7.5e-19	0	0	-4.54	(25)
G_{58}	$N_2A + N_2(A) \rightarrow N_2 + N_2(B)$	7.7e-17	0	0	-4.99	(25)
G_{59}	$N_2A + N_2(A) \rightarrow N_2 + N_2(C)$	1.6e-16	0	0	-1.31	(25)
G_{60}	$N_2(A) + N_2 \rightarrow N_2 + N_2(B)$	1.0e-16	0	1500	-0.32	(25)
G_{61}	$N_2(A) + O \rightarrow N_2 + O$	3.0e-17	0	0	-6.17	(25)
G_{62}	$N_2(B) + O_2 \rightarrow N_2 + 2O$	3.0e-16	0	0	-2.23	(25)
G_{63}	$N_2(B) + N_2 \rightarrow N_2(A) + N_2$	1.0e-17	0	0	-1.18	(25)
G_{64}	$N_2(a1) + O_2 \rightarrow N_2 + 2O$	2.8e-17	0	0	-3.28	(25)
G_{65}	$N_2(a1) + N_2 \rightarrow N_2 + N_2$	2.0e-19	0	0	-8.4	(25)
G_{66}	$N_2(C) + O_2 \rightarrow N_2 + 2O$	3.0e-16	0	0	-5.91	(25)
G_{67}	$N_2(C) + N_2 \rightarrow N_2(a1) + N_2$	1.0e-17	0	0	-2.63	(25)
G_{68}	$N_2(C) \rightarrow N_2(B) + hv$ (photon)	3.0	0	0	-	(25)
G_{69}	$N_2(A) + CH_4 \rightarrow N_2 + CH_4$	3.0e-21	0	0	-6.17	(25)
G_{70}	$N_2(B) + CH_4 \rightarrow N_2(A) + CH_4$	2.85e-16	0	0	-1.08	(25)
G_{71}	$N_2(B) + CH_4 \rightarrow N_2 + CH_3 + H$	1.5e-17	0	0	3.15	(25)
G_{72}	$N_2(a1) + CH_4 \rightarrow N_2 + CH_3 + H$	3.0e-16	0	0	2.1	(25)
G_{73}	$N_2(C) + CH_4 \rightarrow N_2 + CH_3 + H$	3.0e-16	0	0	-0.8	(25)
G_{74}	$O_2^* + CH_4 \rightarrow O_2 + CH_3 + H$	3.0e-21	0	0	-	(25)
G_{75}	$O_2^* + O_2 \rightarrow O_2(a1) + O_2$	1.86e-19	0	0	-3.52	(25)
G_{76}	$O_2^* + O_2 \rightarrow O_2(b1) + O_2$	8.1e-20	0	0	-2.87	(25)
G_{77}	$O_2^* + O_2 \rightarrow O_2 + O_2$	2.3e-20	0	0	-4.5	(25)
G_{78}	$O_2^* + O \rightarrow O_2 + O$	5.0e-18	0	0	-4.5	(25)
G_{79}	$O_2^* + O \rightarrow O_2(a1) + O$	2.7e-18	0	0	-3.52	(25)
G_{80}	$O_2^* + O \rightarrow O_2(b1) + O$	1.35e-18	0	0	-2.87	(25)
G_{81}	$N_2^+ + CH_4 \rightarrow N_2 + CH_3^+ + H$	1.3e-15	0	0	-	(25)
G_{82}	$CH_4^+ + O_2 \rightarrow CH_4 + O_2^+$	5.0e-16	0	0	-	(25)
G_{83}	$E + CH_4^+ \rightarrow CH_3 + H$	2.95e-12	-0.5	0	-	(25)
G_{84}	$E + CH_4^+ \rightarrow CH_2 + 2H$	2.95e-12	-0.5	0	-	(25)
G_{85}	$E + CH_3^+ \rightarrow CH_2 + H$	6.06e-12	-0.5	0	-	(25)

Electron impact reaction rate coefficient computed using off-line Boltzmann solver

- Bolsig+ (Hagelaar and Pitchford, 2005)

$k = k(E/N)$, $T_e = T_e(E/N)$ } $k = k(T_e)$

(Recovers non-local aspects of electron energy transport)

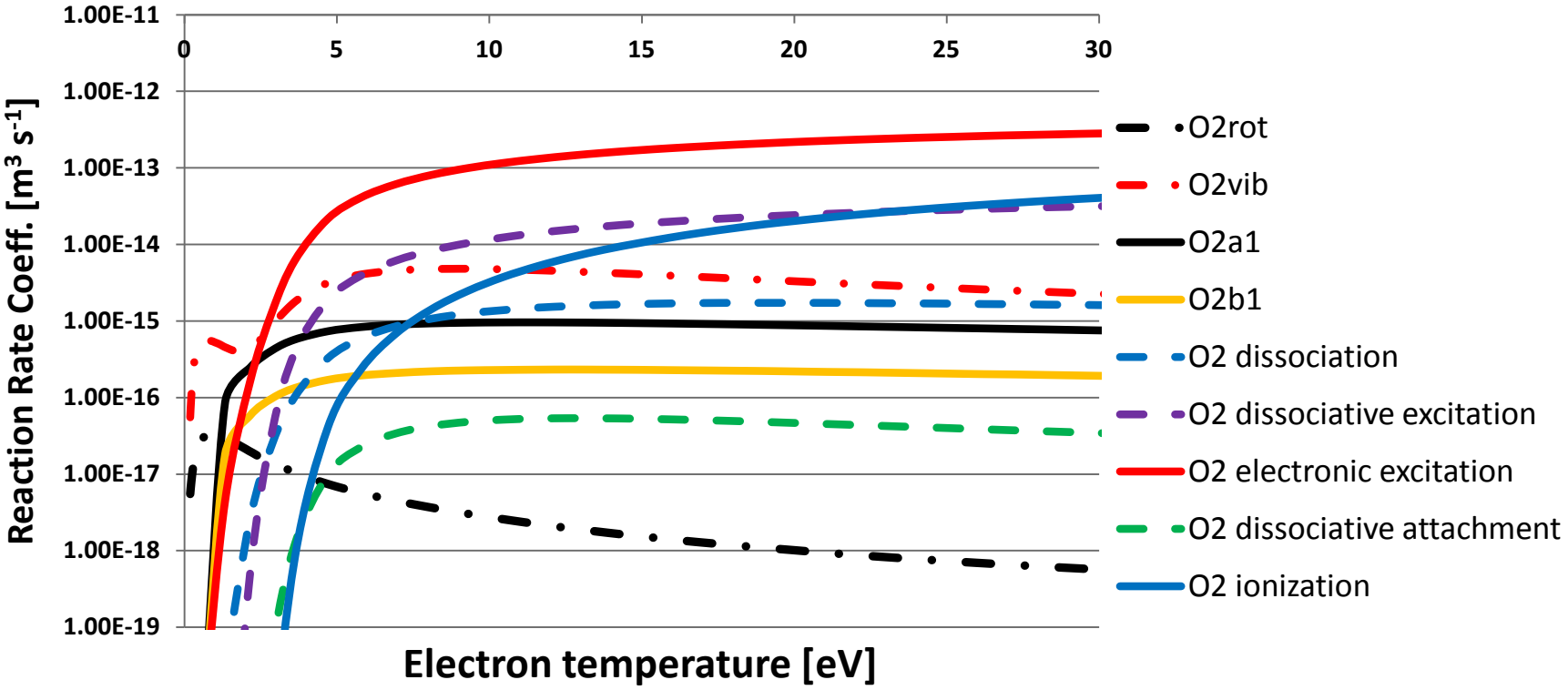

Ref: Hagelaar GJM, and LM Pitchford, Plasma Sources Sci. Technol., Vol. 14, 2005, pp. 722.

Coaxial electrode Nanosecond Pulsed Plasma (NSP)

Reference:
D. Breden, L. L. Raja, C. A. Idicheria, P. M. Najt, and S. Mahadevan, “A numerical study of high-pressure non-equilibrium streamers for combustion ignition application,” *Journal of Applied Physics*, Vol. 114, 2013, pp. 083302-1-14.

Coaxial electrode NSP discharge

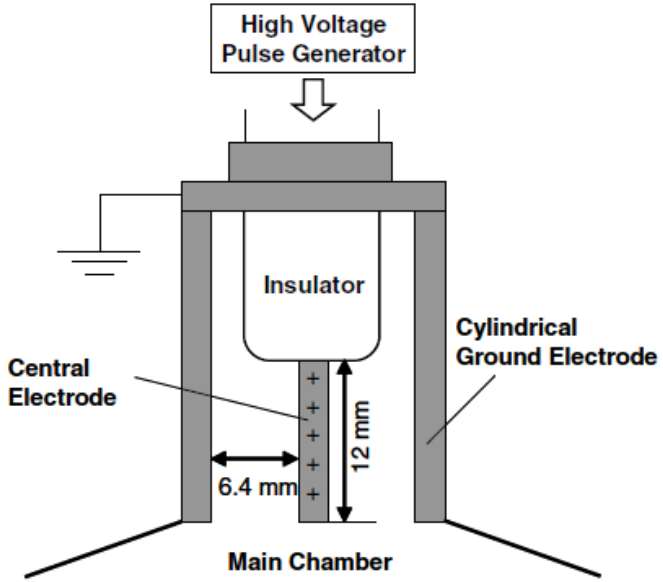

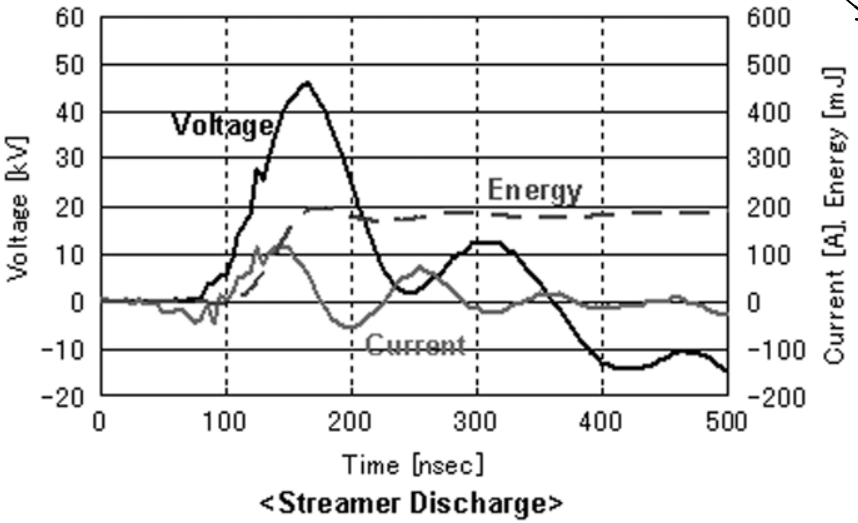

<Streamer Discharge>

Ref: Shiraishi et al. J Phys. D: Appl. Phys., 42, (2009) 135208.

- Describe initial plasma kernel formation stage
  - ~ 10's ns of physical time
- Experimental observations
  - Unbranched streamers propagate from inner high-voltage electrode to outer ground electrode
  - Streamer dia (sub-mm)
  - Brighter discharge near inner electrode
  - Flame spreads from inner electrode to outer ground electrode

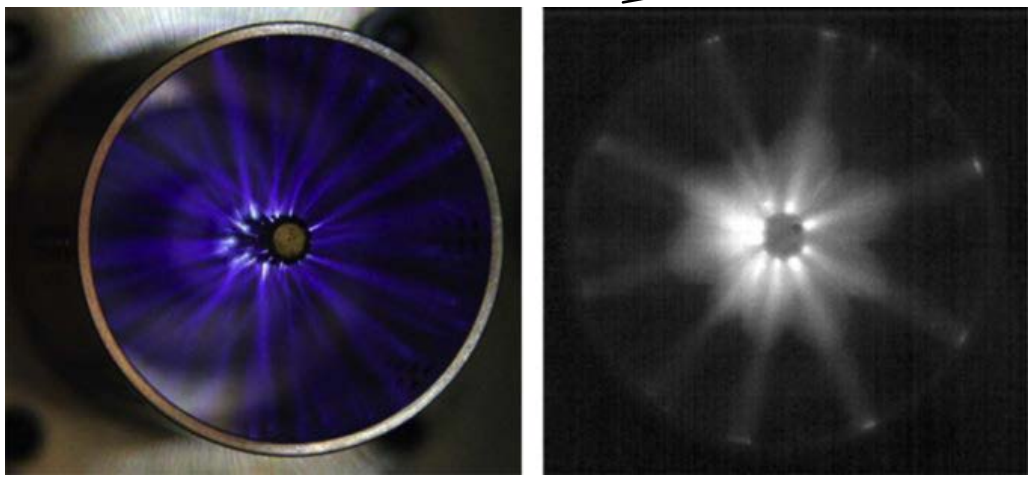

Ref: D. Singleton, S.J. Pendleton and M. Gundersen, J. Phys. D: Appl. Phys., 2011, Vol. 44, 022001.

Coaxial electrode NSP discharge simulation conditions

- Simulation conditions:
  - 10 atmospheres
  - 700 K fixed gas temperature
  - 40 kV applied voltage (E/n ~ 143 Td)
  - lean A/F ratio (40:1 air/methane)

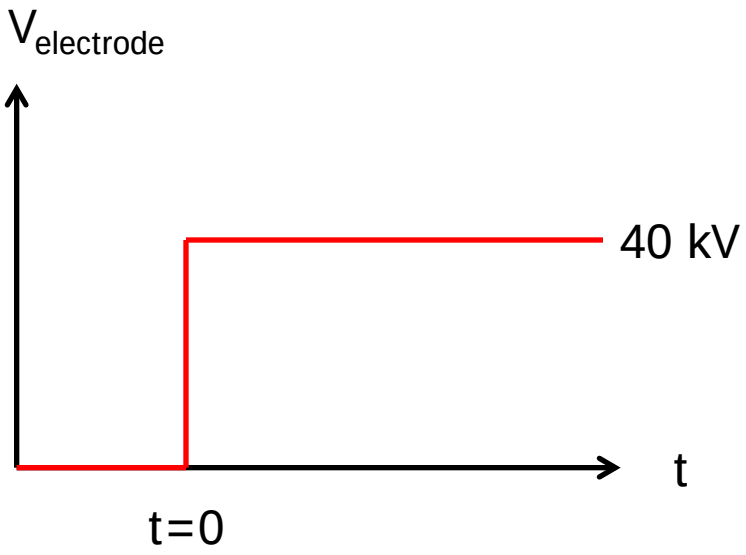

Coaxial electrode NSP plasma simulation domain

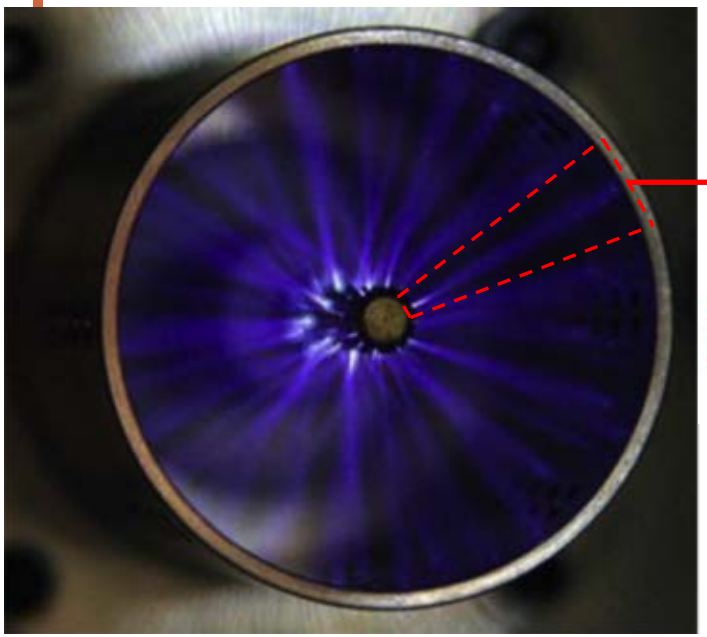

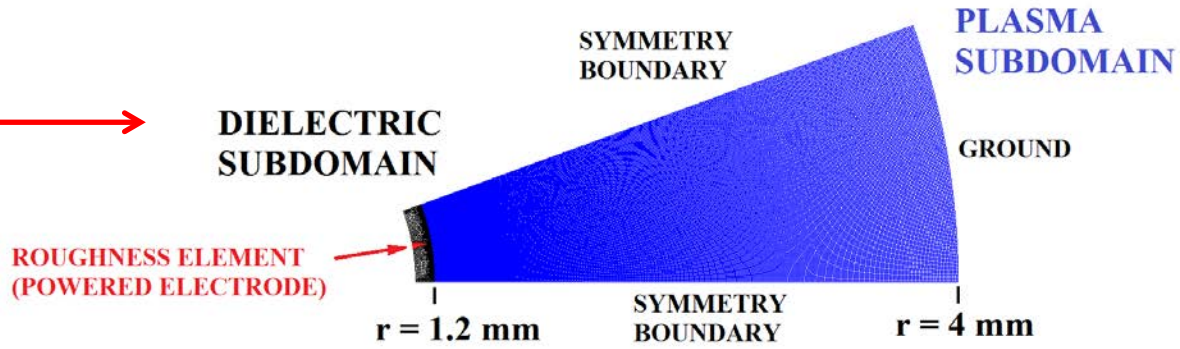

60,000 cells

- Simulation domain : sector of circle
  - 20 deg. sector angle
  - Characteristic size for single streamer propagation
  - Roughness element on inner electrode to pin location of streamer

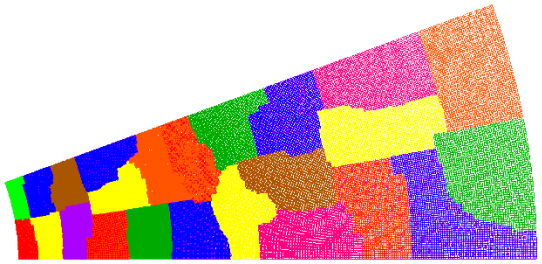

24 processor partition

Sensitivity to roughness element configuration

Conditions: P=10 atm, T_{gas}=700 K, 40 kV, 40:1 A/F ratio (lean)

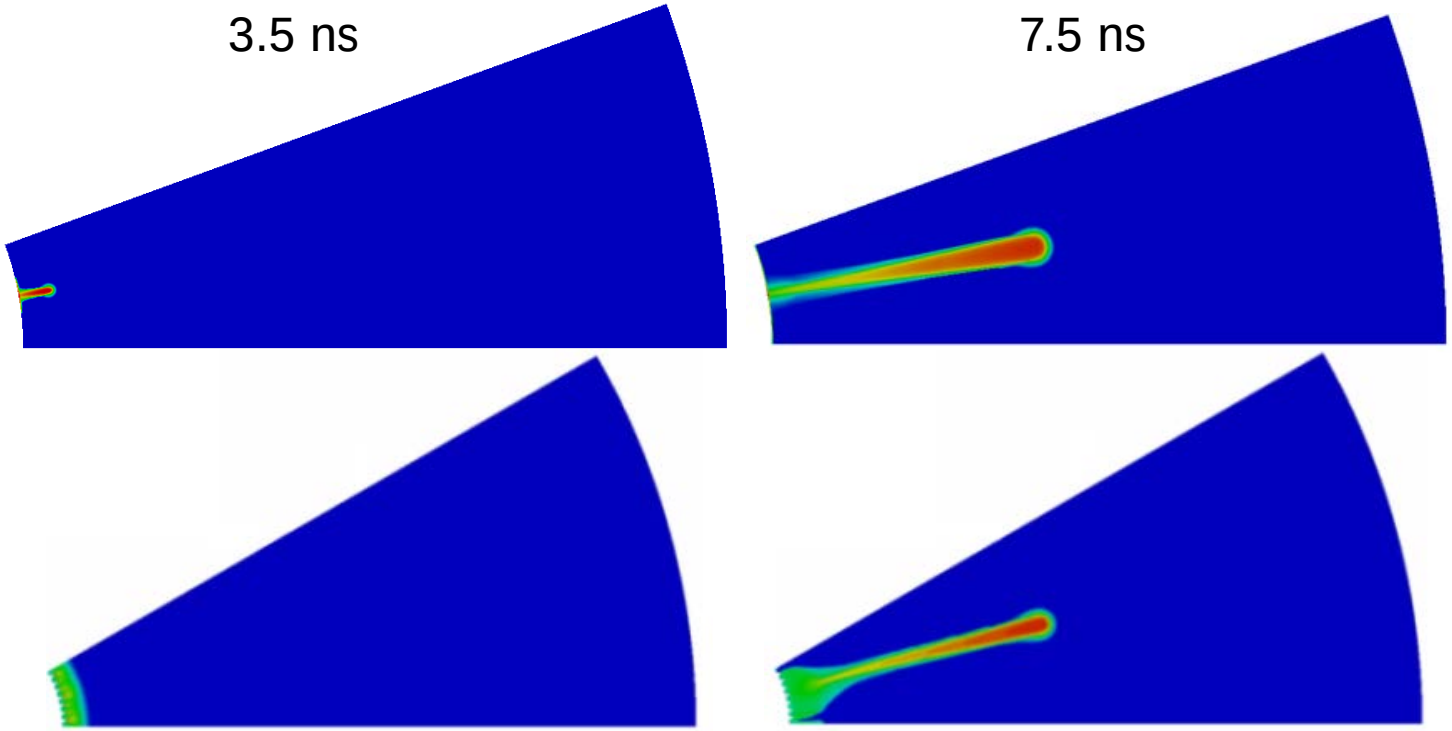

- Verified insensitivity to roughness element configuration
- Verified characteristic sector angle for single streamer

Time evolution of electron density and temperature for coaxial electrode NSP

Conditions: P=10 atm, T_{gas}=700 K, 40 kV, 40:1 A/F ratio (lean)

Electron density transient

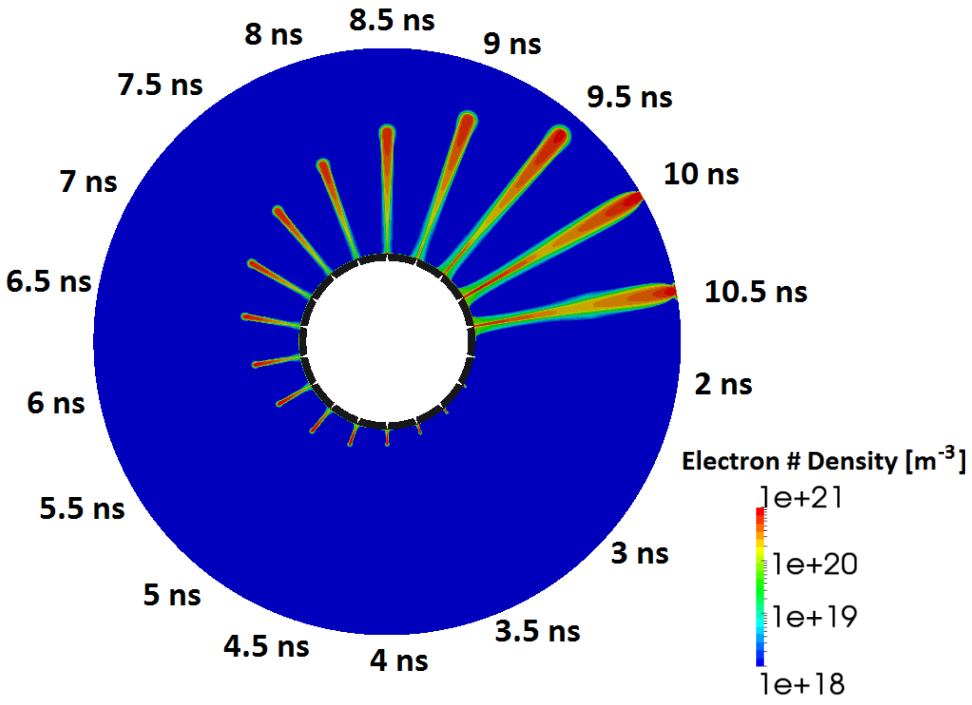

Electron temperature transient

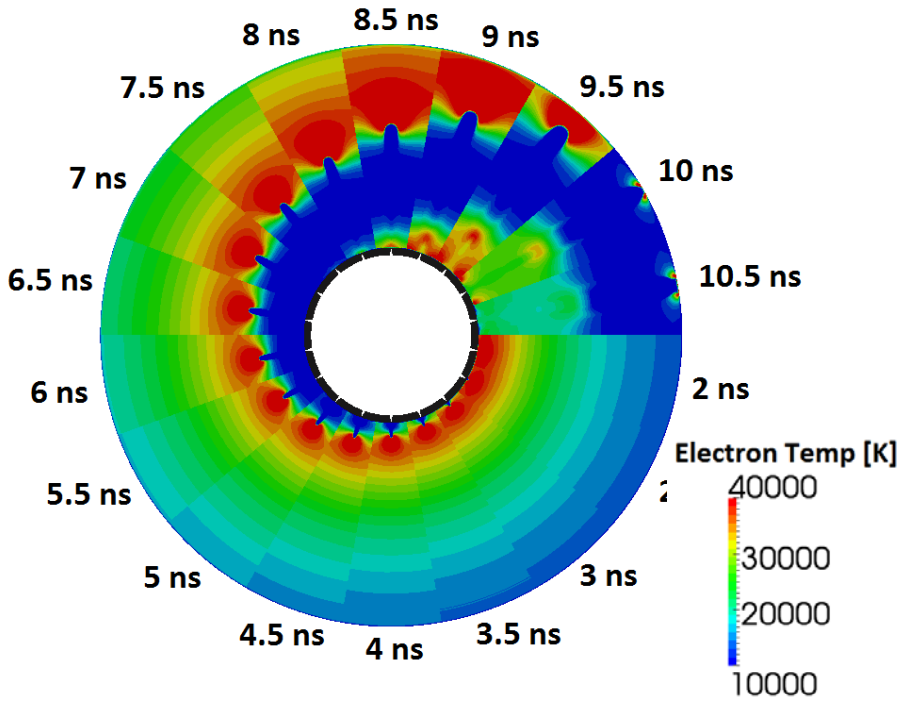

- 2 ns induction time (defined: time to reach threshold of 10^{19} m^{-3})
- Streamers bridge electrode gap in about 10 ns
- N_e(peak)~ 10^{21} m^{-3} , T_e(head) ~4eV, T_e(body) ~1eV
- Secondary streamer (electron attachment luminosity? Self-sustaining?)

Reduced electric field profiles along axis of coaxial electrode NSP

Conditions: P=10 atm, T_{gas}=700 K, 40 kV, 40:1 A/F ratio (lean)

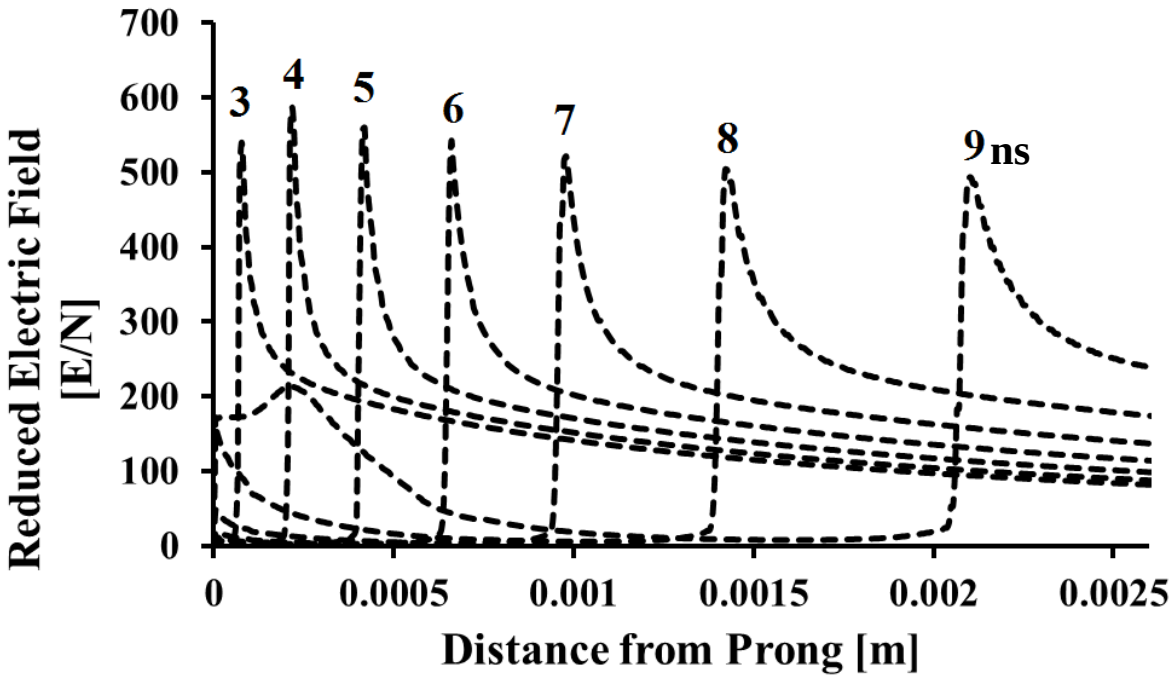

- Recall breakdown E/n about 120 Td (for air)
- Head of streamer has significant over-voltages (~ 500 Td) → high T_e
- Body of streamer has no sustaining E-field (E/n ~ 10 Td) → low T_e
- Secondary streamer formation at end of pulse with E/n ~ 200 Td

Species yields for coaxial electrode NSP (volume-averaged at 9.5 ns)

Conditions: P=10 atm, T_{gas}=700 K, 40 kV, 40:1 A/F ratio (lean)

Positive ions

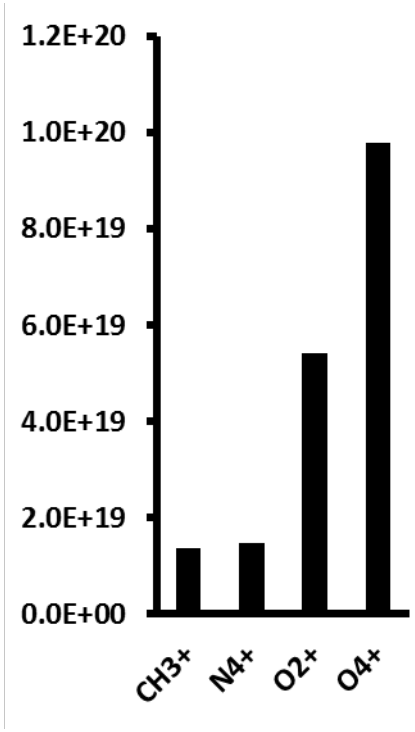

Negative species

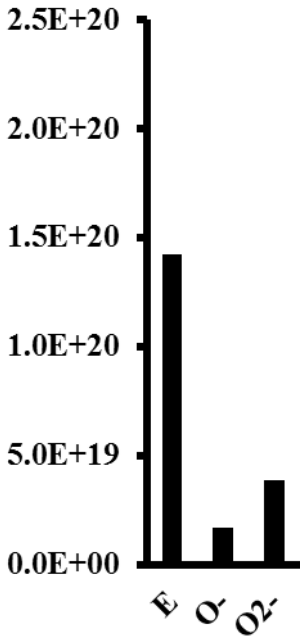

Radicals

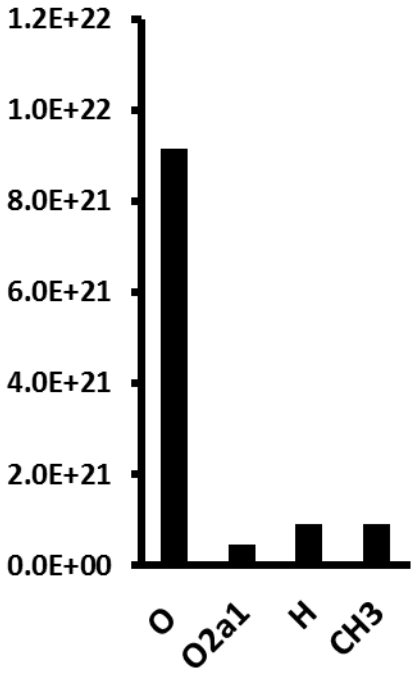

- Charged species (~10^{20} m^{-3})
- Dominant radical O (~10^{22} m^{-3})

Time evolution of radical densities and for coaxial electrode NSP

Conditions: P=10 atm, T_{gas}=700 K, 40 kV, 40:1 A/F ratio (lean)

O radical density transient

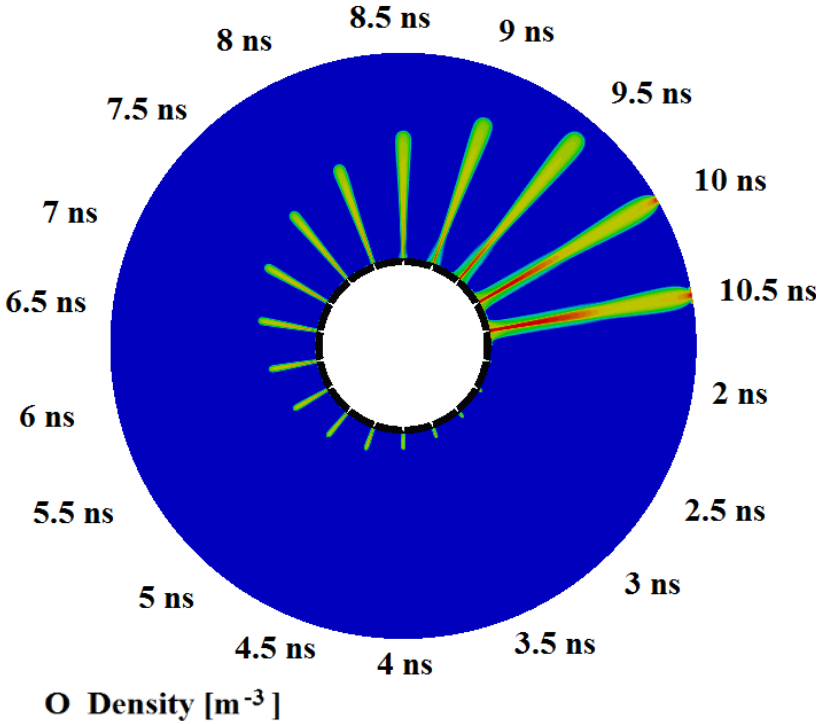

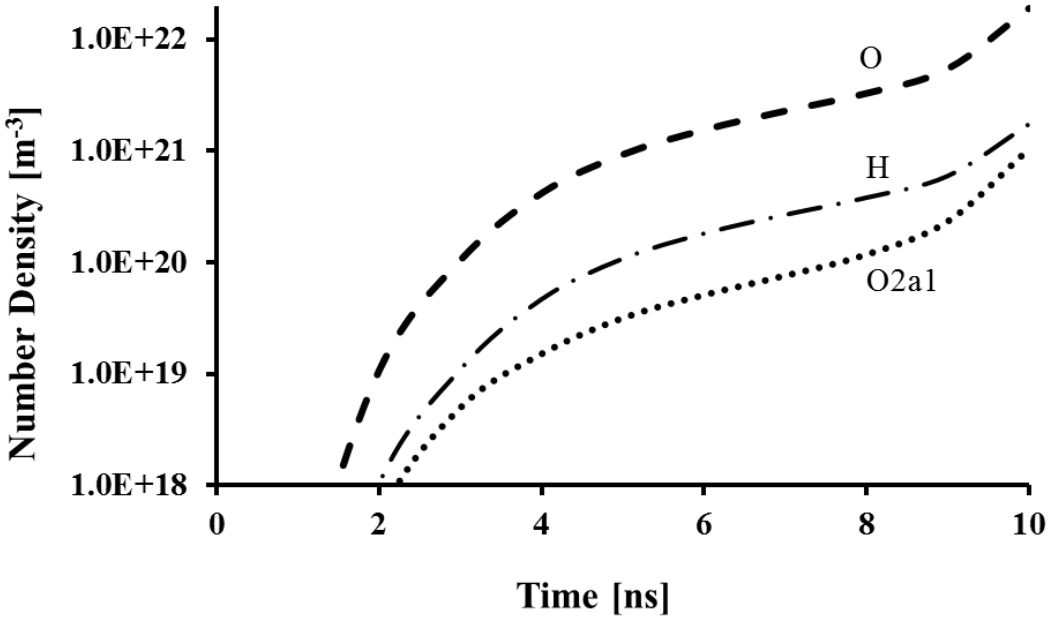

- Secondary streamer has significant impact on overall radical yield

O radical distribution in coaxial electrode NSP at end of transient

- Significant non-uniformity in O radical distribution
  - ~10^{23} m^{-3} at inner electrode
  - Consequence of secondary streamer

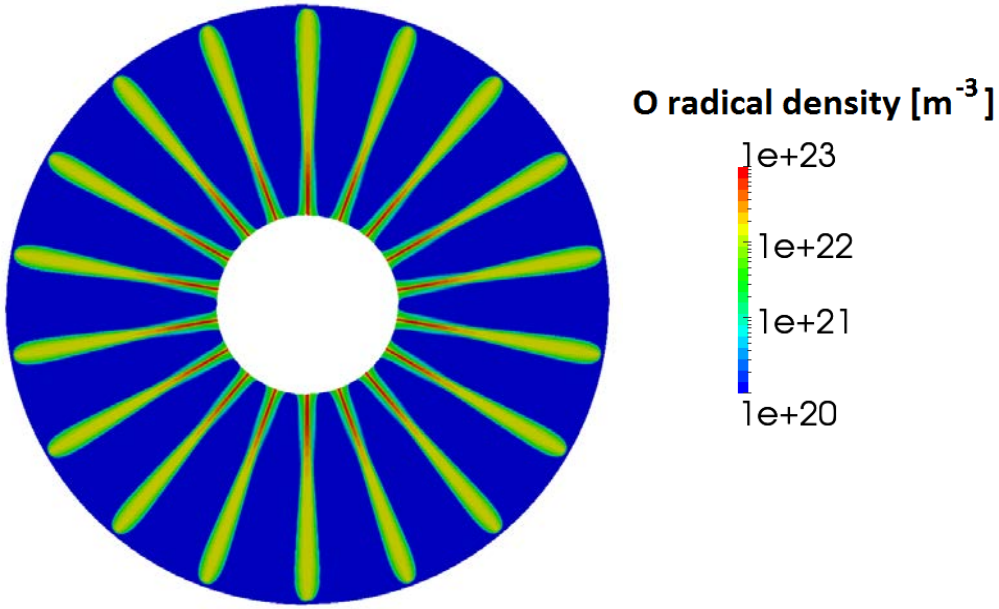

- O radical concentration is evidence for experimentally observed flame spread profile ?

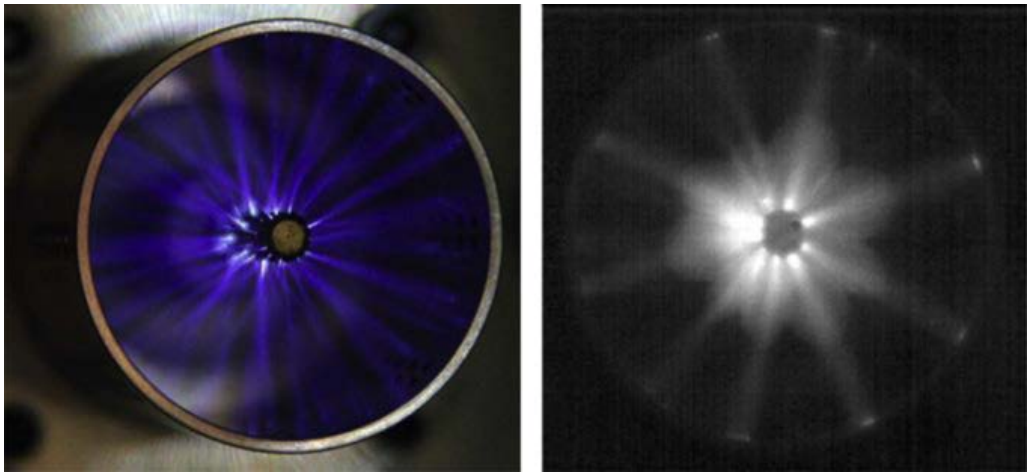

Corona ignition – point to plane at infinity

Reference:
D. Breden, L. L. Raja, C. A. Idicheria, P. M. Najt, and S. Mahadevan, “A numerical study of high-pressure non-equilibrium streamers for combustion ignition application,” *Journal of Applied Physics*, Vol. 114, 2013, pp. 083302-1-14.

Corona igniter

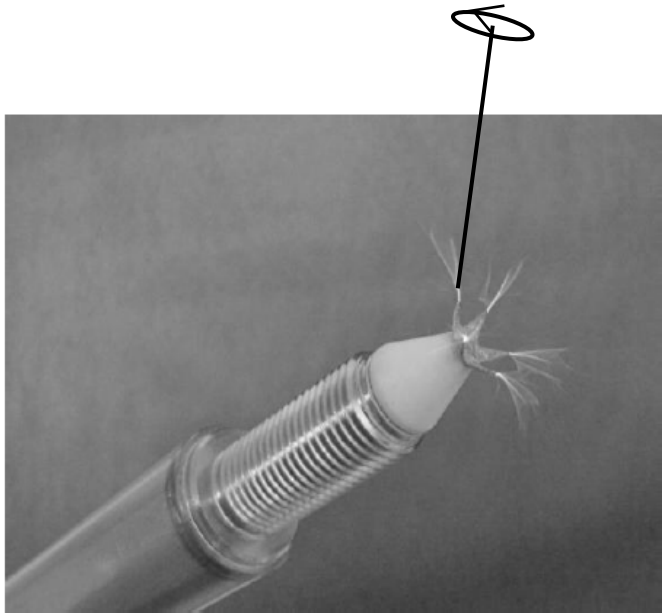

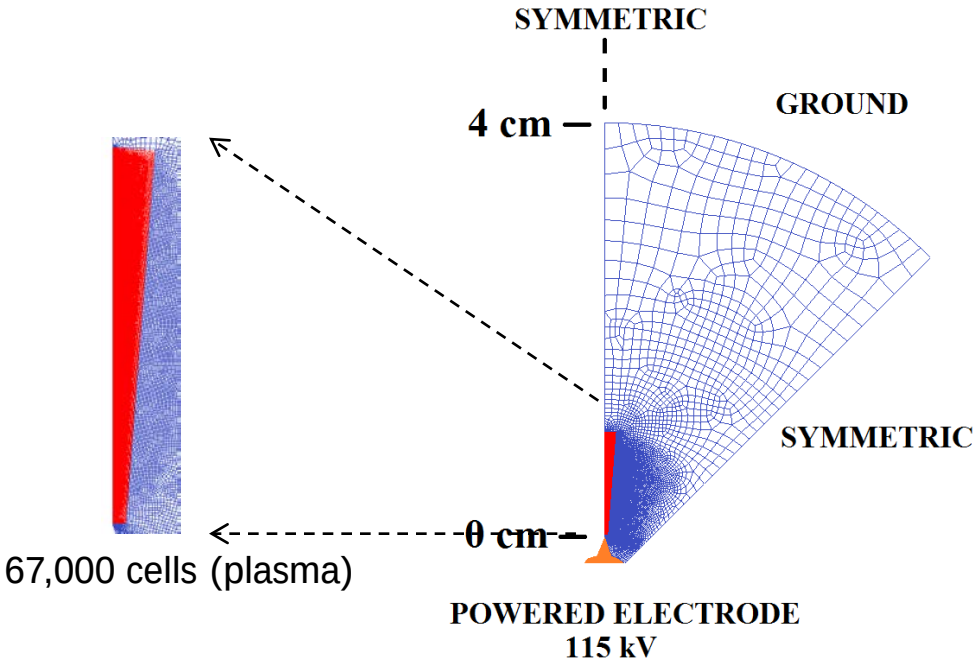

- Simulation conditions:
  - 10 atmospheres
  - 700 K fixed gas temperature
  - 115 kV applied voltage
  - lean A/F ratio (40:1 air/methane)

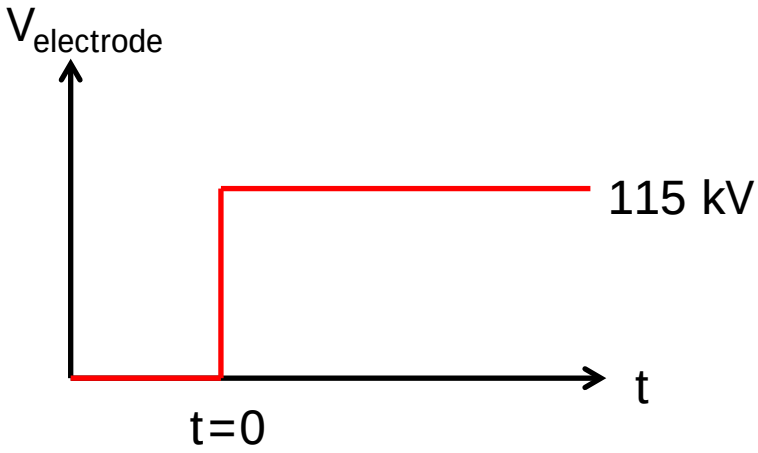

Transient evolution of electron density

Conditions: P=10 atm, T_{gas}=700 K, 115 kV, 40:1 A/F ratio (lean)

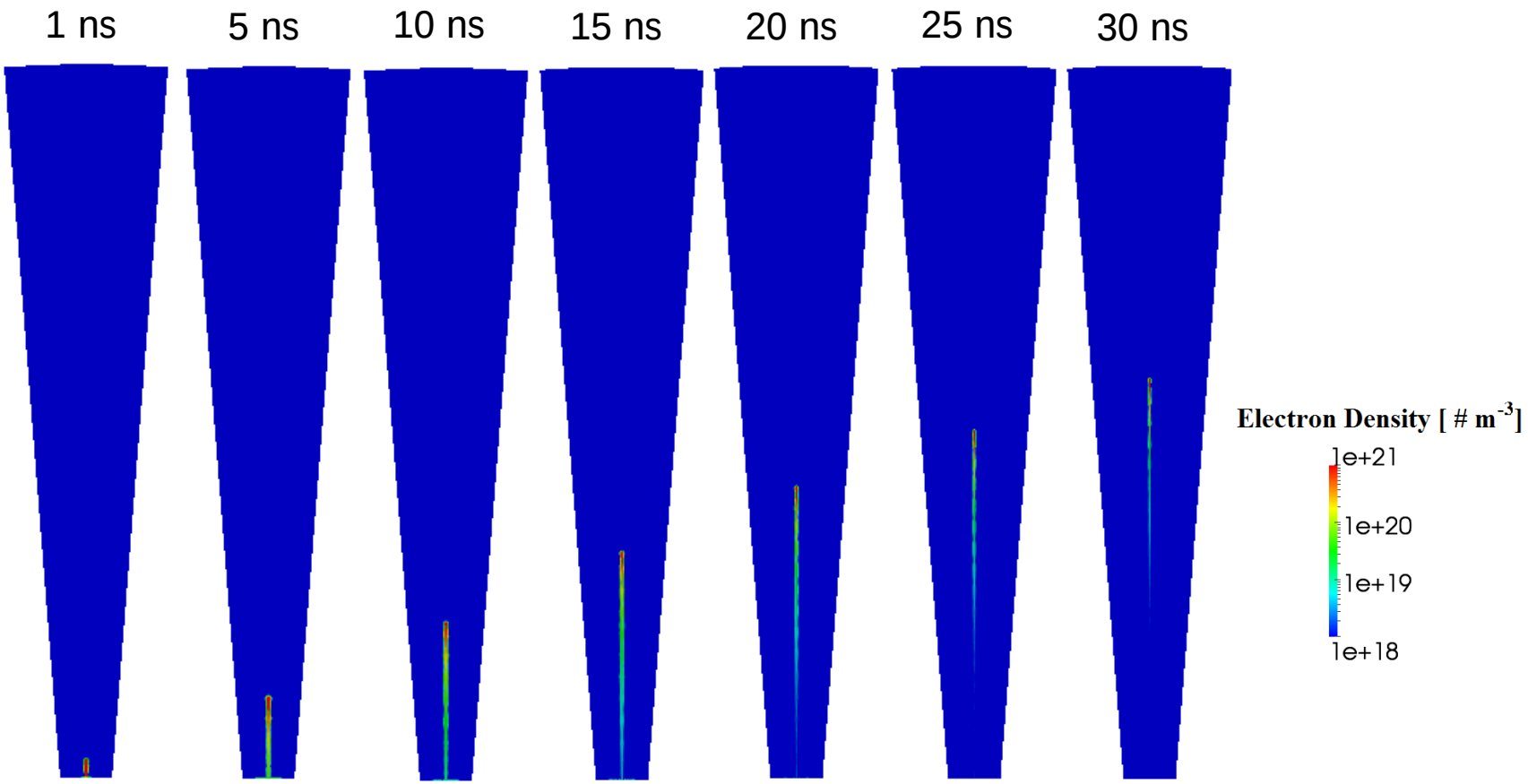

- Peak electron densities in streamer head (~10^{21} m^{-3})
- Electron attachment in body

Reduced electric field profiles along axis of coaxial electrode NSP

Conditions: P=10 atm, T_{gas}=700 K, 115 kV, 40:1 A/F ratio (lean)

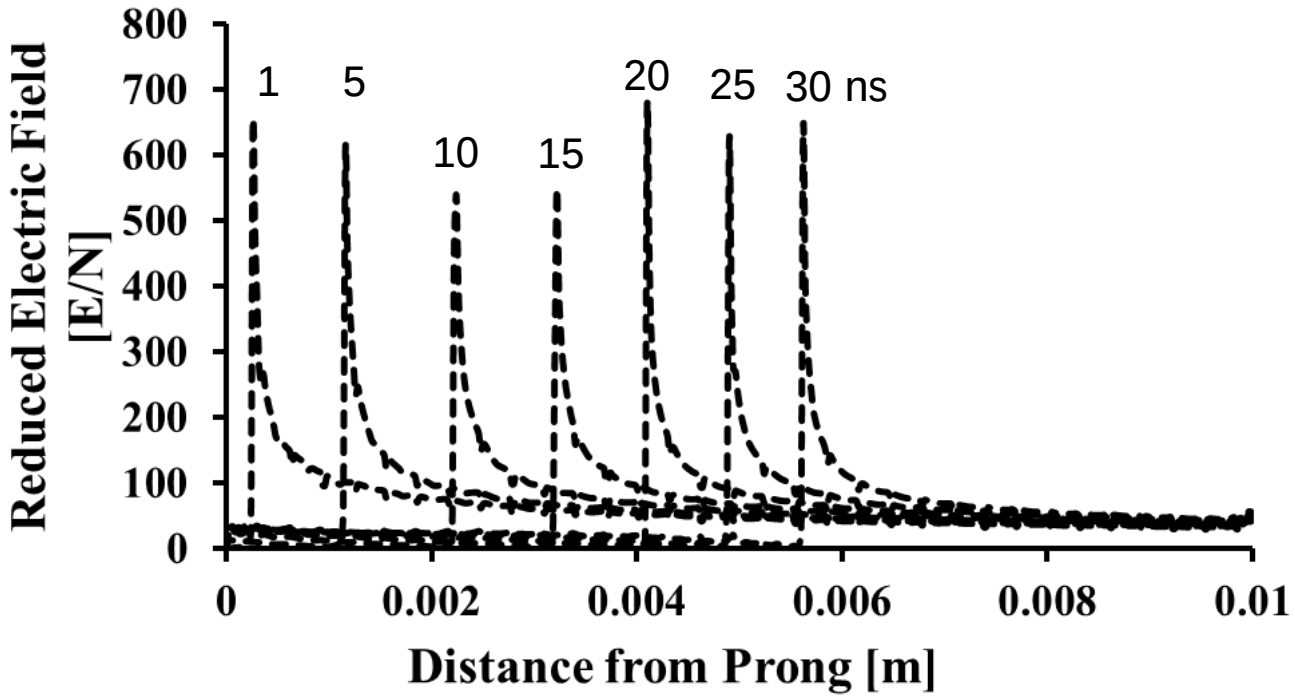

- Recall breakdown E/n about 120 Td (for air)
- Head of streamer has significant over-voltages (~ 500 Td) → high T_e
- Body of streamer has no sustaining E-field (E/n ~ 10 Td) → low T_e
- No secondary streamer formation

Species yields for single electrode geometry (volume-averaged at 30 ns)

Conditions: P=10 atm, T_{gas}=700 K, 115 kV, 40:1 A/F ratio (lean)

Positive ions

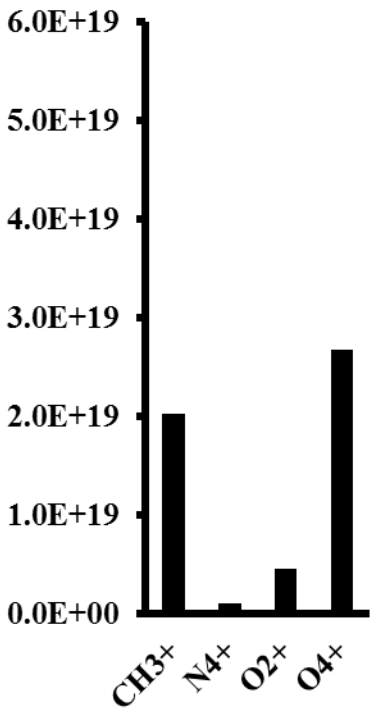

Negative species

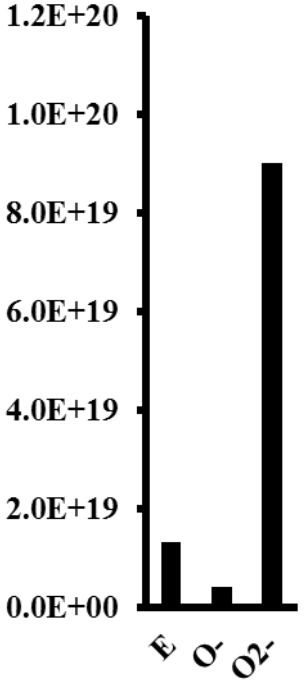

Radicals

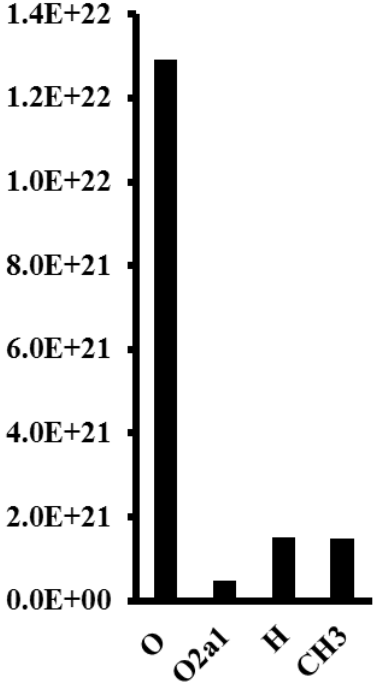

- Charged species (~10^{20} m^{-3})
- Dominant radical O (~10^{22} m^{-3})

Comparison of species yields for Corona and Coaxial electrode geometries

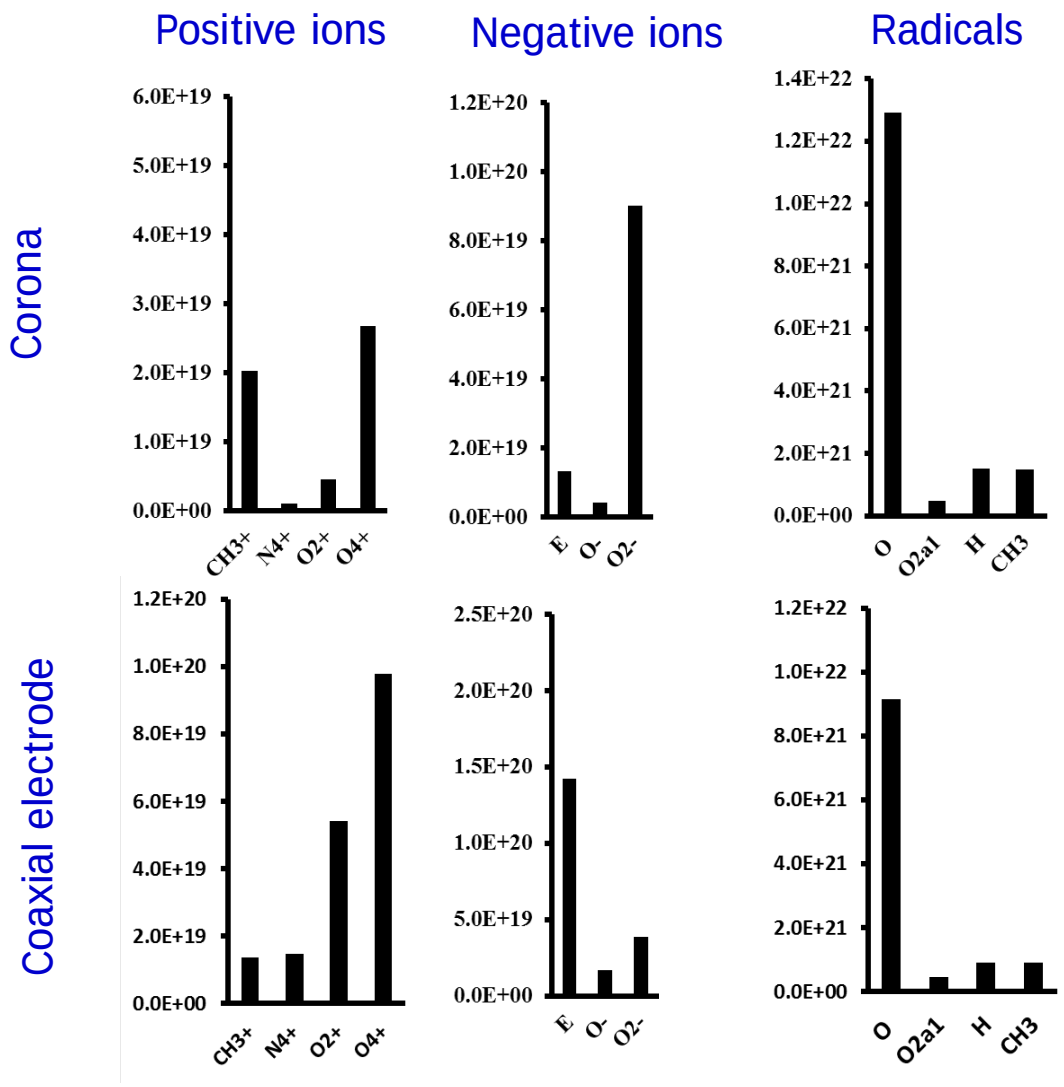

Time evolution of radical densities and for coaxial electrode NSP

Baseline Conditions: P=10 atm, T_{gas}=700 K, 40 kV, 40:1 A/F ratio (lean)

O radical density at 30 ns

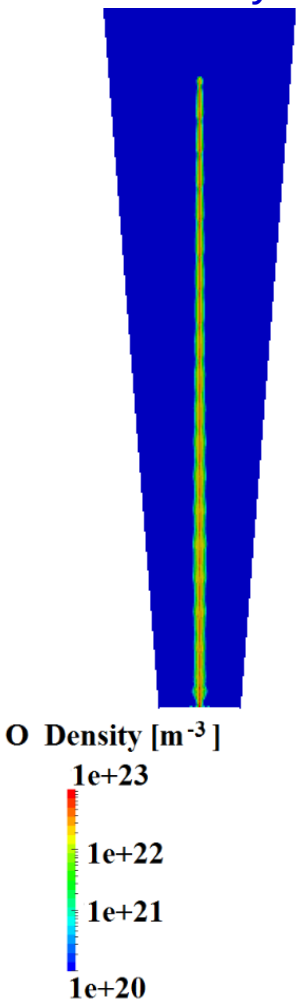

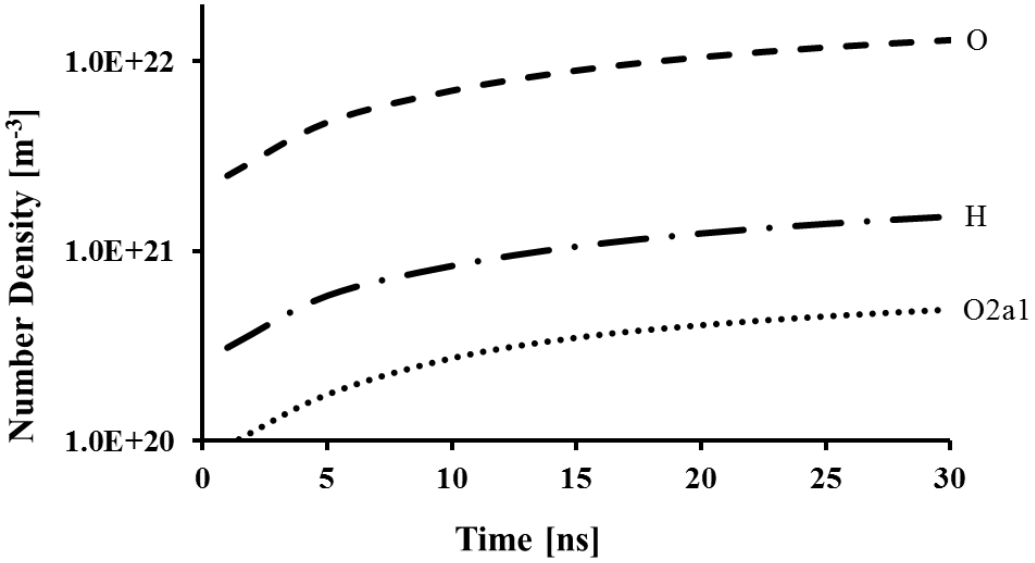

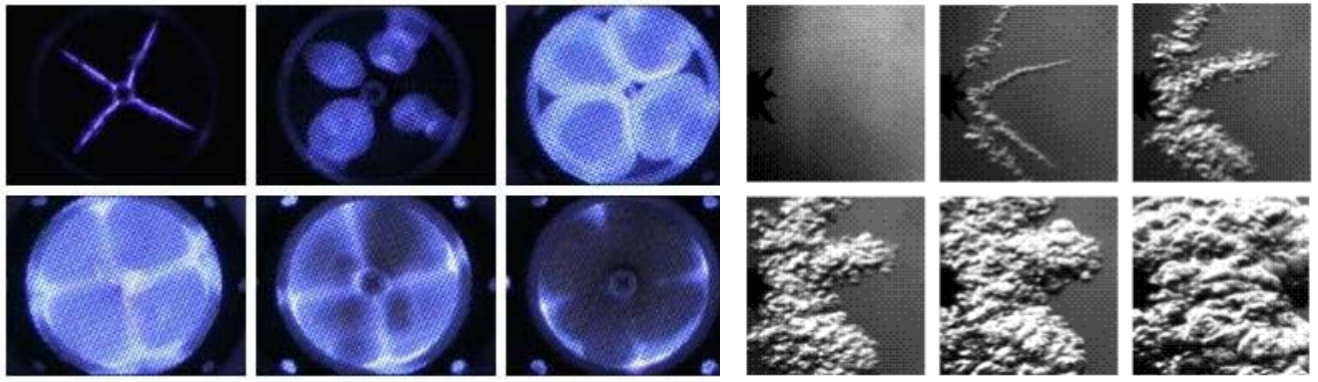

Corona RF excitation

Problem statement for Corona RF excited plasma igniter

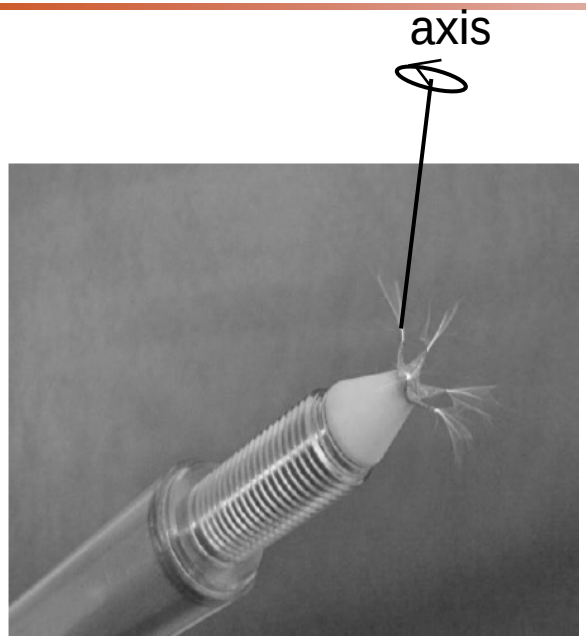

RF excitation :
Freq. ~10 MHz
Voltage ~100kV

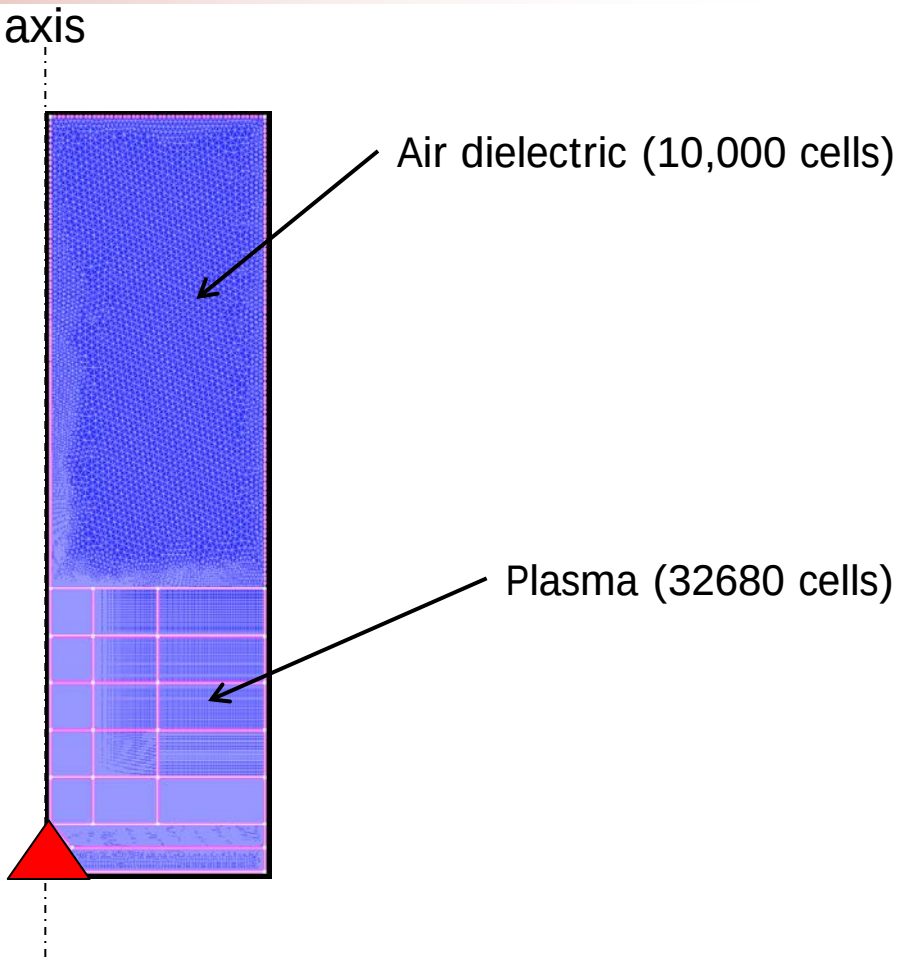

Conditions: P=10 atm, T_{gas}=700 K, 40:1 A/F ratio (lean),
+90kV → -80kV → +80kV pulse train (10 ns each)

Simulation strategy for multi-pulse excitation

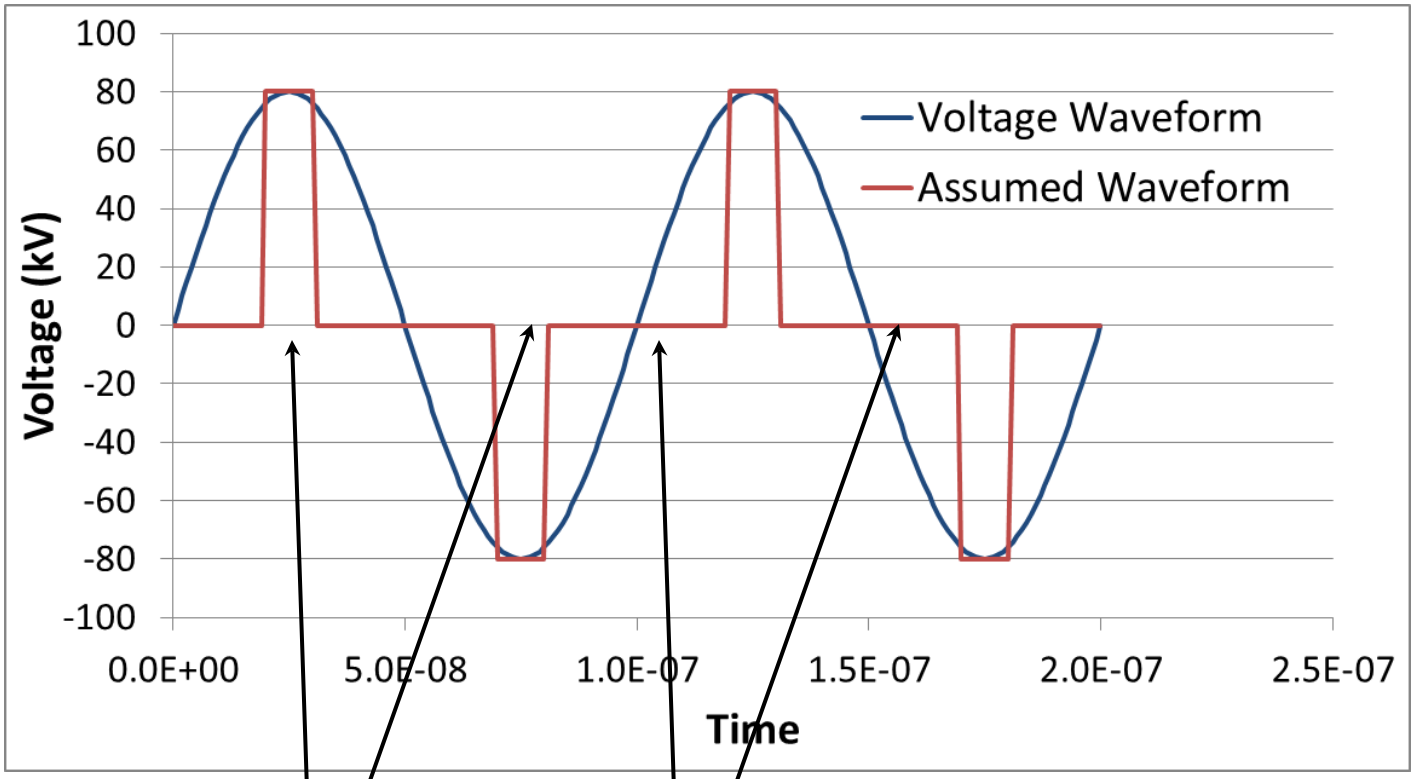

Actual and Assumed Waveforms for a 10 MHz pulse
(check attached spreadsheet)

Discharge structure dependence on excitation polarity

Positive pulse | Negative pulse

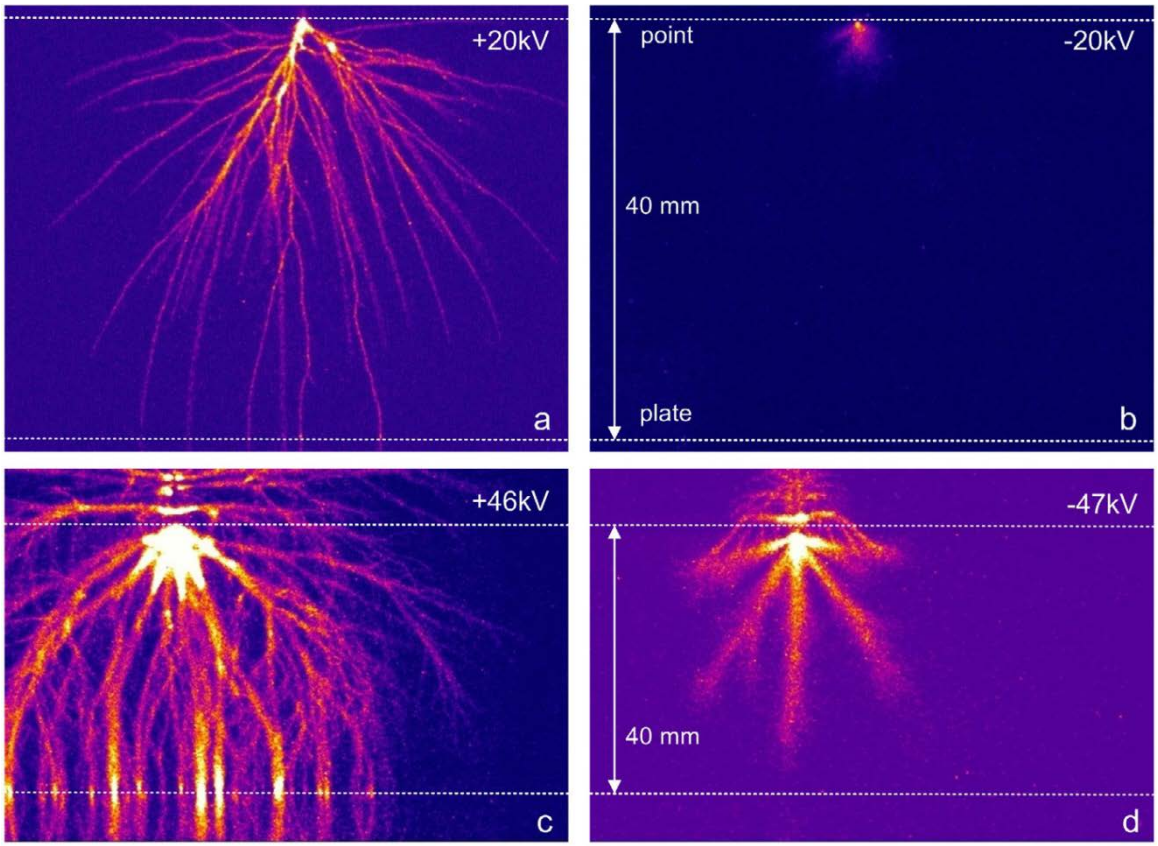

- Air plasma
- 1 bar

- Thin streamers for positive excitation with low over-voltages
- Voluminous glow-like discharge for negative excitation with low over-voltages
- Streamers for high over-voltages (positive and negative excitation)

Ref: Briels, Kos, Winands, van Veldhuizen, Ebert, J. Phys D: Appl. Phys., Vol. 41, 2008, pp. 234004 11p.

Electron density evolution for excitation pulse train

Conditions: P=10 atm, T_{gas}=700 K, 40:1 A/F ratio (lean),
+90kV → -80kV → +80kV pulse train (10 ns each)

Electron density

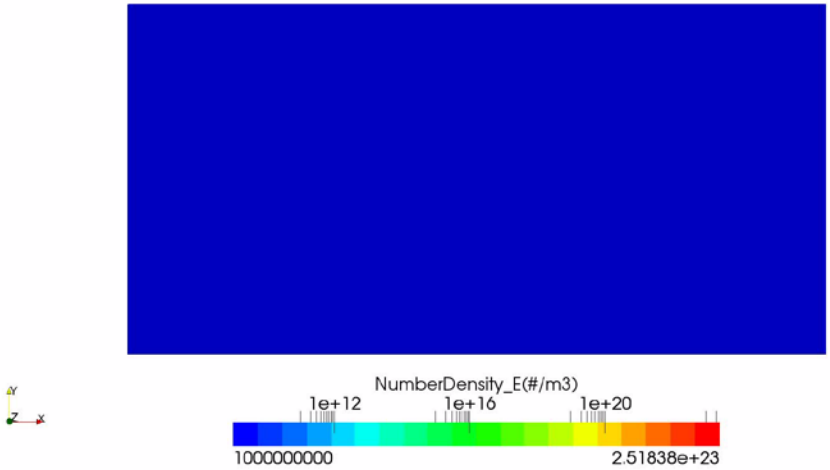

Reduced electric field (E/N)

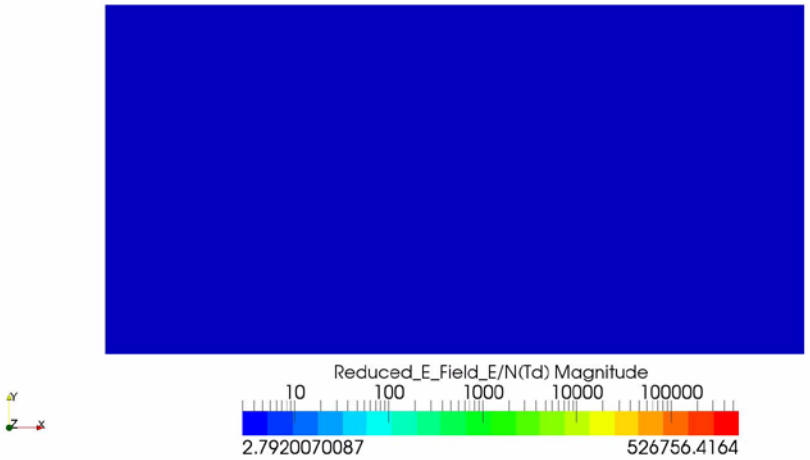

Electron temperature

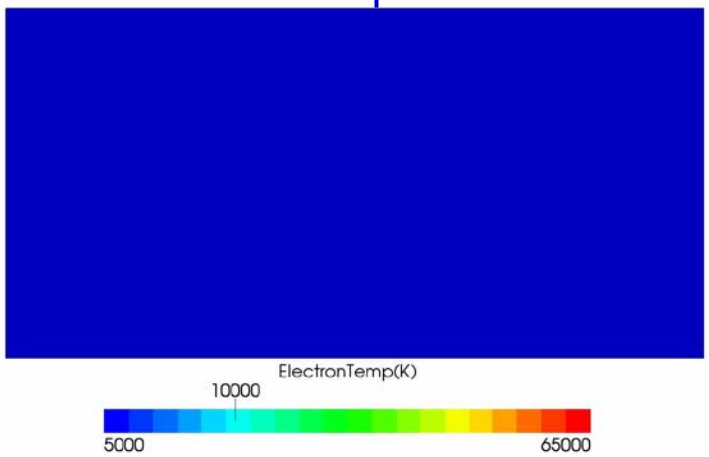

O radical density

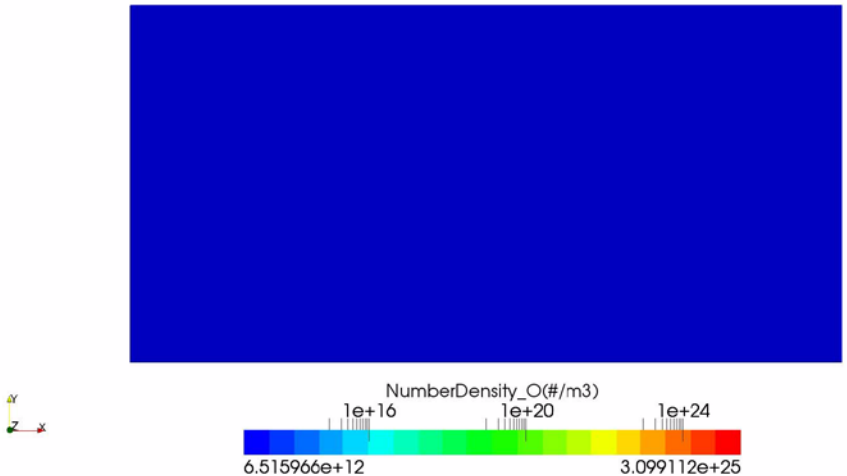

Radical density evolution at end of each pulse

O radical density

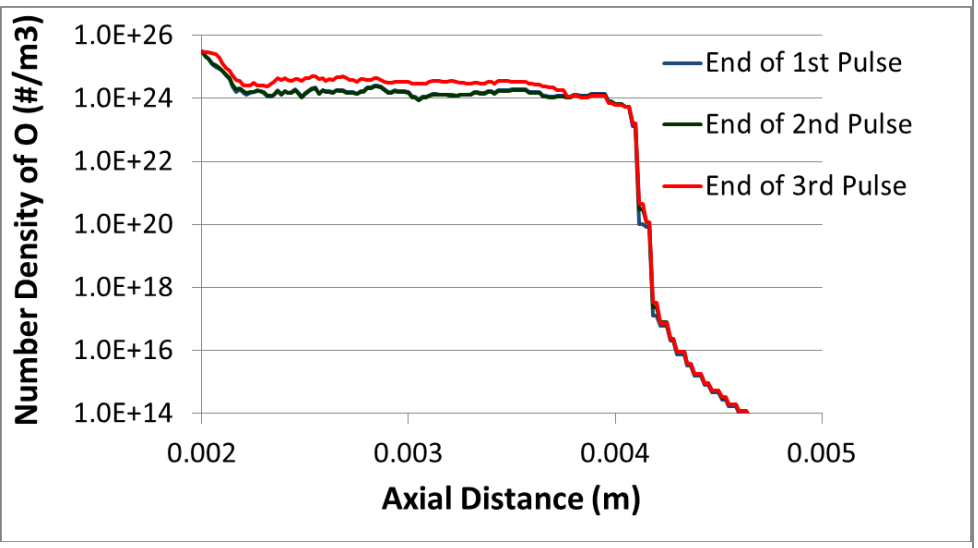

O_3 density

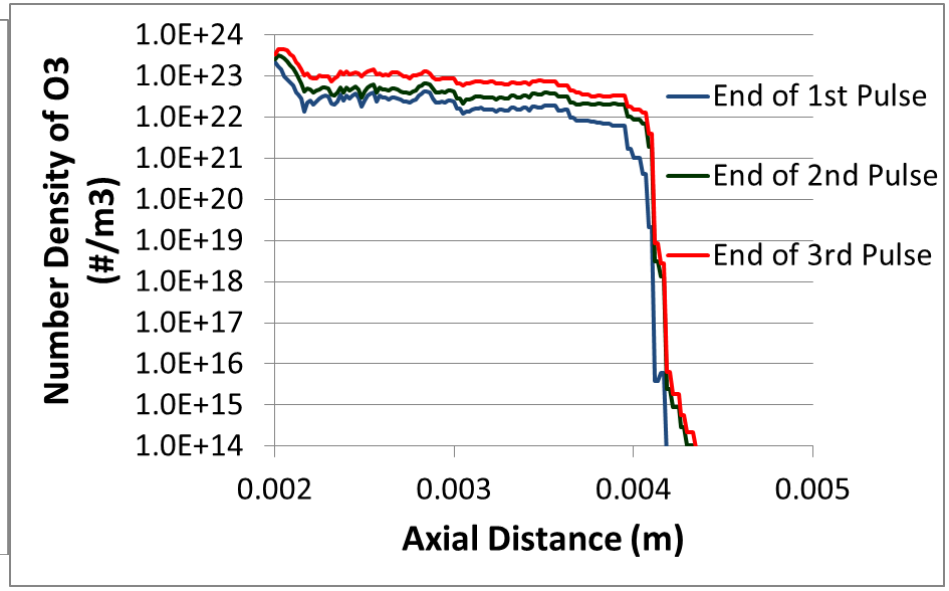

Nanosecond pulsed ignition of supersonic combustion

Reference:

D. Breden and L. L. Raja, “Simulations of nanosecond pulsed plasmas in supersonic flows for combustion applications,” *AIAA Journal*, Vol. 50, No. 3, Mar. 2012, pp. 647-658.

Nanosecond pulsed ignition of supersonic combustion

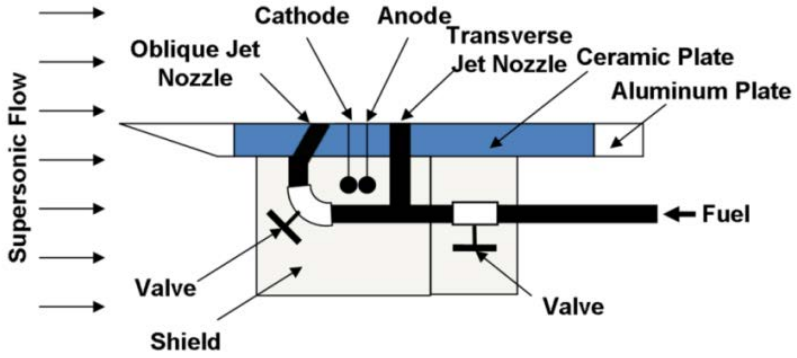

- 7 kV unipolar pulses
- 20 ns pulse width
- 50 kHz pulse freq.

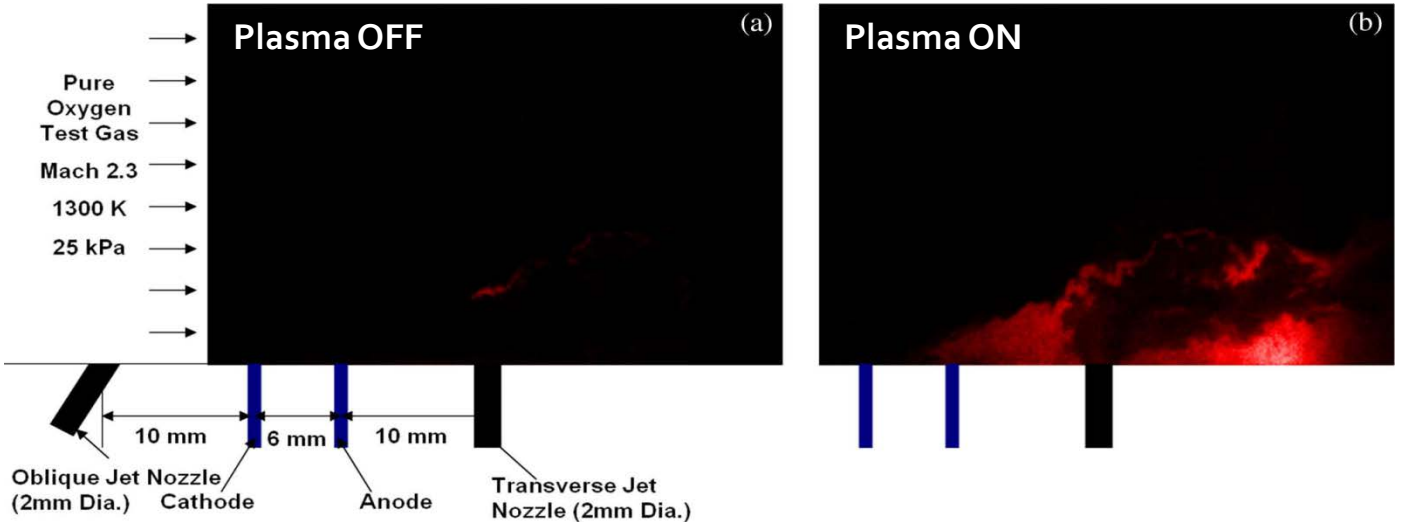

Ref: H. Do, M. G. Mungal and M. A. Cappelli., "Jet Flame Ignition in a Supersonic Crossflow using a Pulsed Nonequilibrium Plasma Discharge," IEEE Tran. On Plasma Sci. Vol.36 , 2008, pp. 2918-2923

Chemical reaction mechanism

H_2-O_2 sub-mechanism :

16 Species

e, O^+, O_2^+, O_4^+, O^-, O_2^- , H^+,H_2^+, O, H, OH, O_2, H_2, $O(^1D)$, $O_2(a^1\Delta_g)$, $O_2(b_1\Sigma_g^+)$

Assumptions:

- Rotational energy immediately heats bulk gas
- Vibrational energy convected out of simulation domain

Geometry, mesh, and operating conditions

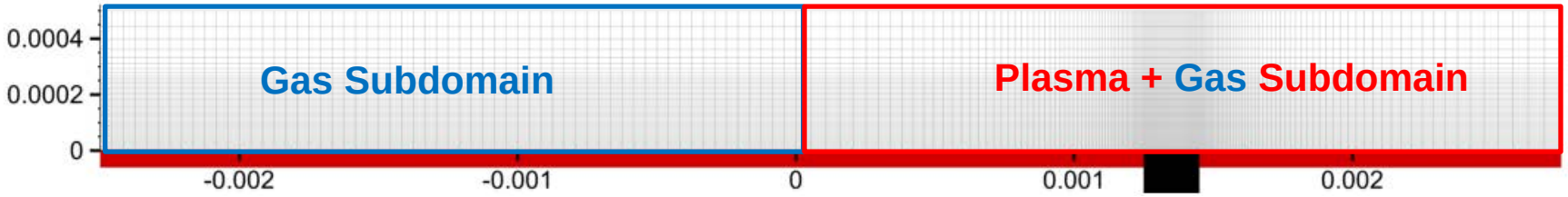

Plasma Mesh

- 8000 cells

0.2 mm electrode

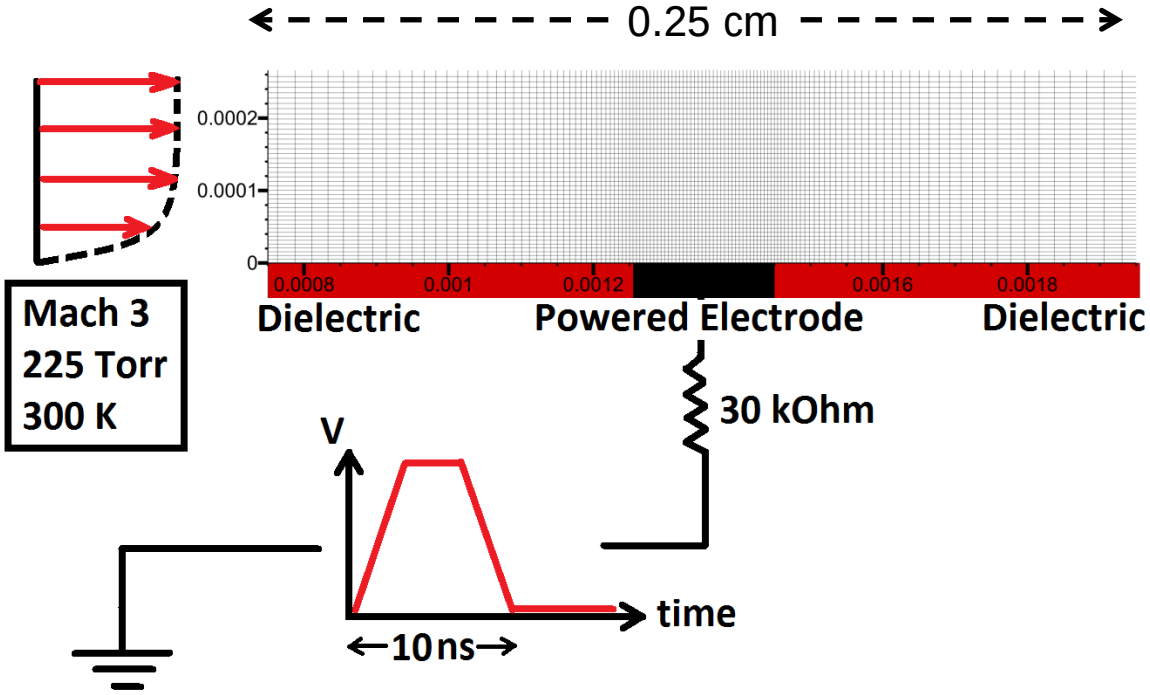

Trapezoidal Pulse

- 10 ns pulse
- 2.5 ns rise/fall time
- 6 kV peak

Unperturbed steady flow

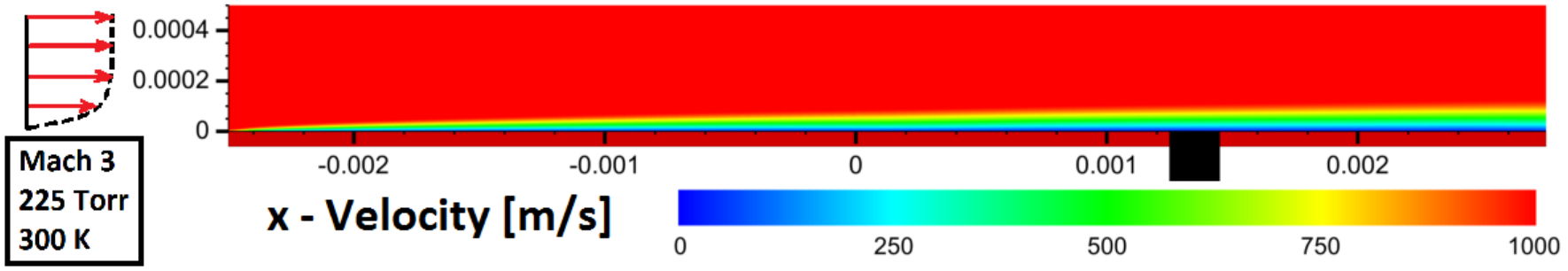

Laminar boundary layer with lower background number density

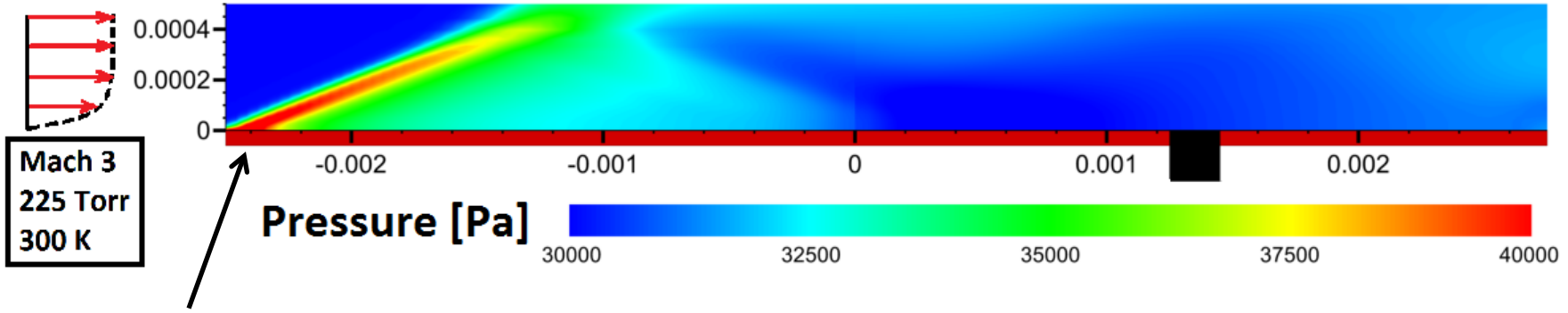

Flat-plate leading edge shock

Electrostatic potential and electron density transients

Potential [V]

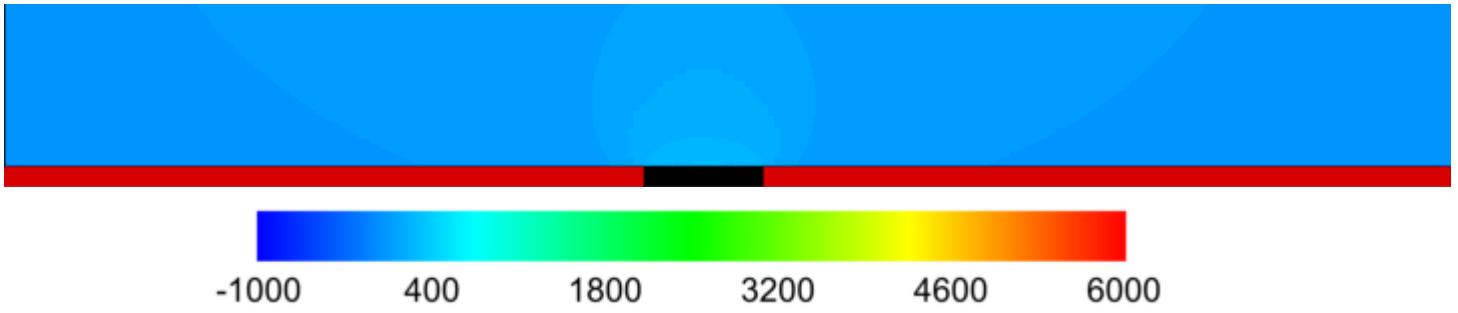

Electrons [#/m^3]

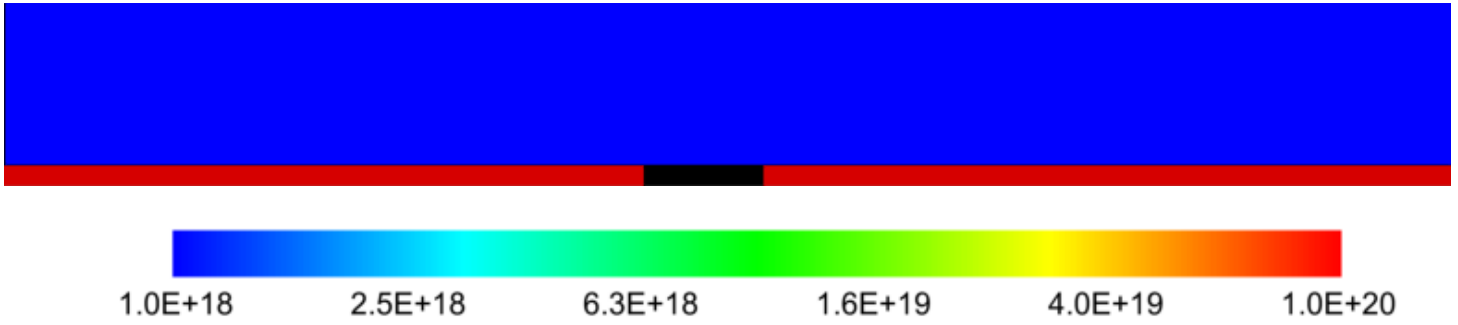

Charged and radical species yields at end of pulse

IONS

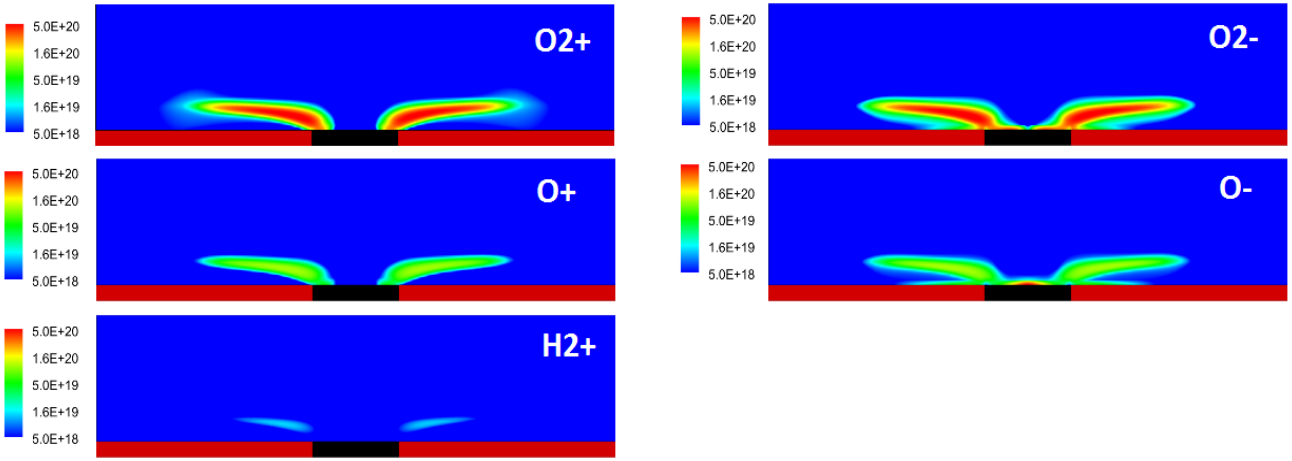

O_2^+ and O_2^- dominant positive and negative charge carriers

RADICALS

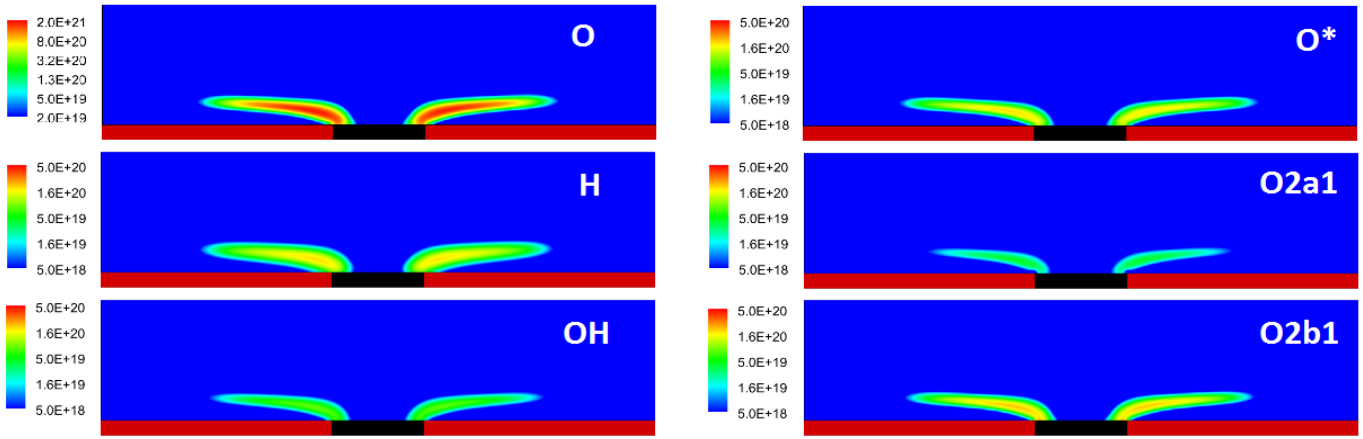

O dominant radical

Gas dynamic response to nanosecond pulsed discharge

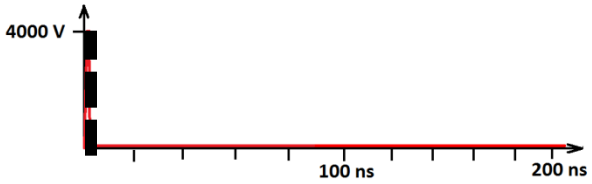

temperature [K]

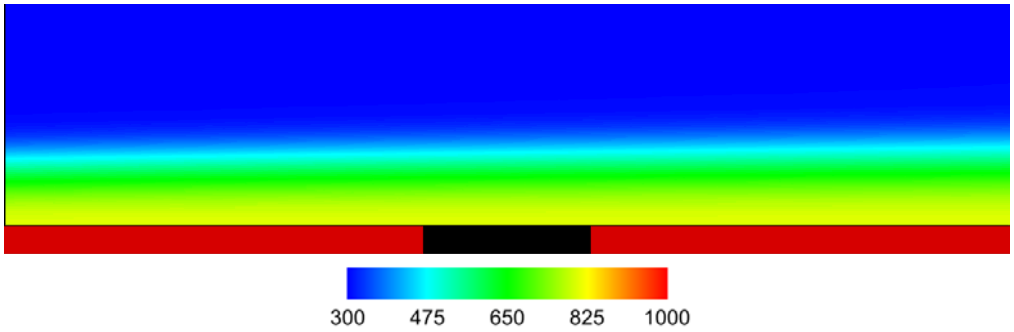

pressure [Pa]

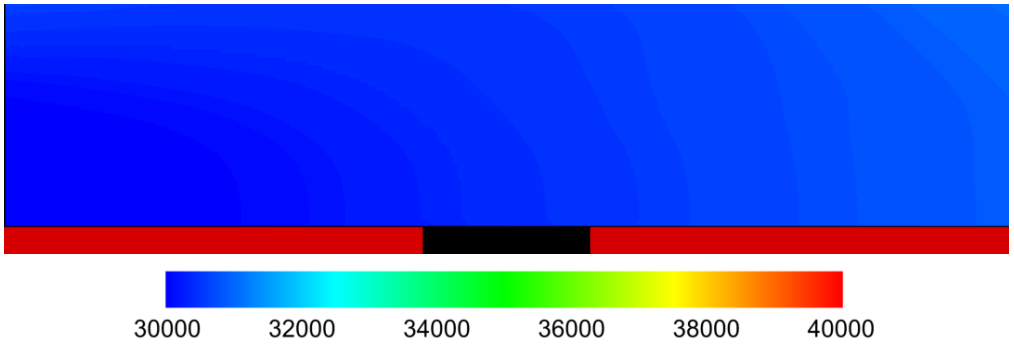

Effect of flow field on discharge dynamics

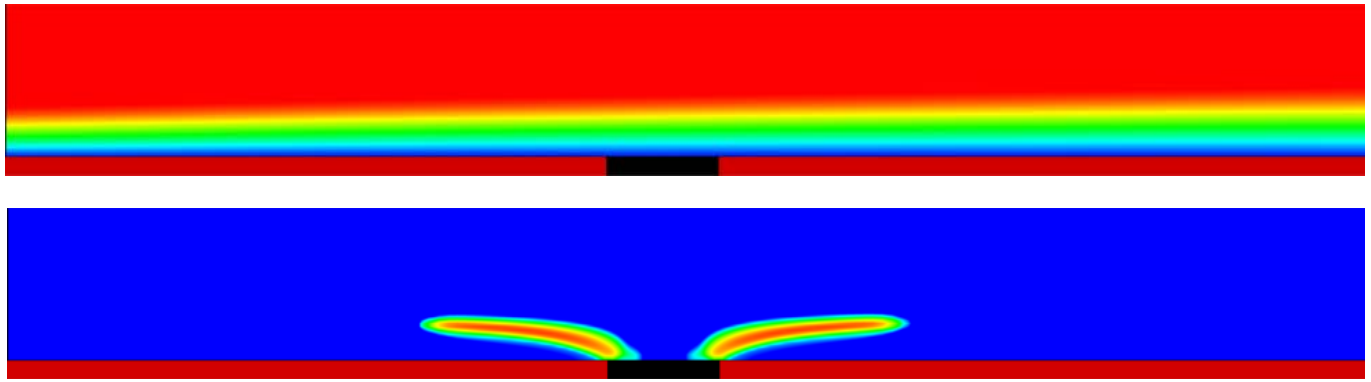

- Lower background number density in boundary layer → higher E/N
- Confinement of streamer to within the boundary layer

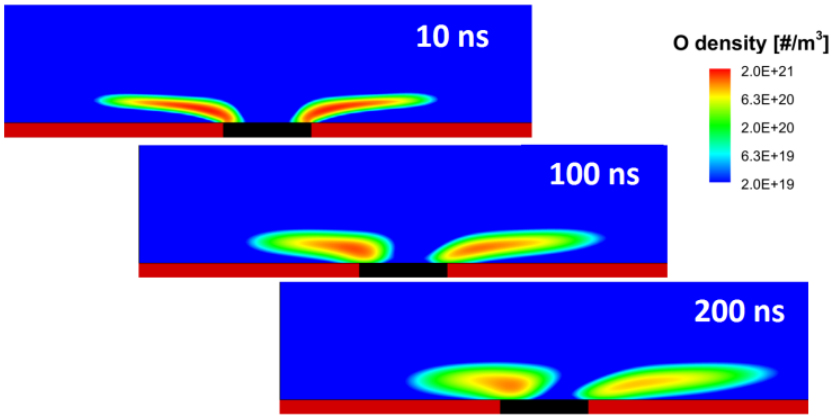

- Flow carries radicals downstream over micro/millisecond timescales

A note on parallel computing for these class of problems

80,000 APPJ mesh for 500 iterations on Lonestar machine at Texas Advanced Computing Center (TACC)

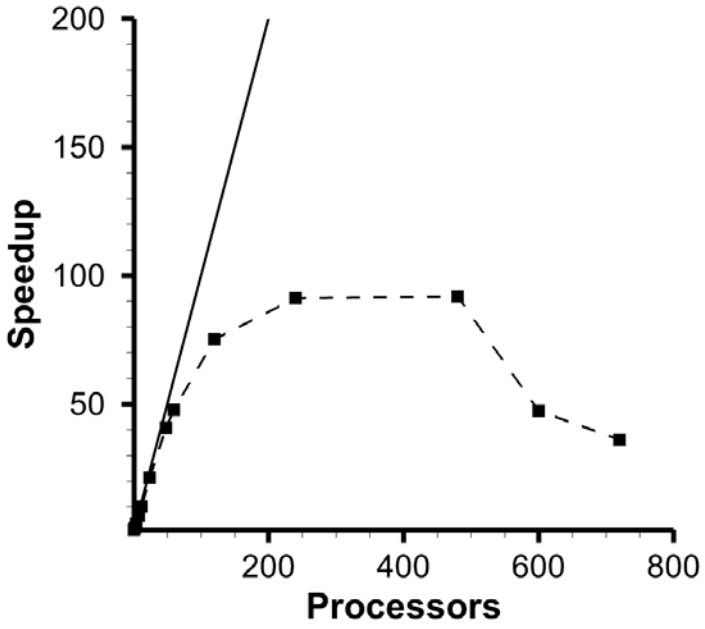

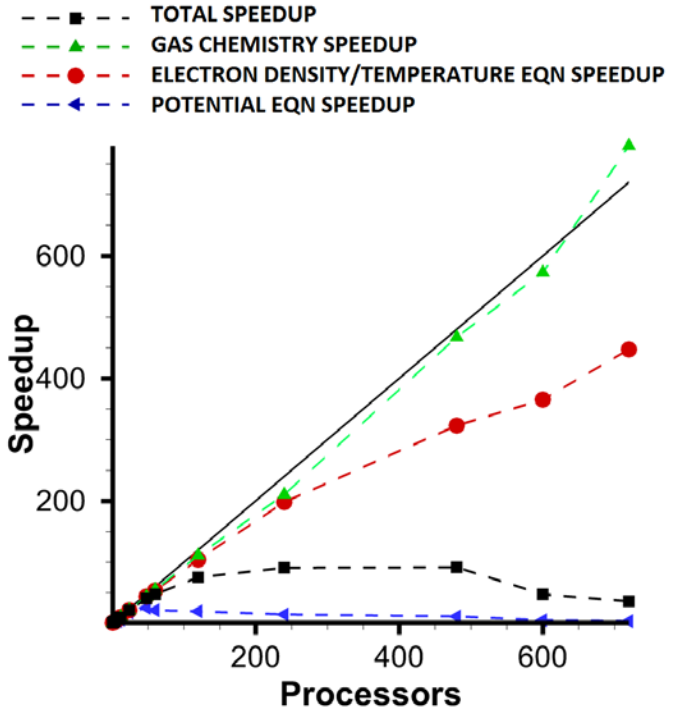

- Problems with large two-dimensional meshes and large chemistries scales well to a few 100 processors, cutting simulation times from ~weeks to ~ 1 day. However further improvement in speed up improvement is limited by algorithmic bottlenecks (specifically the Poisson's eqn).
- New "parallel friendly" discretization approaches to the Poisson's eqn. are required

Summary

- High fidelity simulations of cold plasma (streamer) discharges at high pressure relevant to real application are demonstrated
  - Self-consistent plasma physics, multi-species, multi-temperature, gas chemistry, surface chemistry, gas dynamics
  - Computationally expensive and needs large-scale parallel computing to make simulations feasible
- Simulations provide insights into discharge physics and chemistry and coupling with gas-dynamics
- Extension to large scale problems with high-performance computing requires a rework of established computational plasma modeling approaches

End of Presentation

Plasma kernel formation with active radicals is not a sufficient condition for ignition

- Cold plasma generated radicals are accompanied with no additional gas heating
- Do radicals accelerate combustion (chain initiation and branching) reactions for ignition
- Finally are conditions suitable for flame spread

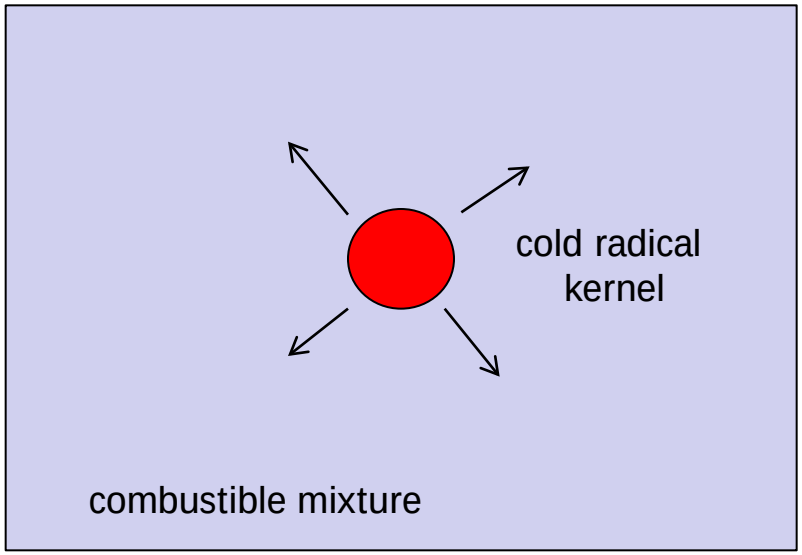

Question : Does the cold radical kernel grow in time or quench ?

Same as classic ignition kernel problem, except here kernel is a cold radical region, rather than hot gas region

Preliminary computational modeling of combustion initiation and flame spread

- Solve reactive gas dynamics problem assuming an initial radical kernel
  - 1D Axisymmetric transient problem
  - 1 mm kernel size (~ multiple overlapping streamer widths)
  - No additional gas heating from plasma
  - 10 atm, 1500 K, lean mixture with EGR (A/F 20:1 + 50 % EGR)
  - 1 % of O radicals (consistent with yield from streamer)

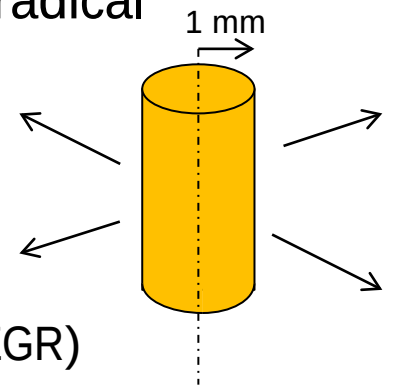

- Chemistry Mechanism: DRM22 with 22 species and 105 reactions
  - Species: H2, O, O2, OH, H2O, HO2, H2O2, CH2, CH3, CH4, CO, CO2, HCO, CH2O, CH3O, C2H2, C2H3, C2H4, C2H5, C2H6, N2

- Reactive Flow model:
  - VizGlow (without plasma calculations) coupled to Compressible Navier-Stokes solver (VizFlow)

Other approaches may be considered for automotive combustion ignition applications

- Principle requirements :
  - Extended plasma kernel size
  - High radical yield
  - Low loss (volumetric; far away from surfaces)

Spark

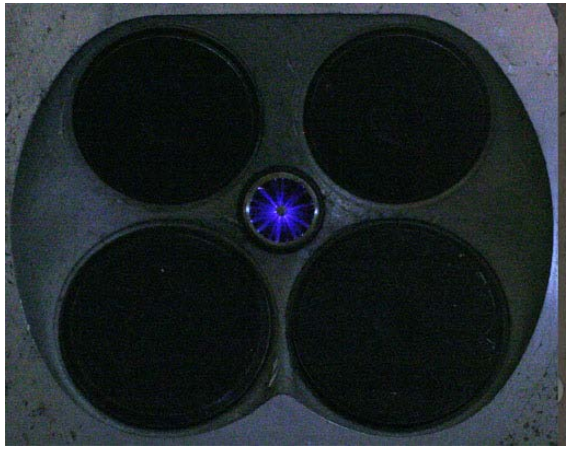

HSP

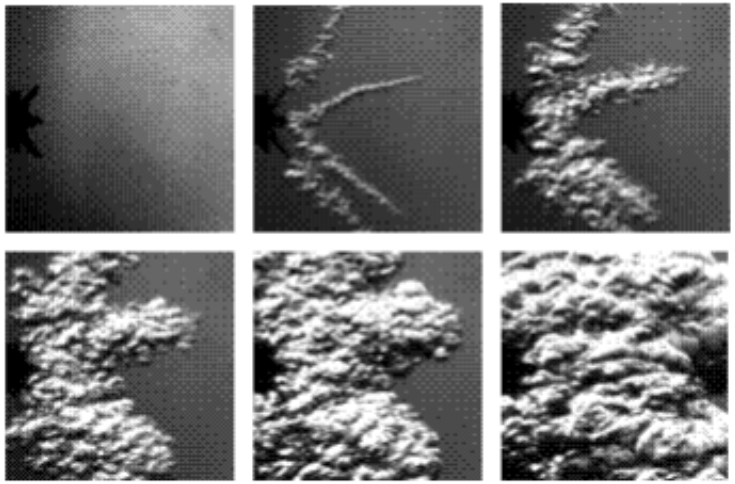

RFEIS or ECCOS

Sub-critical microwave excitation with external plasma initiation is a possibility

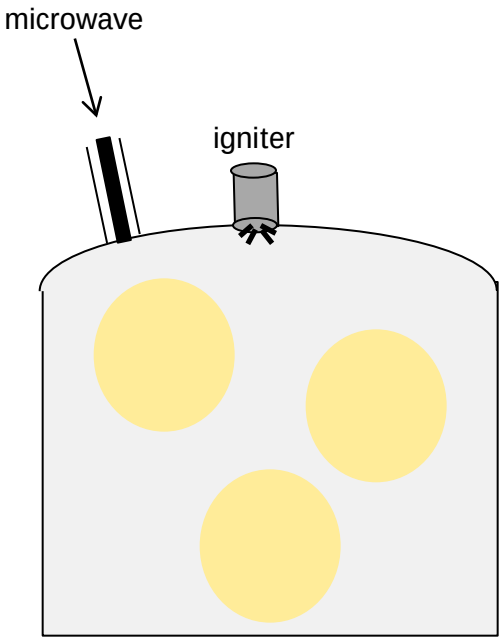

- Coax-fed microwave can provide a volume filling excitation field
- External plasma initiation can be used to keep microwave E-field subcritical

Microwave excitation concept is not new for automotive ignition applications

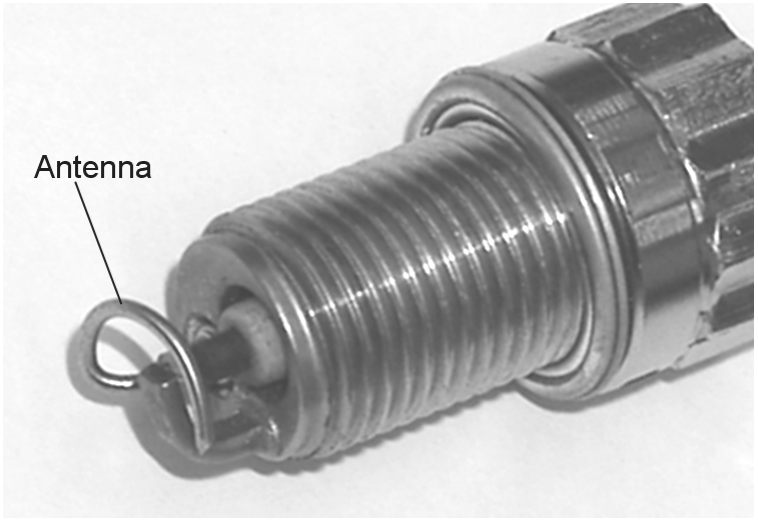

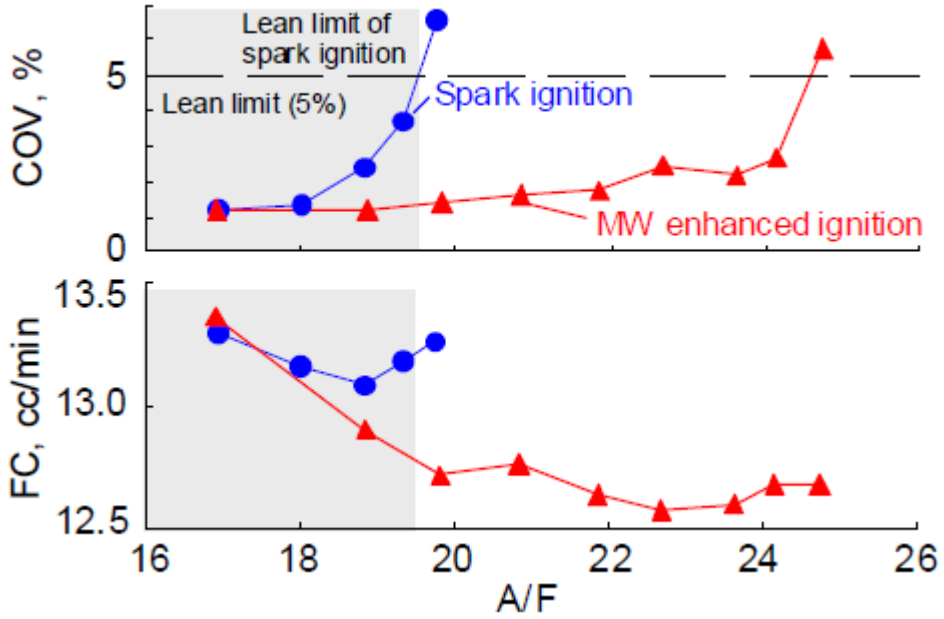

- Igniter erosion concerns with Ikeda concept can potentially be overcome with coax-fed microwave

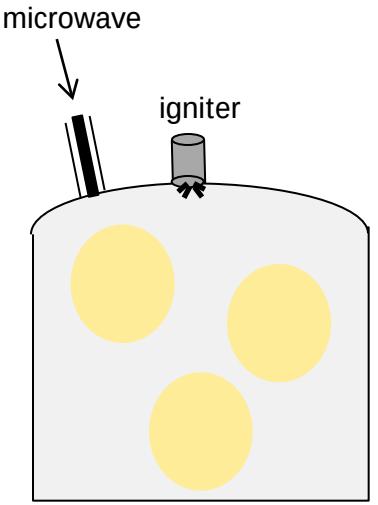

From : Ikeda, et al, AIAA Paper 2009-223.

High-fidelity modeling capability available to simulate microwave plasmas with VizGlow

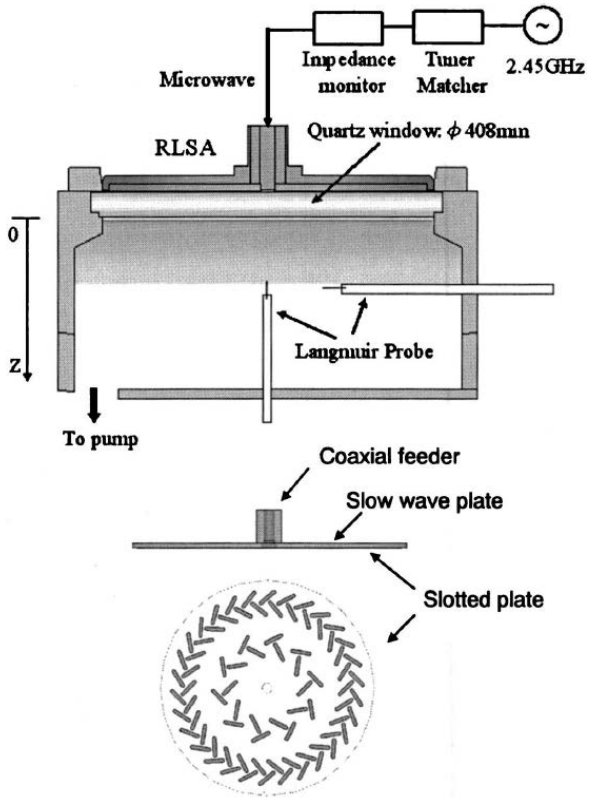

FIG. 1. Schematics of the RLSA for the microwave plasma system.

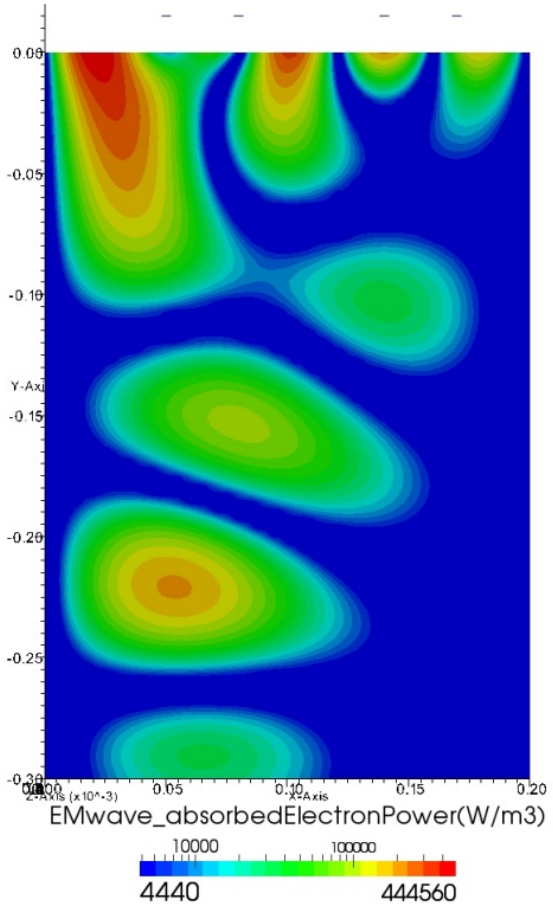

Characteristics of large-diameter plasma using a radial-line slot antenna

C. Tian,[a] T. Nozawa, K. Ishibasi, H. Kameyama, and T. Morimoto
Tokyo Electron Ltd., TBS Broadcast Center, 3-6 Akasaka 5, Minato-ku, Tokyo 107-8481, Japan

1421 J. Vac. Sci. Technol. A 24(4), Jul/Aug 2006 0734-2101/2006/24(4)/1421/4/$23.00 ©2006 American Vacuum Society

Summary

- Presented an overview of non-equilibrium plasma physics relevant to automotive ignition applications
  - Nano-second pulsed plasma are efficient way to generate non-equilibrium plasmas at high pressures
  - HSP, DBD, RFEIS devices leverage this concept in different ways
- High-fidelity simulation studies of HSP presented
  - Streamers produce copious amounts of radicals (particularly O radicals)
  - Radicals are concentrated at inner electrode possibly explaining the dynamics of flame spread from these ignition sources
- Showed initial studies of long time scale processes in ignition
  - Plasma radical kernel → local combustion initiation → gas dynamic relaxation → flame spread
- Extended volumetric radical kernel possible with subcritical microwave + NSP ignition

Trends in automotive combustion engines are driving need for new ignition sources

- Improved engine efficiencies and stringent emission norms are driving new technologies in automotive combustion devices
- Improved efficiencies achievable through 1) increased compression ratios in IC engines and 2) lean combustion
- Lean combustion →
  - Increase in efficiency (power/fuel rate)
  - Decrease in flame temperature

    → low NOx

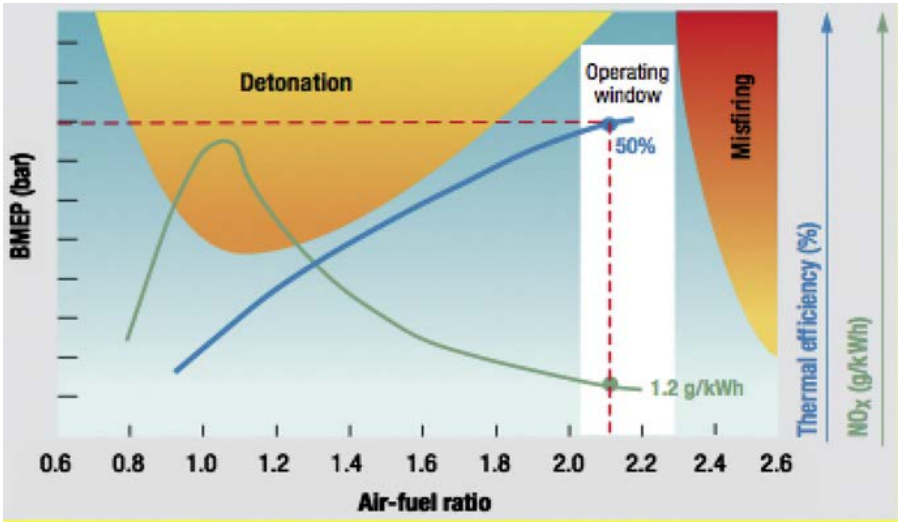

Starikovskiy and Alexsandrov, Prog. Energy Comb. Sci., 2013

- Enabling technologies
  - Direct injection (no air intake throttling losses) → just in time combustion
  - Lean with Exhaust Gas Recirculation (EGR) → low flame temp → lower NOx
- Technological challenges
  - Lean combustion (with EGR) → ignitability issue is key problem

Conventional spark plug based IC engine ignition

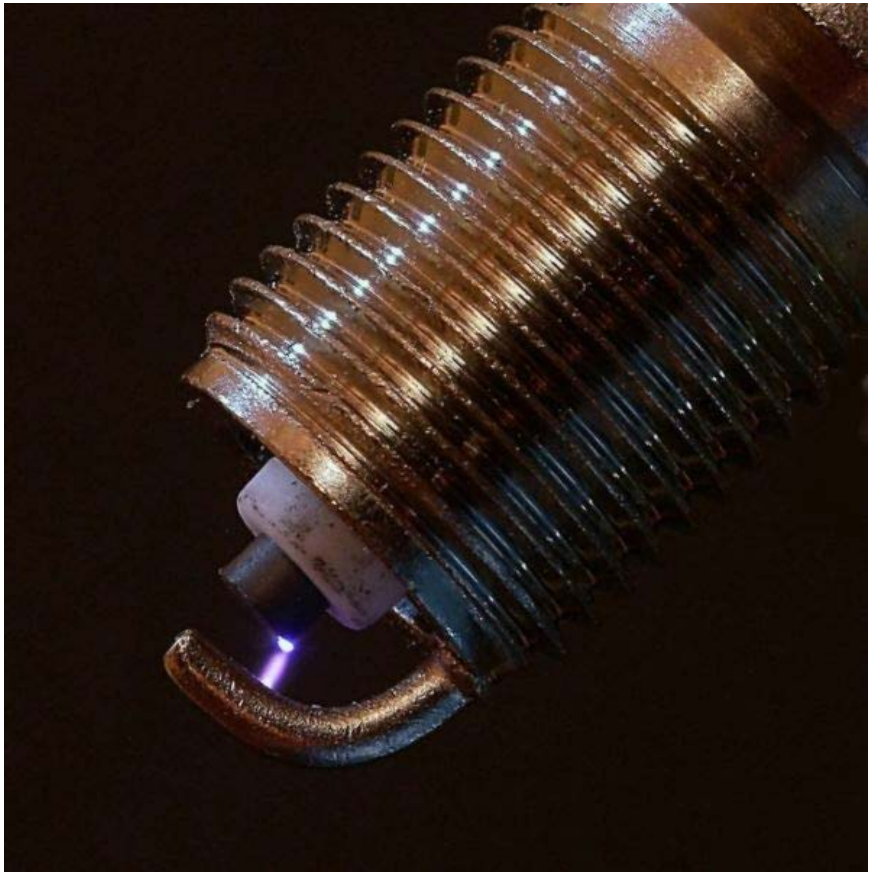

- Combustion ignition via highly constricted/localized spark
- Spark is a thermal plasma with very high sensible temperatures (~ 1000's K)
  -- lifetime/reliability
- Chemical initiators for combustion not the same as in a cold plasma
- Limited control on plasma yield

Nanosecond pulsed and Dielectric Barrier plasma-based ignition

Conventional spark plug

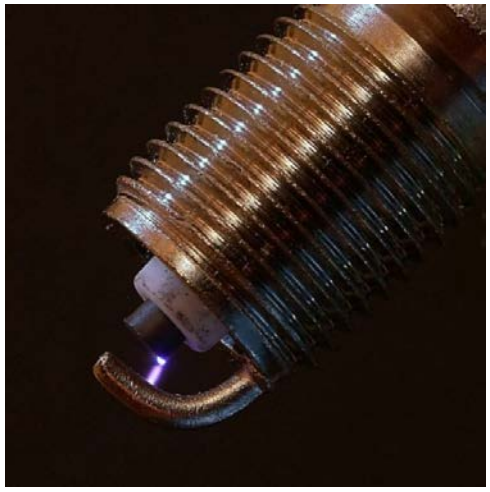

Nanosecond Pulsed

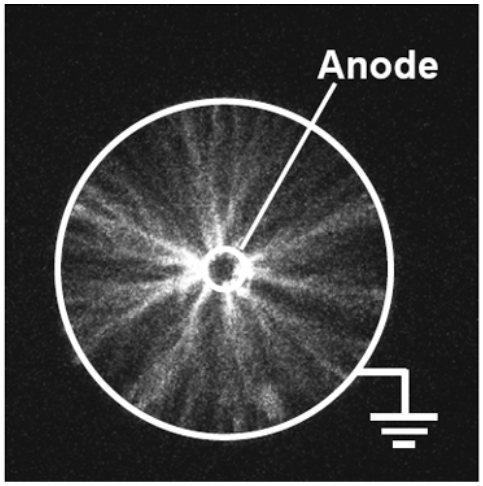

Dielectric barrier

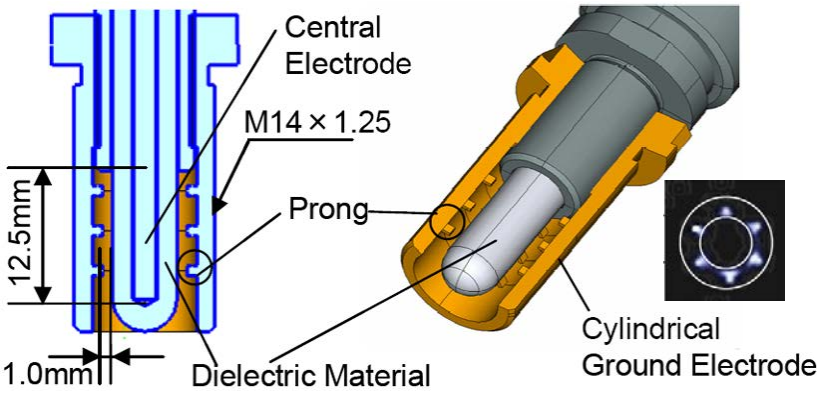

1200 rpm, A/F=15.1(Φ=1.0), ADV: 20 deg.BTDC, iso-octane

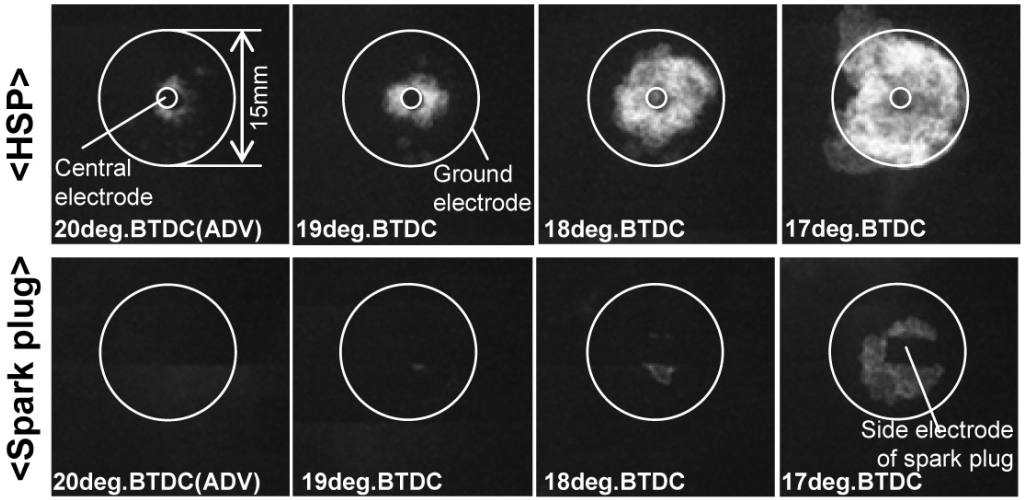

Shiraishi and Urushira, SAE_2011-01-0660

Variety of plasma actuator concepts exist for volumetric and surface flow control

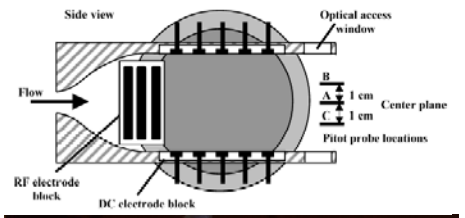

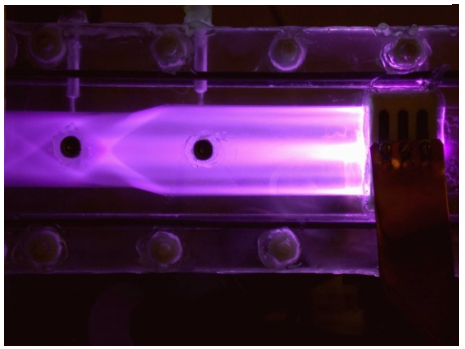

Meyer et al. AIAA J. (2005) OSU

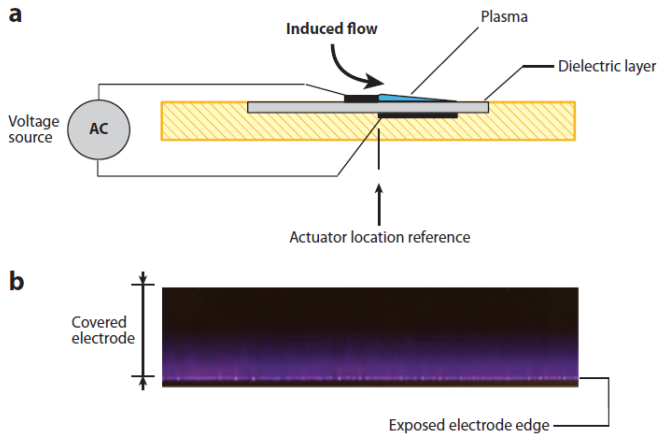

Corke et al., Ann. Rev. Fl. Mech. (2010)

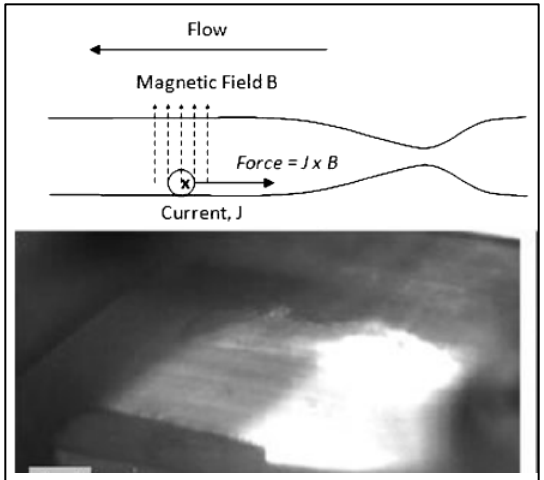

Kalra et al., Expt. Fluids, (2011)

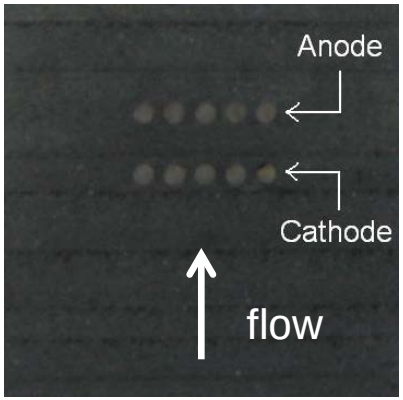

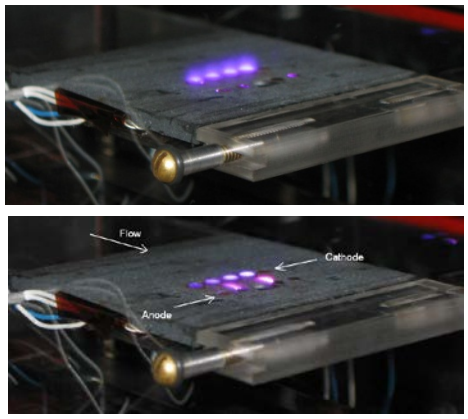

Shin et al., AIAA J. (2007)

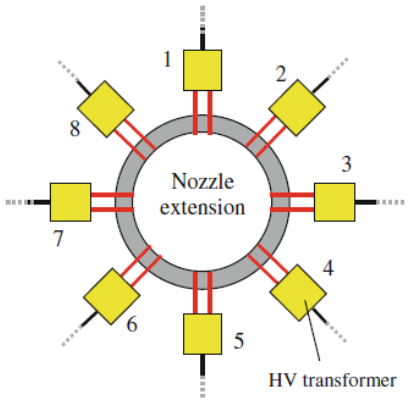

Kim et al., Expt. Fluids, (2010)

Computational issues in the modeling of air plasma interactions with flows

- Extremely high degree of time disparity in component physics

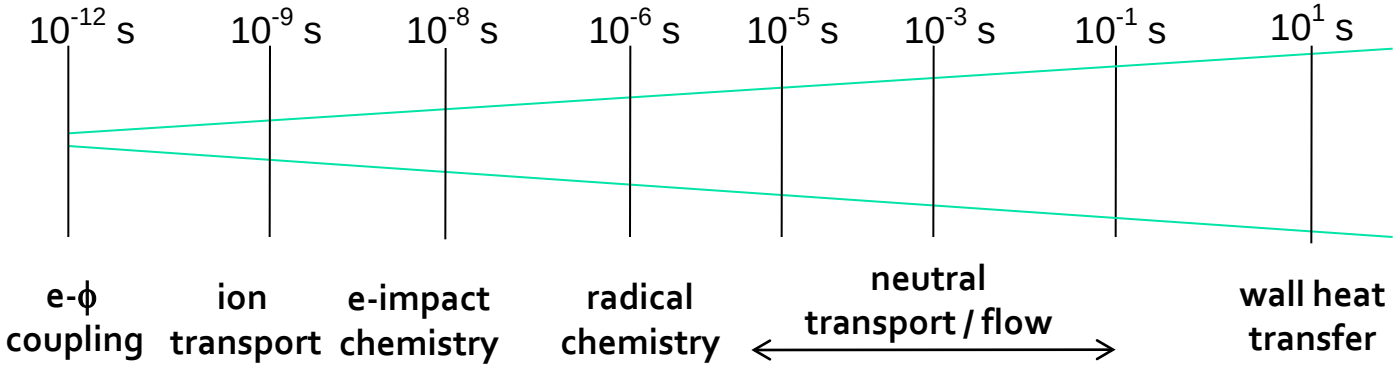

- Spatial stiffness due to discharge structure

Sheaths

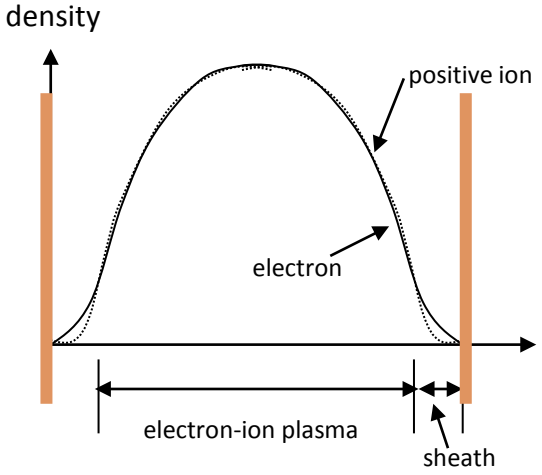

Electronegative plasma

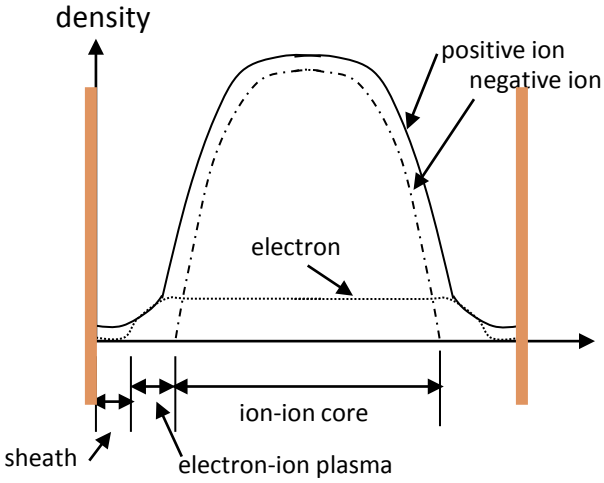

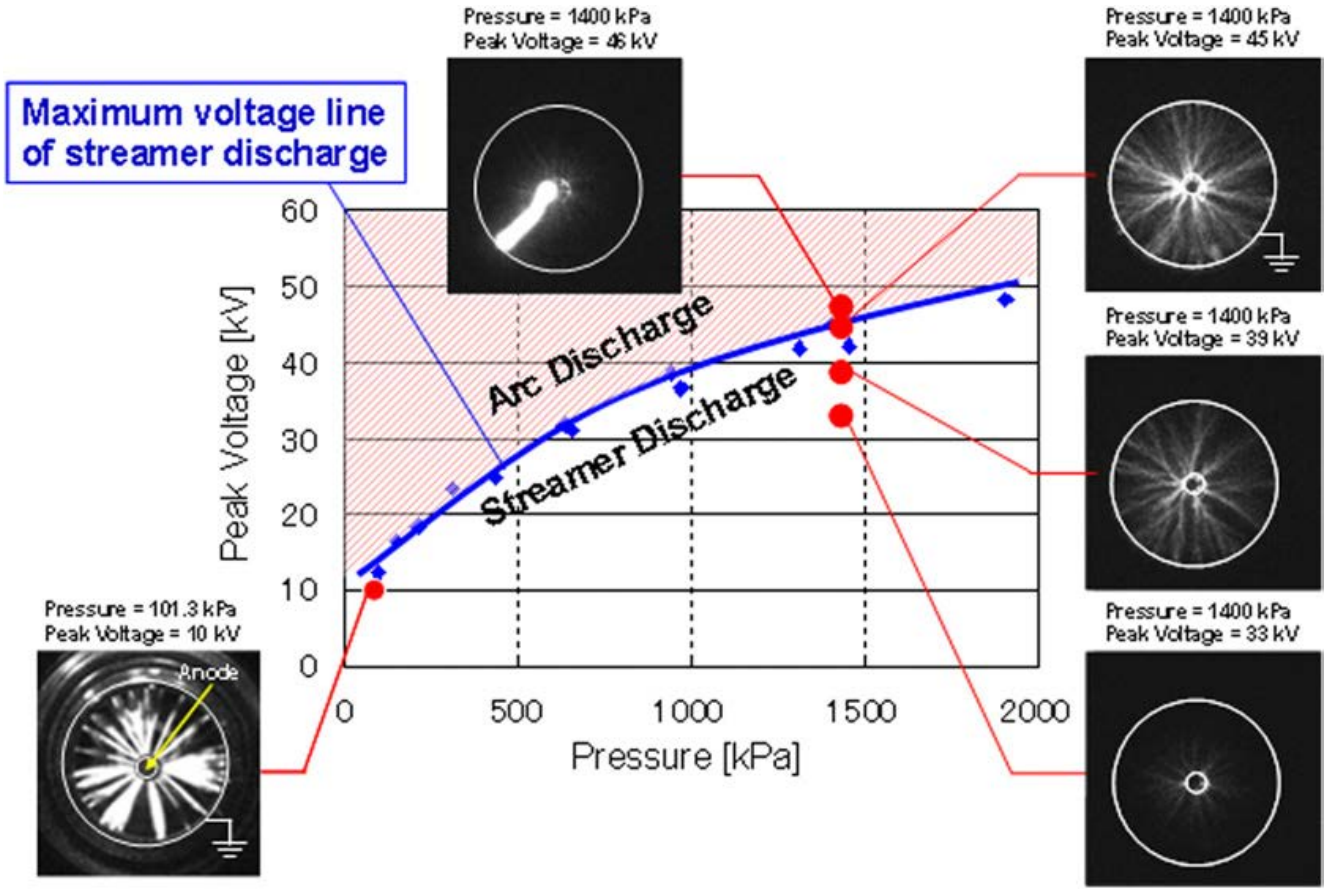

From: Shiraishi et al., J. Phys. D., 42, 2009, 135208.

Photoionization (3-term Helmholtz equation model)

Integral Model (Zheleznyak et al 1982):

$$S_{ph}(\vec{r}) = \iiint \frac{I(\vec{r}\prime)g(R)}{4\pi R^2} dV$$

$$I(\vec{r}) = \frac{P_q}{P + P_q} \xi S_i(\vec{r})$$

$$\frac{g(R)}{P_{O2}} = \frac{exp^{-\chi_{min} P_{O2} R} - exp^{-\chi_{max} P_{O2} R}}{P_{O2}\, R\, ln(\chi_{max}/\chi_{min})}$$

Luque et al* proposed approximating $g(R)/P_{O2}$ using two exponentials functions and expanded by Bourdon et al+ to three terms

$$S_{ph}(\vec{r}) = S^1_{ph} + S^2_{ph} + S^3_{ph}$$

$$S^j_{ph} = \iiint \frac{I(\vec{r})}{4\pi R} A_j P^2_{O2} exp^{-\lambda_j P_{O2} R}$$

The integrals are solutions to three Helmholtz equations:

$$\nabla^2 S^j_{ph} - (\lambda_j P_{O2})^2 S^j_{ph} = -A_j P^2_{O2} I(\vec{r})$$

(j = 1,2,3)

	A_j (cm^{-1} Torr $^{-1}$)	λ_j (cm^{-1} Torr^{-1})
S^1_{ph}	0.0067	0.0447
S^2_{ph}	0.0346	0.1121
S^3_{ph}	0.3059	0.5994

* Luque A, Ebert U, Montijn C and Hundsdorfer W 2007 Appl. Phys. Lett. 90 08150

+ Bourdon A, Pasko NP, Liu NY, Celestin S, Segue P and Maroude E 2007 Plasma Sources Sci. Technol. 16 656

Plasma chemistry mechanism used in studies

- Plasma Chemistry mechanism relevant to plasma time scale (~10's ns)

- Methane-air mixtures
  - 26 Species :

    E, O, N_2 , O_2 , H , N_2^+ , O_2^+ , N_4^+ , O_4^+ , O_2+N_2 , O_2^- , O^- , O_2(a1) , O_2(b1) , O_2* , N_2(A) , N_2(B) , N_2C , N_2(a1), CH_4 , CH_3 , CH_2 , CH_4^+ , CH_3^+ , CH_2^- , H^-

  - 85 Reactions :

    1) electron impact, 2) ion-ion, 3) electron neutral, 4) neutral-neutral

- Methane-air with EGR mixtures
  - 39 Species :

    E, O, N_2 , O_2 , H , N_2^+ , O_2^+ , N_4^+ , O_4^+ , O_2+N_2 , O_2^- , O^- , O_2(a1) , O_2(b1) , O_2* , N_2(A) , N_2(B) , N_2C , N_2(a1), CH_4 , CH_3 , CH_2 , CH_4^+ , CH_3^+ , CH_2^- , H^- ,

    H_2O, H_2O^+, H_2, H^+, H_2^-, OH, OH^+, OH^-, O^+, CO_2, CO_2^+, CO^- , O_3

  - 110 Reactions :

    1) electron impact, 2) ion-ion, 3) electron neutral, 4) neutral-neutral
    Additional : CO2, H2O and O3 reactions

Comparison of baseline and With EGR cases for HSP discharge streamer

Baseline (lean A/F = 40:1)

With EGR (A/F = 20:1 + 50% exhaust)

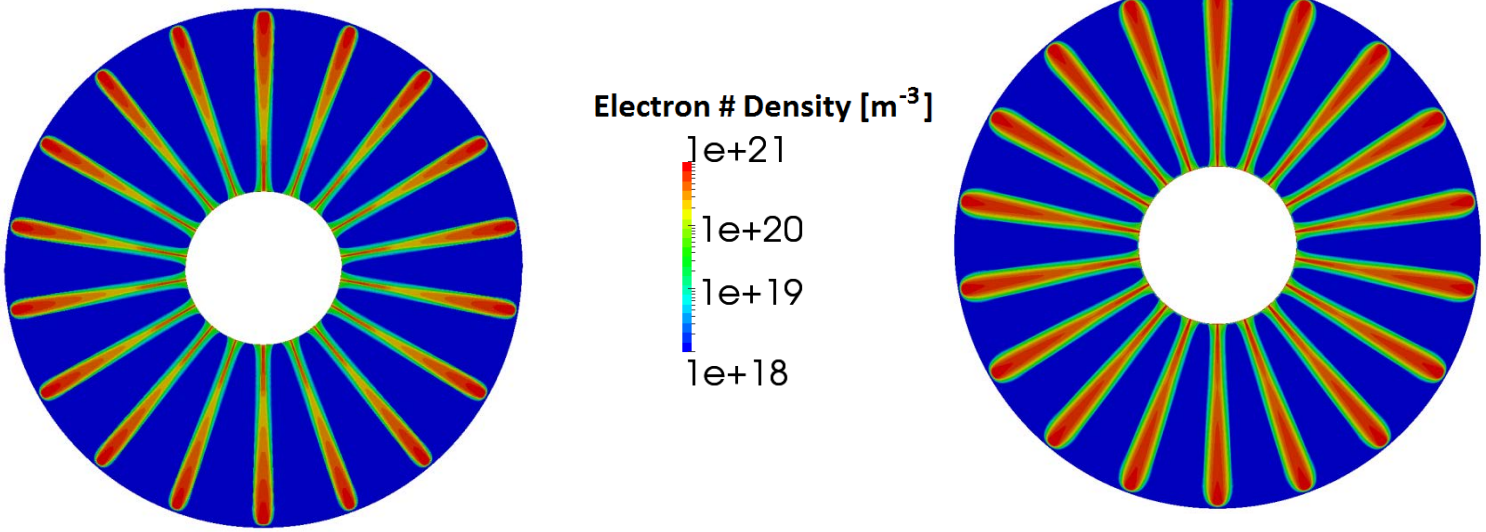

9.7 ns

5.7 ns

- Propagation speeds higher with EGR
- Electron density slightly higher with EGR

Radical densities for baseline and With EGR cases for HSP discharge streamer

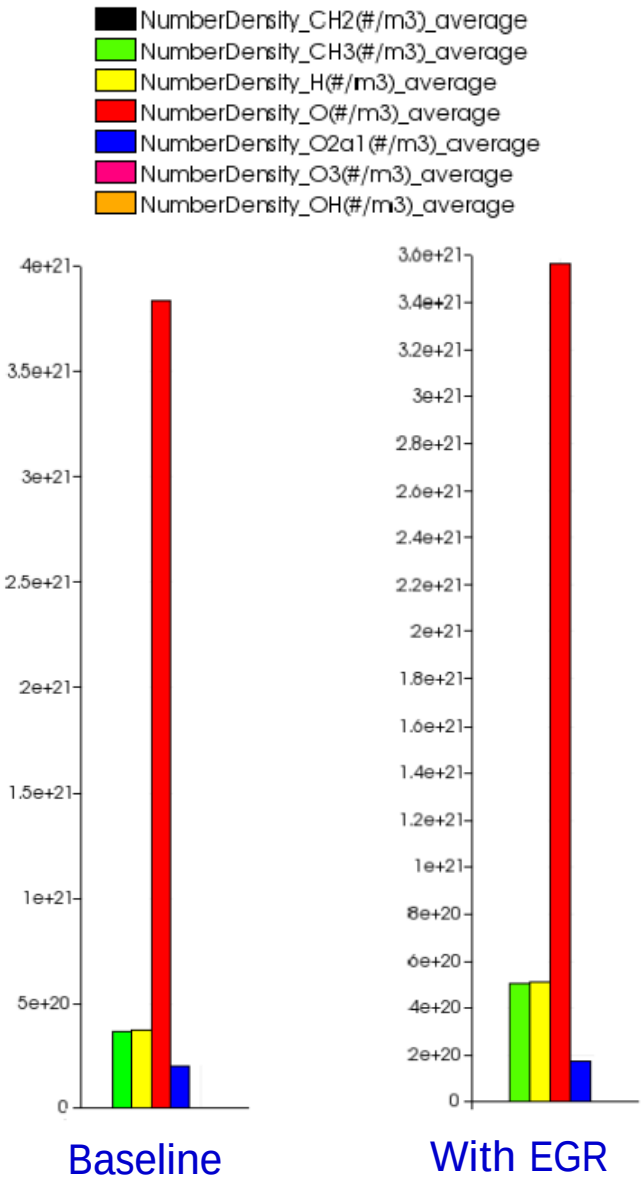

- No significant changes in radical densities for case with EGR

Case 1: Pulse train of -90kV → +90 kV → -90 kV (gas temperature 700K)

Pulse Durations:

1st pulse: 7 ns

2nd pulse: 7 ns

3rd pulse: 7 ns

Evolution of Number Density of Electrons

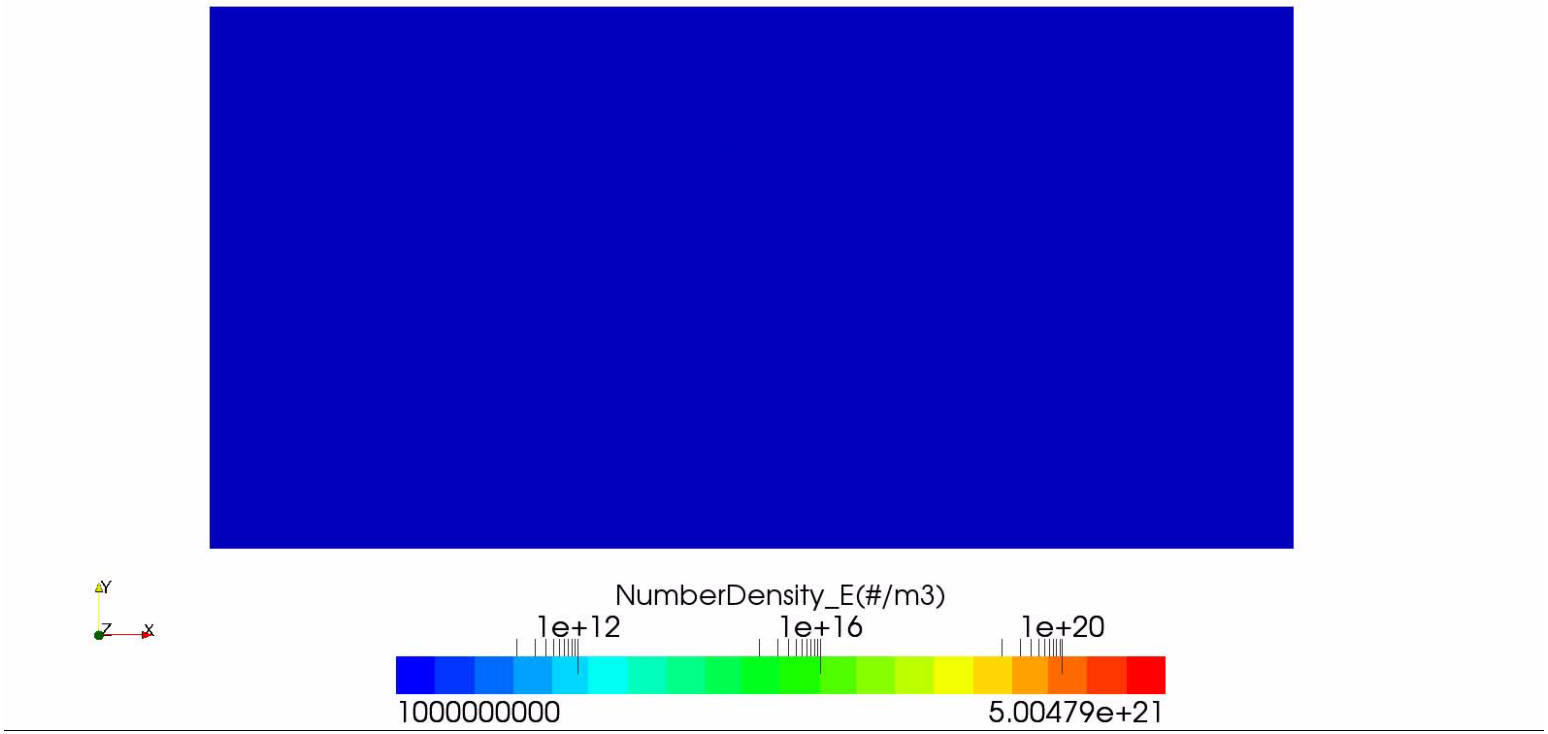

Evolution of Number Density of O radicals

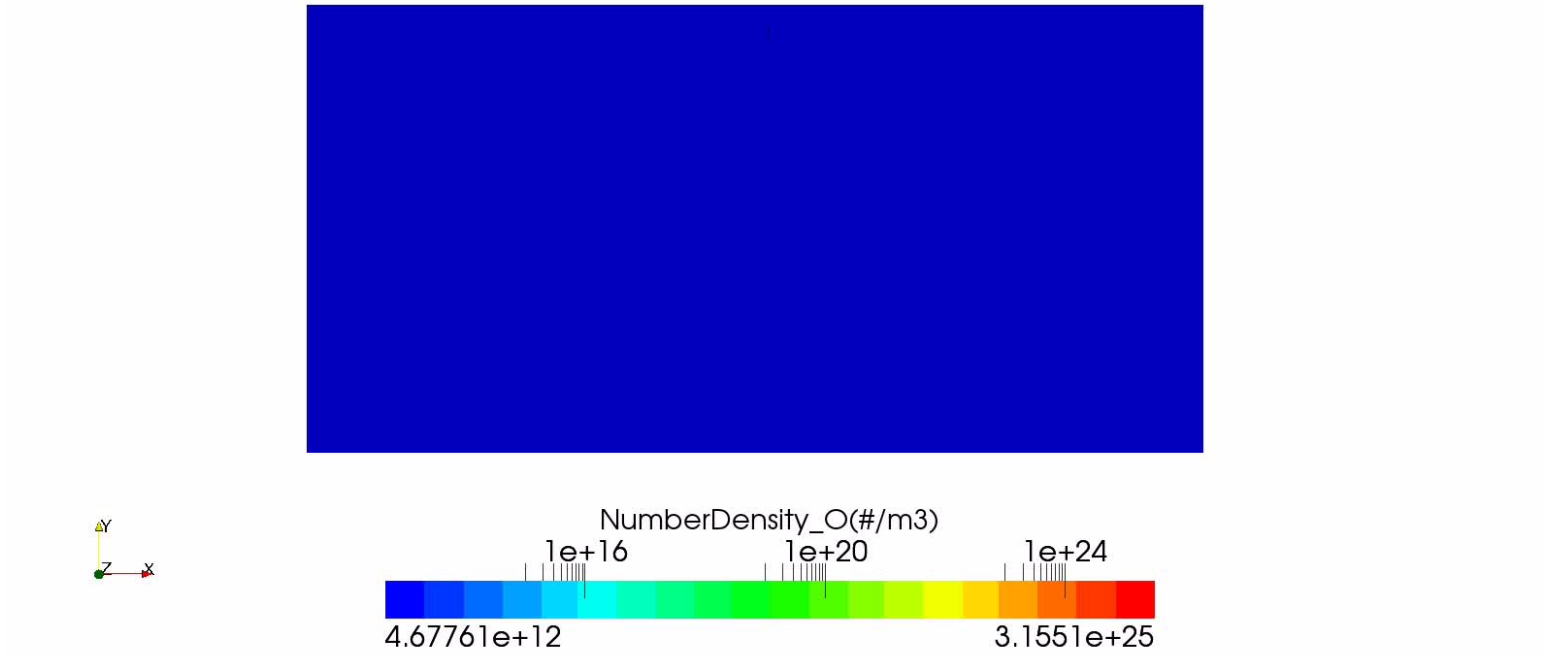

Evolution of Electron Temperature (K)

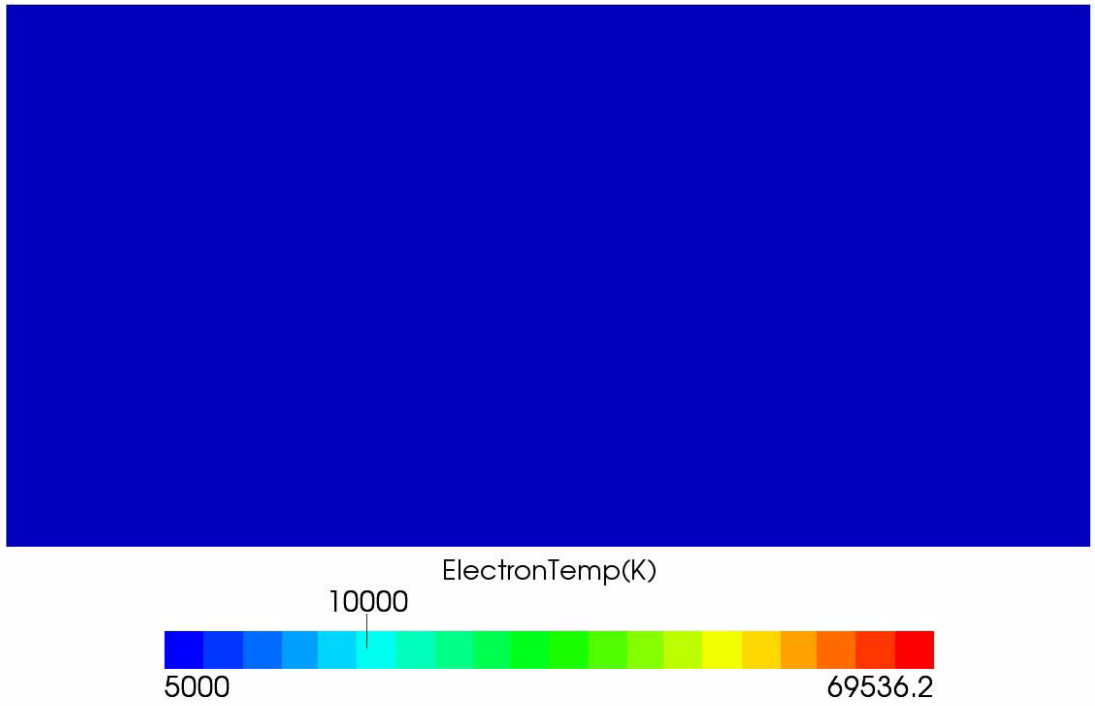

Evolution of Reduced Electric Field (E/N)

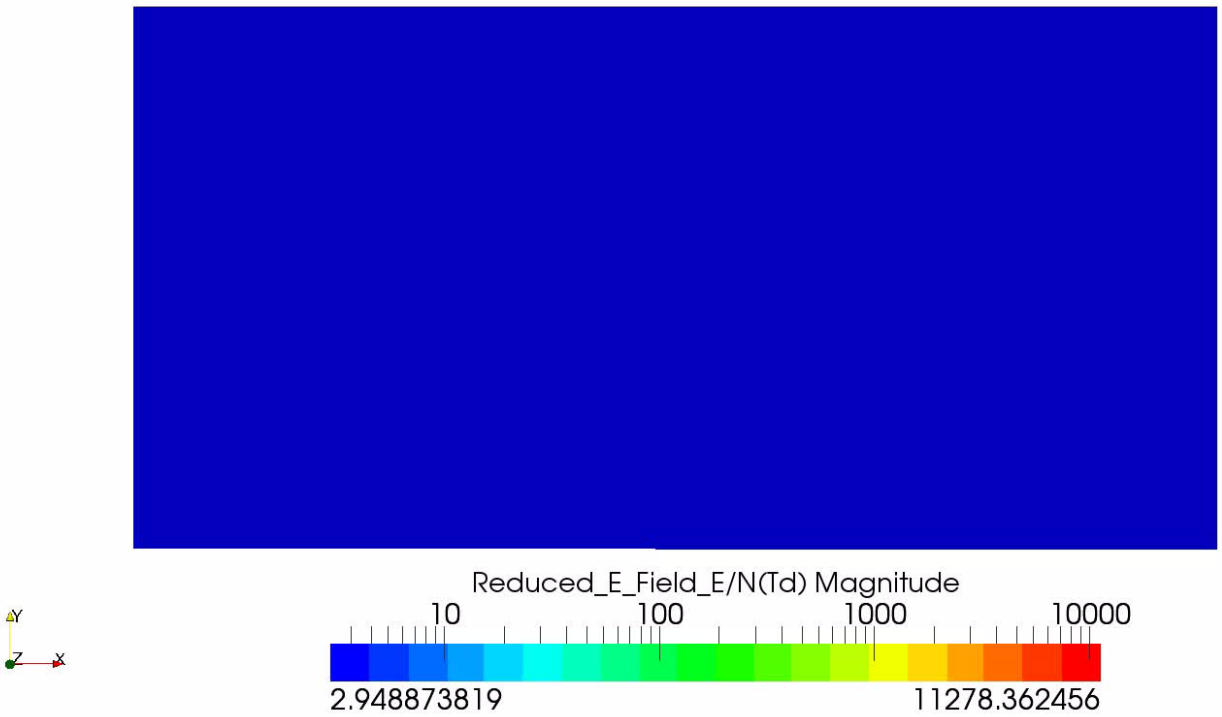

O Radical Number Density at End of Different Pulses

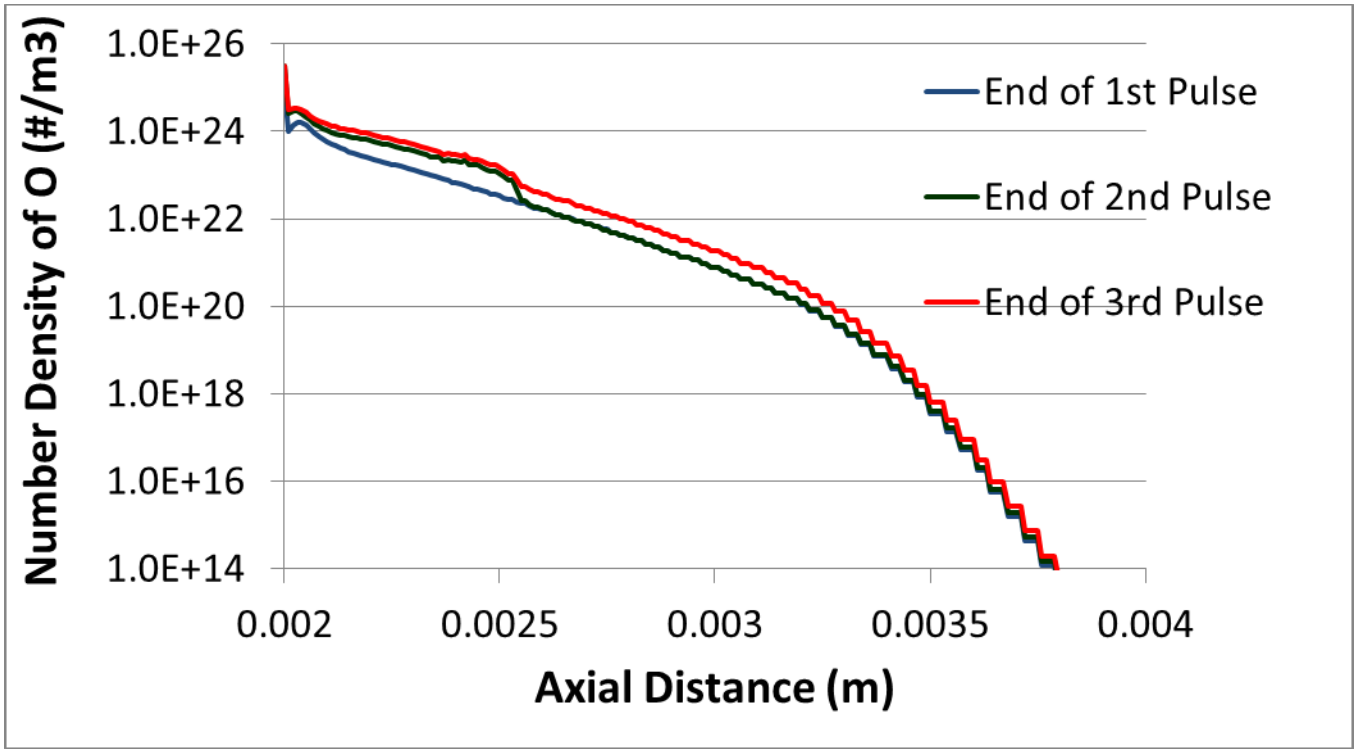

O3 Radical Number Density at End of Different Pulses

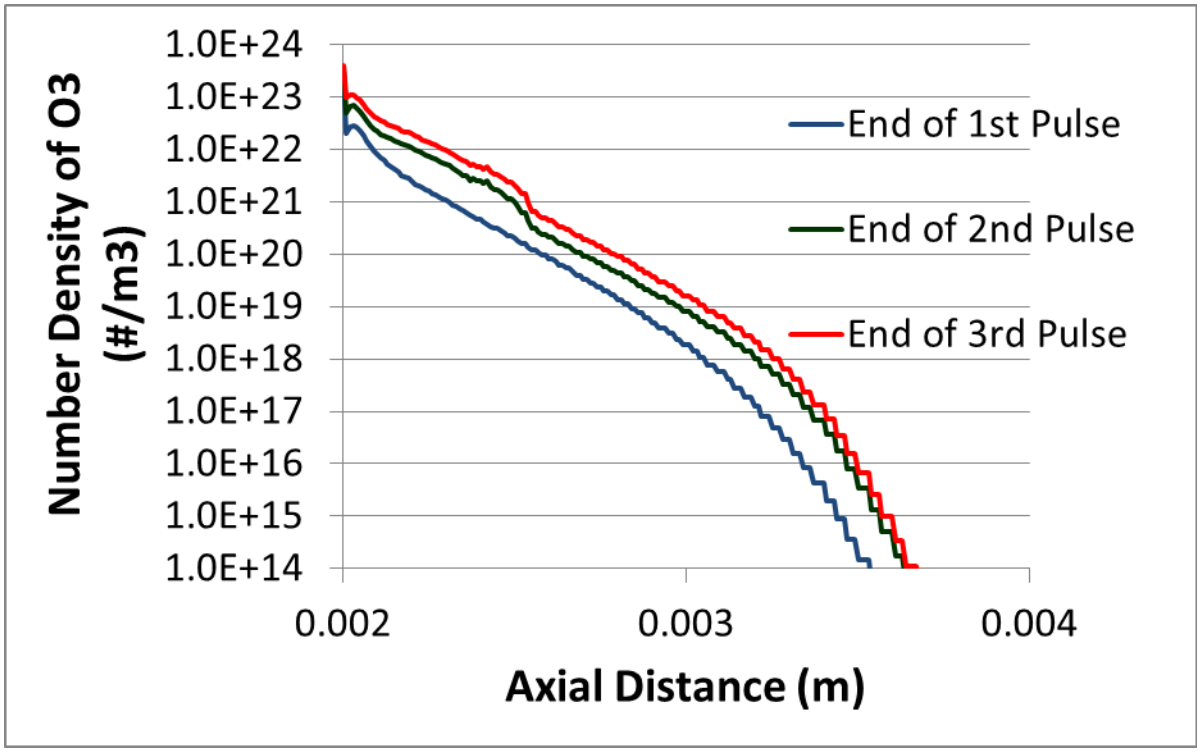

Voltage Amplitude Comparison

Voltage: Streamer Propagation

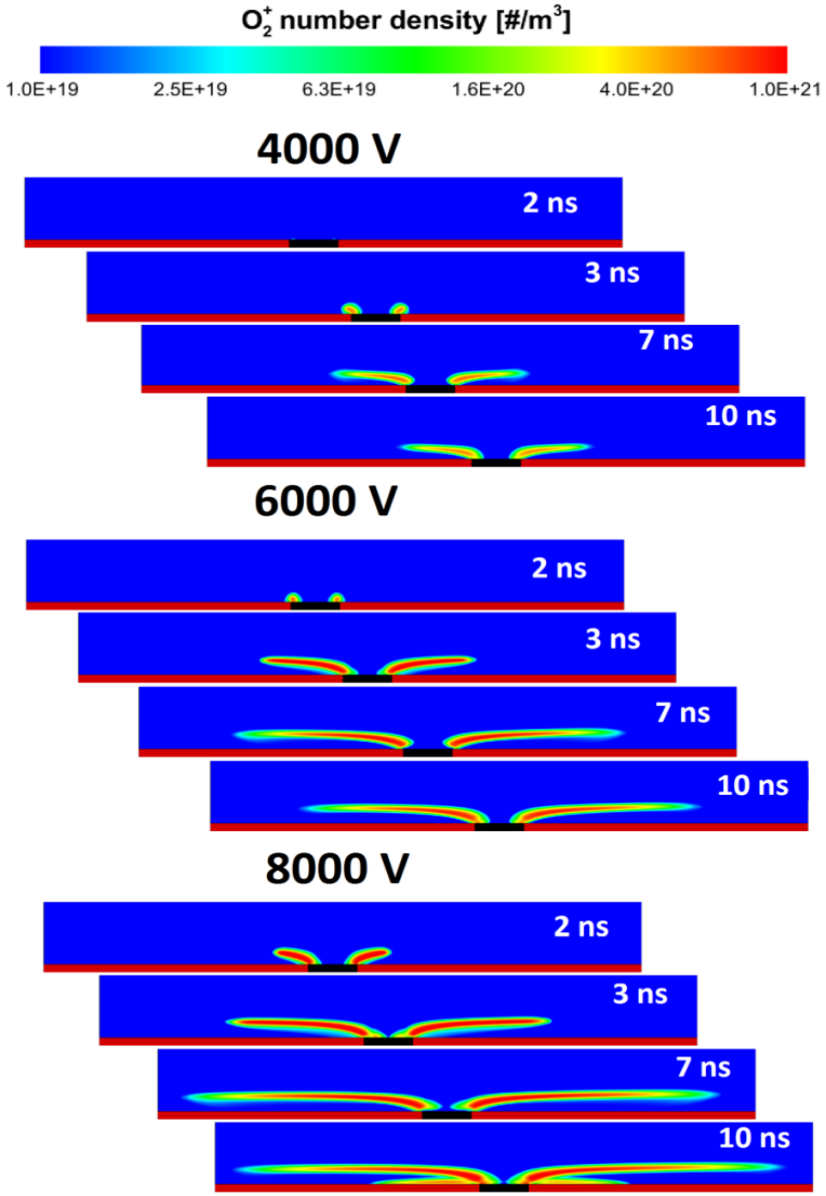

Higher voltages result in stronger Electric Field

Streamers propagate further as voltage increases

Voltage : Thermal Effects

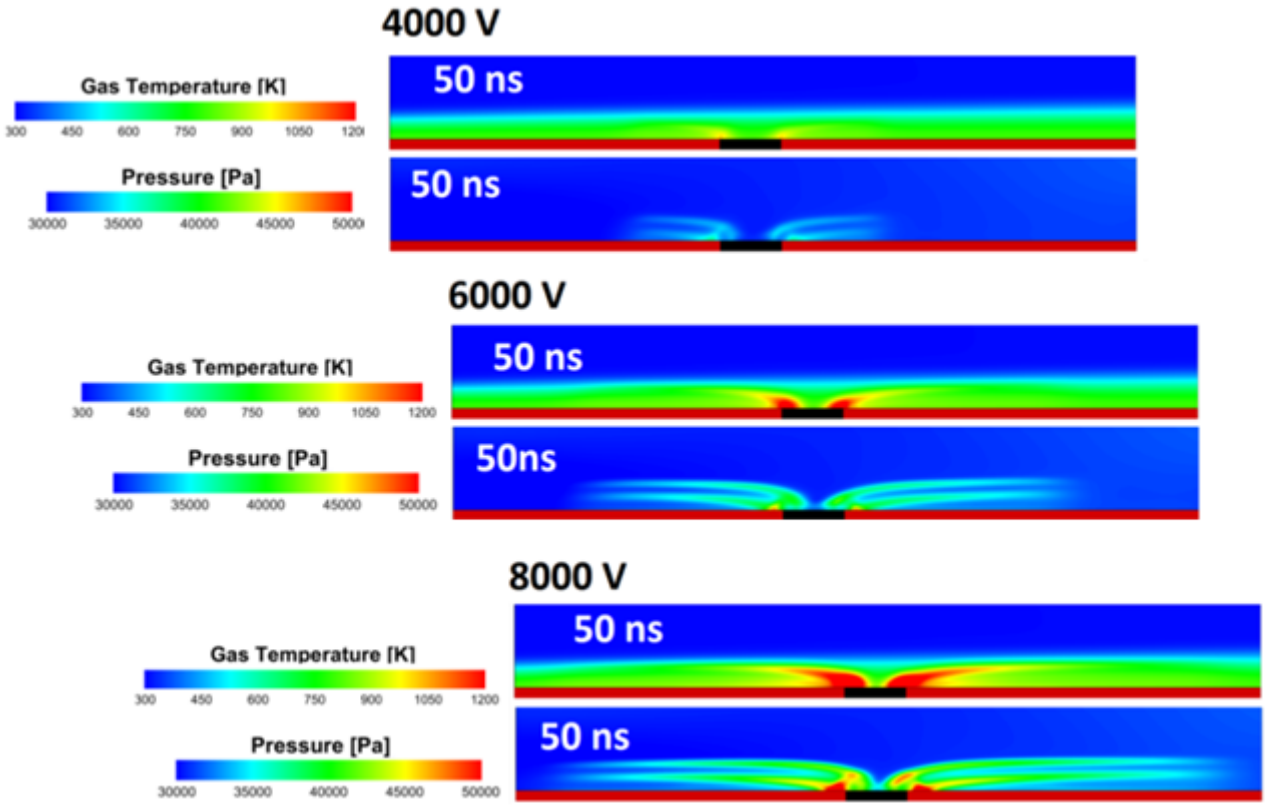

Stronger Electric fields result in greater ion Joule heating

Conclusions

- **O radicals dominant species in plasma (~0.5% peak mole fraction)**
- **Ion Joule heating dominates gas temperature increase and results in blast waves**
- **Increasing Voltage increases peak densities, gas heating and volume of plasma formed**
- **Chemistry (electropositive vs electronegative plasma) affects –**
  - **Streamer propagation distance/speed**
  - **Region of plasma formation (inside/outside boundary layer)**
  - **Intensity of gas heating for different polarities**
- **Anodic pulses appear more efficient for supersonic combustion**
  - **Radicals produced over greater volume**
  - **Less power lost to heat (for O_2-H_2)**